Engineered microvasculature platforms to study tumor-host-matrix interactions during metastatic seeding

By

Michelle B. Chen

B.S. Mechanical Engineering (2012), University of Toronto
S.M. Mechanical Engineering (2014), Massachusetts Institute of Technology

Submitted to the Department of Mechanical Engineering in Partial Fulfillment of the Requirements for the Degree of

Doctor of Philosophy in Mechanical Engineering

at the

MASSACHUSETTS INSTITUTE OF TECHNOLOGY

February 2017

Author .. Signature redacted .....
Department of Mechanical Engineering
January 15, 2017

Certified by . Signature redacted .....
Roger D. Kamm
Professor of Mechanical Engineering
Professor of Biological Engineering
Thesis Supervisor

Accepted by ..... Signature redacted .....
Rohan Abeyaratne
Chairman, Department Committee on Graduate Theses
Graduate Office

Engineered microvasculature platforms to study tumor-host-matrix interactions during metastatic seeding

By

Michelle B. Chen

Submitted to the Department of Mechanical Engineering on January 15, 2017 in Partial Fulfillment of the Requirements for the Degree of Doctor of Philosophy in Mechanical Engineering

Abstract

Distant metastases, which result in >90% of cancer related deaths, is enabled by hematogenous dissemination of tumor cells via the circulation. In particular, tumor cell extravasation is thought to be an essential and potential rate-limiting step, as most metastases are found in the extravascular space rather than intraluminal at distant organs. However, mechanistic insights into the cellular and molecular players during extravasation are limited due to technical challenges in observing real-time events *in vivo*. Increased understanding of the extravasation cascade is critical in uncovering new opportunities for therapeutic intervention during early metastatic dissemination.

In this thesis, we develop an *in vitro* model of the human microcirculation with the capability to recapitulate several discrete steps of hematogenous dissemination, including tumor cell circulatory transport, arrest, and transendothelial migration. The microdevice features self-organized human microvascular networks through which tumor cells can be perfused and tracked over time via standard confocal microscopy. In addition to improved throughput for parametric studies, robust and rapid scoring of extravascular cells combined with high spatio-resolution imaging for deciphering cell morphological dynamics can be easily achieved due to excellent optical accessibility.

To demonstrate the ability to obtain novel biological insights, we apply the assay to decipher the roles of tumor integrins in modulating extravasation. In particular, we deplete integrin beta-1 in tumor cells and isolate the specific defects in the extravasation cascade. Dynamic imaging revealed that β1-depleted cells lacked the ability to sustain protrusions into the subendothelial matrix in contrast to control cells. Specifically, adhesion via α3β1 and α6β1 to subendothelial laminin was a critical prerequisite for successful transmigration, as well as basement membrane breaching. Combined with validation from in vivo metastasis assays, we find that tumor beta-1 integrin is a critical mediator of extravasation and metastases formation.

Furthermore, we demonstrate the potential of our assay to recapitulate the complexities of the host microenvironment via modular addition of non-cancer host cells. Specifically, we explore the interactions of circulating human neutrophils with tumor cells and demonstrate that their interactions can exert pro-extravasation effects through neutrophil-derived IL-8. Through high spatio-temporal resolution imaging, we further identify novel mechanisms through which neutrophils are sequestered and confined at the vicinity of trapped tumor cells during flow conditions, and how the spatial localization of their secreted factors can act to facilitate tumor transmigration.

Key words: Metastasis, extravasation, microfluidics, tumor cell migration, neutrophils, integrins

Thesis Committee:

Thesis advisor: Roger D. Kamm, Professor of Mechanical and Biological Engineering, MIT
Alan J. Grodzinsky, Professor of Mechanical and Biological Engineering, MIT
Richard O. Hynes, Professor of Biology, MIT

Acknowledgements

I would like to thank my advisor, Prof. Roger Kamm for his continuous support and guidance throughout the course of my work at MIT. I am grateful for all the opportunities that he has given me throughout the years, whether it was opportunities to collaborate, travel to conferences or providing me with all the endless resources and freedom to pursue my research interests. Because of this, I was able to grow as an independent scientist. I am also grateful for the support of Prof. Alan Grodzinsky as a member of my committee and a valued advisor in all aspects of my research. I would like to thank Prof. Richard Hynes for taking me under his wing and mentoring me in world of cell biology, as a both a committee member and collaborator. Through collaborations his lab, I have learned an incredible amount in the world of cell biology in such a short period of time.

I would also like to thank all the members of the Kamm Lab who have worked tirelessly with me along the way. In particular, I would like to thank Sebastien Uzel for his valuable expertise on micro-fabrication, as well as his sharp eye for detail. His work ethic is truly inspiring and has always pushed me to be a better scientist. I thank Ran Li for his countless insights and for being a valued colleague with whom I could bounce ideas off of. I am also grateful for the help from Jordan Whisler for teaching me everything there is to know about microvascular networks, as well as Vivek Sivathanu, Dr. Michael Mak and Dr. Moeendarbary. I could always rely on these friends for a critical eye, support, and inspiration, especially when things got tough. I am also grateful for the mentors and collaborators from other labs who have been instrumental in helping me achieve my goals, especially Dr. John Lamar, Julia Froese, Dr. Bigyan Bista, Dr. Fred Lam, and Dr. Asaf Spiegel.

Lastly, I thank my family, as they continue to support me daily from 2000 miles away over the last 9 years of being away from home. My sister and mother have always encouraged me while may dad has taught me what it means to be an excellent and upright scientist and scholar, and that as long as I follow my passion even the hardest times will pass.

This work is supported by a National Science Foundation Graduate Research Fellowship and the MIT Rosenblith Fellowship.

Table of Contents

Chapter 1

Background and Motivation

1.1 The metastatic cascade

Cancer metastasis, the spread of cancer cells from a primary tumor site to a secondary organ, accounts for 90% of deaths among cancer patients[1]. In order for cancer cells to transmigrate and colonize a distal organ, they must overcome several barriers in a series of steps termed the "metastatic cascade"[1]. Tumor cells of epithelial origin at the primary site undergo an epithelial-to-mesenchymal transition[2] (EMT), acquiring the capability to invade and migrate through the tumor basement membrane, as well as the stromal matrix surrounding the epithelial tissues. This enhanced migratory ability allows cancer cells to spread throughout the primary tumor site, and can be further promoted by chemical (growth factors), cellular (tumor-associated stromal cells), and mechanical (interstitial flow) cues within the tumor microenvironment[3]. The growth of the tumor can also initiate angiogenesis, allowing blood vessels to extend into the tumor tissues[4]. Besides supplying cancer cells with nutrients, these tumor-associated blood vessels also provide cancer cells with a route of escape from the primary tumor. Once a migrating cancer cell come into contact with a blood vessel or lymphatic, it can transmigrate through the endothelial wall and enter the circulation in a process called intravasation. In the blood stream, these circulating tumor cells can travel to the secondary site, and exit the blood vessel by extravasation. These extravasated cancer cells can *recolonize* the secondary site[1]. Taken together, cancer metastasis is a complex process that involves a series of distinct steps (**Figure 1**).

Recognizing the complexity of this process and the corresponding challenges associated with studying them *in vivo*, it is perhaps not surprising that a full understanding of the critical mechanistic details of metastatic disease is lacking. For similar reasons, there is a marked absence of drugs available to treat metastatic cancer by inhibiting one or more of the steps of the metastatic cascade. These key shortcomings have led in recent years to a rapid expansion of new *in vitro* technologies, especially in the field of microfluidics, to study metastasis and to create assays with the potential to screen for drugs with therapeutic value.

1.2 Tumor cell extravasation cascade

Extravasation, the first step of seeding metastases, involves a cascade of events consisting of (1) tumor cell arrest and formation of stable adhesions (2) transmigration through a tight endothelial barrier, and (3) subsequent invasion into the surrounding subendothelial basement membrane and matrix (**Figure 1**). There have been two general hypotheses regarding the mode of arrest of circulating tumor cells (CTCs) in a blood vessel: mechanical trapping of cells and/or active preferential adhesion of the tumor cell onto the endothelium in a distant organ. James Ewing proposed that metastasis at distant organs is dictated by the anatomy of the blood and lymphatic vessels and blood circulatory paths between primary and secondary tumor sites [5]. CTCs, due to their relatively large size (~15-20 microns in diameter), may become physically trapped in the microcirculation, become activated, and eventually transmigrate [6]. However, Steven Paget's "seed and soil" hypothesis suggests that there exist interactions between different tumor cell types and specific organ microenvironments that guide their metastatic spread. The vasculature of such organs may be primed with surface receptors/molecules or secrete chemokines that cause specific tumor cell types to preferentially "home and seed" at that particular tissue environment. This is supported by the observation that breast cancer cells frequently metastasize to the bone [7]. Although two distinct phenomena have been described, is it clear now that the two theories may not be mutually exclusive; in fact, it has been suggested that tissue/organ tropism can be influenced both by physical trapping and interactions between "seed cells" and "receptive soils" [8].

Although the mechanisms of tumor cell *intravasation* have been widely studied, the precise cellular interactions and molecular alterations associated with extravasation are poorly understood[9]. Single tumor cell extravasation events are challenging to capture in real-time and high definition *in vivo* partly due to the optical inaccessibility of visceral organs; thus, most data are gathered endpoint assays that indirectly observe tumor cells via quantification of secondary tumor formation[10,11]. Furthermore, *in vivo* models are limited in their ability to isolate discrete steps in the extravasation cascade, rendering it difficult at times to fully understand the mechanistic details of the extravasation process.

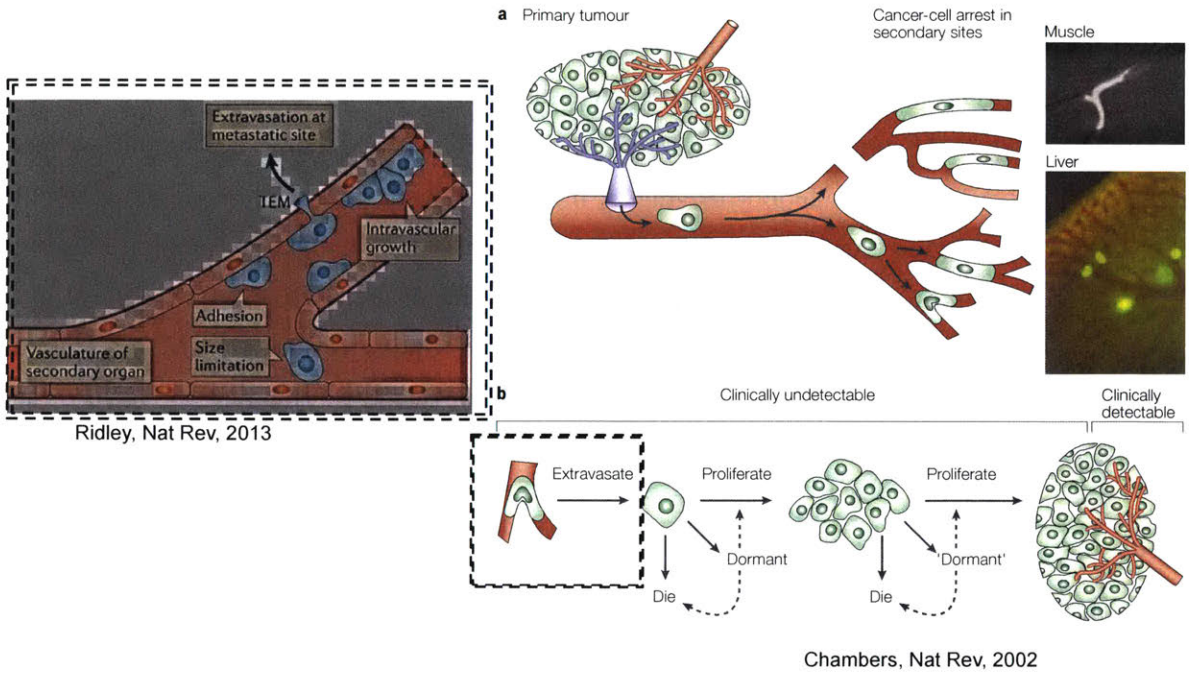

Figure 1. The metastatic cascade and extravasation. Cells from the primary tumor invade into the surrounding tumor stroma and eventually access the microcirculation via intravasation. Circulating tumor cells can then travel to a distant site, extravasate, and proliferate to form a secondary metastases. Extravasation (dotted box inset) involves a cascade of events starting with tumor cell arrest due to adhesion or size limitation, followed by transendothelial migration and migration into the perivascular matrix. Figures adapted from [12,13].

1.3 *In vitro* models of the metastatic cascade

Although no *in vitro* model can fully replicate the complexity of the *in vivo* metastatic milieu, considerable effort has been devoted to the development of more sophisticated *in vitro* technologies to facilitate our understanding of tumor cell invasion, migration, and interactions with the vasculature. Conventional cell culture assays including petri dishes and Transwell/Boyden chambers have proven to be pivotal in enhancing our understanding of cellular interactions in metastasis by recreating discrete events in a complex cascade and offering tight control of certain critical experimental parameters. However, there remain several needs that most traditional *in vitro* assays cannot yet satisfy. These include the recapitulation of spatial and temporal chemokine gradients, mechanical stresses, and relevant spatial organization of multiple cell types.

Microfluidics has made great strides in the field of cell biology, allowing scientists to fabricate sophisticated 3D models feature highly controlled microenvironments. Devices can easily accommodate

different cell types which can be arranged in physiologically relevant configurations to mimic the *in vivo* tumor microenvironment[14]. Chemokine gradients and mechanical forces such as interstitial fluid pressure on tumor cells or shear stresses on endothelial cells can be readily applied, controlled and quantified [15]. Cells can be embedded and cultured in 3D ECM hydrogels that mimic the *in vivo* cell migration scenario, but still be amenable to high resolution imaging as the small volume and/or thickness of cell culture chambers generally provide excellent optical clarity [14]. High spatio-temporal resolution imaging in experimental metastasis assays is important as it enables characterization of the morphological details during tumor cell invasion and migration, and endothelial cells during transendothelial migration. As such, microfluidic technologies have emerged as a promising approach to develop intricate *in vitro* cancer models and recapitulate the different steps in the metastatic cascade.

In vitro assays to study extravasation

The most commonly used and accepted *in vitro* model to study tumor-endothelial interactions in the context of metastasis is the Boyden chamber/Transwell assay, which provide a relatively simple and high throughput method for parametric cell migration studies, and overcome some limitations of *in vivo* experiments by increasing throughput, ease of quantification of transmigration events and the ability to employ human cell culture [16]. Generally, an endothelial cell layer is grown to confluence on a porous membrane insert and tumor cells are seeded on top of the layer and allowed to transmigrate. The number of cells transmigrated can then be quantified by collecting the cells on the underside of the membrane. More recently, similar assays incorporating a 3D ECM matrix beneath the endothelial monolayer have increased the physiological relevance by recapitulating the subendothelial ECM into which tumor cells transmigrate [17]. A subluminal-to-luminal transendothelial migration assay has also been developed to model intravasation, which features a thin layer of ECM on the bottom of a Transwell filter with layer of endothelial cells seeded onto this basement membrane-like matrix [18]. However, "top-down" assays where the endothelium and matrix and layered on top of each other in the x-y plane usually do not allow for real time and high resolution monitoring of tumor cell morphological dynamics during transmigration.

Recently, microfluidic cell culture platforms have emerged to address the need for greater resolution, higher throughput, control of the cellular microenvironment and enhanced physiological relevance compared to traditional cell culture methods. Much effort has also been devoted to the design of microfluidic assays for observing the early stage of metastatic seeding. Methods of engineering vasculature can be applied in this scenario, including self-organized formation of microvascular networks

and endothelial monolayer formation on hydrogel surfaces or porous membranes (**Figure 2**). Recently, the Takayama group described a microfluidic chip consisting of two chambers separated by a thin membrane onto which an endothelial monolayer is cultured[19]. The design resembles a traditional Transwell assay but with the added advantages of microfluidic systems including high resolution imaging and application of relevant fluid shear stresses. Tumor cell adhesion and arrest on the endothelium can be observed dynamically and in high resolution and it was demonstrated that breast cancer cell receptors CXCR4 and CXCR7 are involved in the adhesion of tumor cells to the endothelium. Similarly, Shin et al developed a microfluidic platform to recapitulate the metastatic cascade on a single chip, beginning with intravasation followed by arrest and adhesion on an endothelial monolayer. It was demonstrated that E-selectin expression and shear stress values dictated the adhesion of colon cancer cells onto the endothelium[20]. These types of "top-down" devices are particularly amenable to visualizing the morphological dynamics of the endothelium (e.g. endothelial junction behaviors).

In a different approach, microfluidic devices consisting of microchannels connected by 3D ECM hydrogels, tumor cells are seeded in one channel, arrest onto and extravasate across an endothelial cell (EC) monolayer oriented perpendicular to the image plane and migrate into a collagen gel. Using a system of this design, tumor cell transmigration events were shown to occur in the first 24 hours and were accompanied with an increase in endothelial monolayer permeability [21]. A similar type of microfluidic device was designed by Zhang et al, where one main endothelialized channel is connected vertically with 5 separated matrix-filled channels. HUVECs are grown to confluence on the hydrogels at the ends of the matrix channels and tumor aggregates are seeded into the endothelial channel where extravasation events can be observed [22]. In another study, a "multi-stepped" device is designed where tumor cells must first deform past 10-micron gaps between PDMS posts, which mimics the narrow capillaries through which tumor cells traverse in the circulation[23]. A portion of these deformed cells are then collected and transferred to a "transmigration chamber" consisting of an endothelialized channel connected to Matrigel filled channels, similar to that described in Zhang et al[22]. These types of monolayer-based assays are particularly amenable to imaging of tumor cell morphological dynamics, as migration occurs in the plane of view; however the details of the endothelium during transmigration are compromised (such as morphological dynamics of endothelial junctions). Moreover, there is the capability to incorporate chemical gradients orthogonal to the endothelial barrier, which may be useful to test hypotheses involving the dependence of transmigration on chemotactic agents. However, in these assays, the number of observable transmigration events is often limited due to the small surface areas between posts (required to prevent gel bursting), frequent sprouting of ECs into the gel, as well as difficulties in ensuring a continuous monolayer at the junction of PDMS posts and the hydrogel surface. Confirming the barrier

integrity at each of these focal points via immunofluorescence or diffusive permeability measurements would be laborious but an essential step if the assay were to be used for extravasation. Other challenges with monolayer-based assay include the artifactual dependence of transmigration rates on the degree of endothelial confluency and geometrical over-simplification as extravasation occurs in complex 3D μVNs with vessel segments of 5-30 μm in diameter instead of >100 μm [24] or an "infinite" flat plane of endothelial cells [21,23]. Additionally, in many monolayer systems (especially Transwell filters), nearly all tumor cells seeded at t=0 will translocate across a monolayer over a 24-48 hour time frame[25]. When compared to much lower extravasation rates of 40-60% at 24 hours that are typically found in mouse[26,27] and zebrafish [28]models for a variety of cell lines, this suggests that endothelial monolayers exhibit much greater permissiveness to tumor cells compared to *in vivo* microvasculature. We note however, that this value can vary widely depending on the cell type and *in vivo* model used. Lastly, while monolayer assays have adequately modeled many microvascular behaviors, they do not readily allow simultaneous application of lumenal flow with a 3D tubular organization.

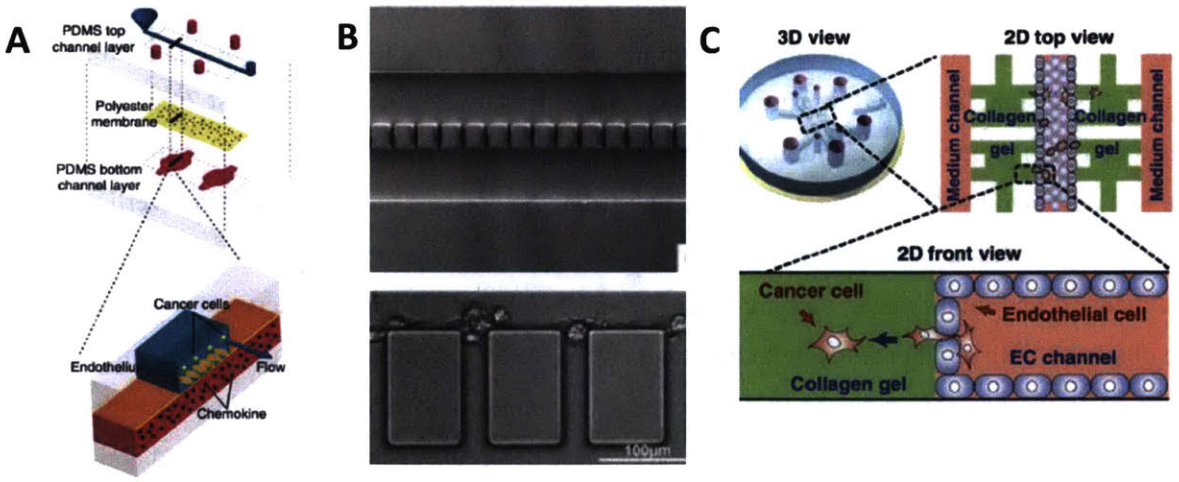

Figure 2. Microfluidic models of extravasation. (A) An extravasation model featuring an endothelial monolayer on top of a porous membrane sandwiched between two microchannels. The endothelium can be subject to physiologically relevant shear stresses while tumor cells are allowed to transmigrate from the top to the bottom microchannel (reproduced with permission from [29]). (B) Tumor cells can be observed to transmigrate across a confluent endothelial monolayer and into the 5 matrigel-filled microchannels connected perpendicular to the endothelial channel (reproduced with permission from [22]). (C) An endothelial monolayer is grown to confluence on the side of a gel-region to mimic the vascular barrier. Tumor cells are seeded in the "lumen" and extravasation events can be observed in the x-y plane of view (Reproduced with permission from [21]).

1.4 *In vivo* models of extravasation

Current *in vivo* and *ex vivo* models for visualizing extravasation include mouse [30–34] zebrafish [35] and chorioallantoic membrane (CAM) assays[36–38]. While murine models remain the gold standard for recapitulating metastatic seeding, the organs in which tumor cells arrest are generally not very optically accessible to allow live single cell imaging, rendering it difficult to assess extravasation rates; these are more suitable for end point *ex vivo* analyses[33,34]. CAM and zebrafish assays have previously been demonstrated to be much more optically accessible partly due the "planar" nature of the capillary beds, allowing intravascular and extravasated cells to be more clearly differentiated. However, the ability to resolve the dynamics of tumor cell protrusion kinetics with a large number of data points is still limited, likely due to the technical challenges associated with tumor cell injection and live imaging in intact organisms. Quantification of extravasation events in murine systems is often subjective due to the tortuosity of in vivo vasculature and tissue processing, and precise measurements relies on high resolution imaging (60X), greatly increasing data collection times, and are generally unsuitable for highly parametric studies. One heavily employed method to score extravasation is by counting how many tumor cells are retained in the lung after a certain time post-injection, with the assumption that extravasated cells will remain detectable while non-extravasated cells are lost due to shear or immune factors. However, recent analysis of mouse lung tissues fixed at 24 and 48 hours reveal a non-negligible proportion of "retained" tumor cells to be intravascular, so these assumptions are questionable [27]. Furthermore, all of the above systems feature non-human host cells, which may be problematic if specific human tumor-human host cell interactions are not conserved, particularly in the case of various types of immune cells. Lastly, intravenous injection of tumor cells in most of these systems often require significant technical expertise, which can limit the number of qualified users and even compromise the reproducibility of results. Moreover, procedures such as intra-cardiac injection of tumor cells often result in very few number of tumor cells found in the sites of dissemination, rendering it difficult to gather sufficient amount of data points.

1.5 Motivations for employing microfluidics

Despite the challenges still associated with *in vitro* transmigration assay, there remains untapped potential for applying microfluidic technologies to study tumor-endothelial interactions. In combination with gold-standard *in vivo* methodologies, microfluidics are well-poised to address the following needs in an extravasation assay which are challenging to achieve *in vivo* (**Figure 3**):

- Isolation and discretization of specific steps in the intravasation and extravasation cascade (adhesion, transendothelial migration, basement membrane breaching) to facilitate understanding of the mechanism of action of different cellular proteins or drugs
- Ability to recapitulate physiologically relevant spatial patterning and organization of multiple cell types at the metastatic site
- Facilitates 3D cell culture in ECM or ECM-like hydrogels
- High spatial resolution imaging of tumor-endothelial interactions during intravasation and extravasation via conventional microscopy techniques
- Facilitates real-time visualization transmigration events, allowing close observation of the dynamics of the endothelium and tumor cells
- Allows for highly controlled and tunable microenvironments, such as precise application of relevant spatio-temporal chemical gradients, mechanical stresses, and complex interactions between different cell types [14,39].
- Relatively lower cost and higher throughput than conventional *in vivo* model
- Relatively lower reagent volume compared to conventional *in vitro* cell culture methods

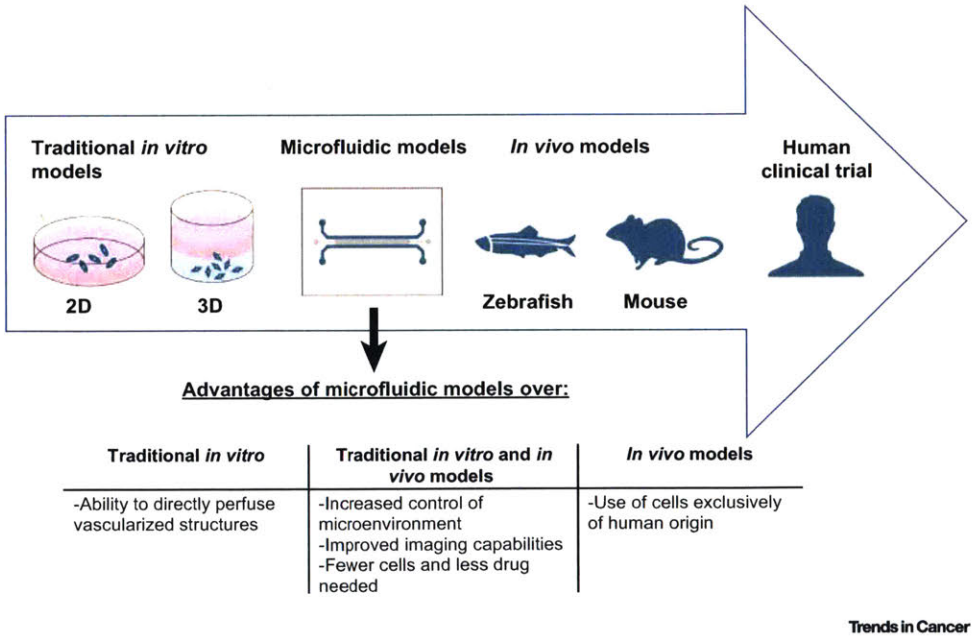

Figure 3. Overview of the various types of extravasation models and the potential advantages microfluidic platforms compared to traditional in vitro models and in vivo models. Figure adapted from[40].

1.6 Thesis aims and overview

Overview

Despite the fact that metastasis is the leading cause of cancer related deaths, many of the biological mechanisms that drive this key process remain poorly understood. In particular, tumor cell extravasation is thought to be an essential and potential rate-limiting step, as most metastases are found in the extravascular space rather than intraluminal at distant organs. Extravasation is made possible by a complex orchestration of various cell-cell adhesion, cell-matrix adhesion and biochemical signaling events. Additionally, it is know widely believed that extravasation events can be modulated by non-cancer host cells, such as circulating platelets, leukocytes and various stromal cells (**Figure 4**).

It is not surprising that the complexity of these processes opens many questions regarding the role and importance of both individual and combinations of factors that modulate extravasation. Addressing these questions can be greatly facilitated by *in vitro* technologies that enable (1) visualization of single tumor cell extravasation dynamics at high spatiotemporal resolution combined with (2) rapid, highly parametric and robust quantitation of extravasation events. When combined with gold-standard *in vivo* models, a deeper understanding of extravasation can be achieved and potentially contribute to improved methods for screening of possible therapeutic agents targeted at the extravasation step.

Thus the goals of this thesis are:

1) Engineer a micro-scale model of the extravasation microenvironment that closely mimics the *in vivo* scenario, while achieving both high throughput-screening capabilities combined with high spatio-temporal resolution visualization of cell morphology and motility.

2) Apply assay to obtain novel insights into the identities and spatio-temporal organization of cellular and molecular players involved in various cell-cell/cell- matrix interactions in the extravasation microenvironment, which are otherwise challenging to obtain *in vivo.* Understand how these interactions modulate extravasation.

Thesis aims

In Chapter 2, we describe the development of a microfluidic-based assay to recapitulate the extravasation microenvironment and characterize the vascular function and extravasation dynamics. The validity, sensitivity and throughput of the platform is demonstrated via identification of various factors that modulate extravasation rates.

In Chapter 3, we employ our extravasation assay to decipher, in high spatial resolution, the roles of tumor integrin beta-1 in modulating the extravasation process. Integrins are established as regulators of numerous tumor cell functions including adhesion, migration, invasion, proliferation and survival [41]. However, the precise steps in the extravasation cascade mediated by beta-1 remain unclear, partly due to challenges in observing these events *in vivo*. We demonstrate the ability of our assay to isolate the specific defects in the extravasation cascade associated with beta-1 depletion and identify novel insights into its roles in in tumor-endothelial adhesion, transendothelial migration, and basement membrane (BM) anchorage. Combined with validation from *in vivo* metastasis assays, we show that tumor beta-1 integrin is a critical mediator of extravasation and metastases formation.

In Chapter 4, we apply our platform to recapitulate and decipher the interactions between tumor cells and circulating neutrophils, and mechanisms through which this modulates tumor cell extravasation. It is widely believed that the metastatic potential of disseminated tumor cells can be modulated by both cooperative and antagonistic interactions between host microenvironment and tumor cells[42]. In particular, tumor cells encounter a variety of blood cells throughout their transit in the circulation, such as neutrophils, the pre-dominant circulating granulocyte in humans. To explore this, we first modify our platform to enhance throughput and robustness and apply it to demonstrate that neutrophils can exert pro-extravasation effects through the neutrophil secreted factor, IL-8. Through high spatio-temporal resolution imaging, we further identify novel mechanisms through which neutrophils are sequestered and confined at the vicinity of trapped tumor cells, and how the spatial localization of their secreted factors can act to facilitate tumor transmigration.

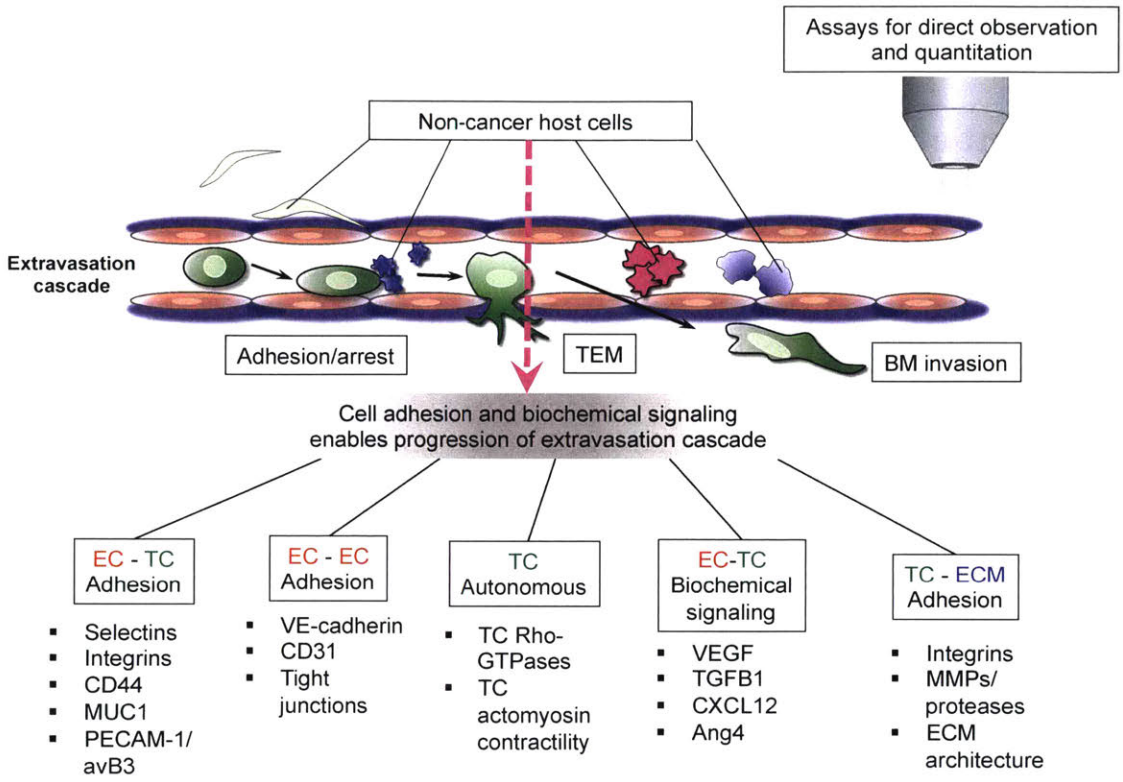

Figure 4. Tumor cell extravasation is a complex orchestration of various cell-adhesion and biochemical signaling events. Furthermore, there may exist cooperative interactions between non-cancer host cells and tumor cells which further dictate the extravasation cascade.

Chapter 2

Development of microfluidic assays for visualization and quantitation of tumor cell extravasation dynamics*

2.1 Introduction

Extravasation involves a cascade of events consisting of (1) tumor cell arrest on the endothelium resulting in the formation of dynamic contacts that give rise to significant cytoskeletal changes, and (2) tumor cell transendothelial migration (TEM) and subsequent invasion into the surrounding matrix[43]. Although the mechanisms of intravasation have been widely studied, the precise cellular interactions and molecular alterations associated with extravasation are poorly understood. In fact, most data are gathered from low-resolution *in vivo* studies and endpoint assays that indirectly observe tumor cells via quantification of secondary tumor formation in existing animal models As such, direct observation of tumor cell arrest on and subsequent migration across an endothelium in a precisely controlled and physiologically relevant microenvironment would provide important insight into extravasation mechanisms.

Currently, *in vitro* models such as the Boyden chamber-Transwell assays provide a relatively simple and high throughput method for parametric cell migration studies, yet do not allow monitoring of the entire process of extravasation and are limited in their physiological relevance[44,45]. Conversely, *in vivo* models of extravasation such as rat-tail vein injection of tumor cells mostly do not allow for high-resolution visualization of extravasation events. More recently, intravital microscopy performed on optically transparent transgenic zebrafish has enabled high spatial and temporal resolution imaging[35]; however, as with most *in vivo* platforms, the ability to perform parametric studies is restricted. Recently, microfluidic technologies have been developed to enable high resolution and dynamic study of both tumor cell intravasation and extravasation[21,46]. In the latter, devices consist of microchannels connected by 3D ECM hydrogels, where tumor cells are seeded in one channel, arrest onto and extravasate across an endothelial cell (EC) monolayer and into a hydrogel. However, the use of polydimethylsiloxane (PDMS)

* Sections of this chapter have been published previously. See Reference 89.

posts to contain the gel often prevents the formation of a continuous, low-permeable EC monolayer. It is also difficult to predict how changes in stiffness between the PDMS and gel affect extravasation mechanisms. Furthermore, most studies of extravasation or TEM across planar EC monolayers are limited in their physiological relevance.

3D microvascular networks (μVNs) have been widely explored *in vitro* and are particularly amenable to the study of vascular biology and modeling of disease in a more physiologically relevant configuration than endothelial lined tubes or monolayers. μVNs can be formed from self-organized, physiologically relevant vascularization processes, including sprouting angiogenesis and vasculogenesis. Recently, several groups have developed microfluidic platforms capable of generating perfusable 3D μVNs[47-49]. While no *in vitro* system can fully recapitulate the complexity of an *in vivo* situation, such vasculature have the potential to more closely model the *in vivo* tumor cell extravasation environment.

In this chapter, present the development of a microfluidic platform for the modeling of the entire process of extravasation from within *in vitro* μVNs assembled via vasculogenesis. Our platform offers key advantages over existing *in vitro* extravasation models by enabling all of the following: (1) high temporal and spatial resolution of extravasation events, (2) the ability to perform parametric studies in a tightly controlled and high throughput microenvironment and (3) increased physiological relevance compared to 2D and 3D planar monolayer models. We employ our model to demonstrate the effect of inflammatory cytokine stimulation on endothelial barrier function and TEM efficiency, and the positive correlation between metastatic potentials of different tumor cell lines and their extravasation capabilities. We demonstrate high spatiotemporal visualization of the sequential steps of extravasation from *in vitro* μVNs, and observe the TEM patterns of different tumor cell subpopulations including mechanically entrapped cells, single arrested tumor cells and cell clusters. Findings from our platform result in a deeper understanding of tumor cell extravasation mechanisms and demonstrate our assay's potential to be employed for the discovery of factors that could inhibit this crucial step in metastasis.

2.2 Assay design

Recapitulation and study of the critical steps in early metastatic seeding requires a system with several capabilities: 1) a microvascular network with dimensions and barrier functions comparable to the human microcirculation, 2) the ability to perfuse circulating tumor cells into the network with the option to maintain intravascular flow for the remaining duration of the experiment, and 3) imaging of extravasation events with high spatiotemporal resolution. To meet these requirements, we have developed a simple, easy to use *in vitro* microfluidic-based assay featuring perfusable μVNs. The user can achieve

rapid and robust quantitation of tumor cell extravasation efficiency, and if required, perform higher spatiotemporal resolution imaging of the morphological dynamics of tumor and endothelial cells during transmigration. The assay consists of 5 key sequential elements: (1) device fabrication and sterilization, (2) injection of endothelial and fibroblast cell-laden fibrin gels, (3) device culture until formation of a mature perfusable μVN, (4) perfusion of tumor cells, (5) live tracking of tumor cell extravasation and proliferation events and data analysis.

Formation of in vitro μVNs in microfluidic devices

The device builds upon the microfluidic gel chamber designs previously published in our lab[50]. It features three hydrogel regions (each 800 μm wide x 1300 μm long x 110 μm high) each separated by media channels that allow delivery and exchange of soluble factors and small particles. Upright micro-posts separated by 100 μm delineate the boundaries of each gel region, simultaneously allowing surface tension-assisted filling of cell-laden hydrogels and paracrine interactions between endothelial cells and flanking fibroblasts. Human umbilical vein endothelial cells (HUVECs) and human lung fibroblasts (FBs) suspended in fibrin gels are injected into the central region and side regions, respectively (**Figure 5**). Once seeded, single HUVECs elongate, form vacuoles and connect with neighboring cells to form patent lumens ranging from 8 to 96 μm in diameter within 4-5 days (**Figure 6**). Paracrine signaling from stromal cells in the flanking gel regions help to prevent the premature regression of μVNs (compared to HUVEC mono-culture)[51], such that the characterization of extravasation events is not affected by changes in network morphology. Vessels are relatively quiescent, with individual vessel diameters increasing by 5.1±4.7% from days 4 to 5, and 5.7±5.4% from days 5 to 6. Similarly, the normalized number of vessel branches exhibited no statistically significant changes, indicating minimal EC remodeling and apoptosis. The number of devices seeded per experiment is up to the discretion of the user – we have robustly shown that 24 independent devices can be seeded in one sitting without compromising cell viability. While it is possible for human microvascular endothelial cells (HMVECs) to be used instead of HUVECs, we have observed that the current protocol with HMVECs yields significantly less perfusable and interconnected vascular networks. Further optimization of initial ECM composition and exogenous growth factors is required if HMVEC culture is desired.

Microfluidic devices were fabricated via standard soft lithography as described previously[50]. Fibrinogen solution was prepared by reconstituting 5 mg/mL or 10 mg/mL of bovine fibrinogen (Sigma, MO) in PBS and dissolving the mixture in a 37°C water bath for 2 h. The solution was then filtered using a 0.2 μm filter and stored at 4°C. Human umbilical vein endothelial cells (HUVECs) (Lonza, MA) were

cultured in supplemented endothelial growth medium (EGM-2, Lonza) and grown to passage 5 before they were trypsinized and resuspended at a concentration of 8 million cells/mL in a solution of EGM with 0.15U/mL GM-6001 (PeproTech, NJ) and thrombin (0.5 U/mL, Sigma). The cell suspension was then mixed in a 1:1 ratio with 20 µL of 5mg/mL fibrinogen to achieve a final concentration of 4 million cells/mL and immediately injected into the HUVEC gel channel. Normal lung fibroblasts (NHLFs) (Lonza, MA) cultured in supplemented FGM (Sigma, MO) until passage 5 were similarly dissociated and suspended with the 10 mg/mL fibrinogen solution to reach a final cell density of 9 million cells/mL, and was injected into the NHLF channel. Devices were placed in a humidity box at room temperature and gels were allowed to cure for 20 minutes before filling the media channels with supplemented EGM. Media was replenished every 24 h for the duration of the culture. All cells were maintained in a humidified incubator at 37°C and 5% CO_2.

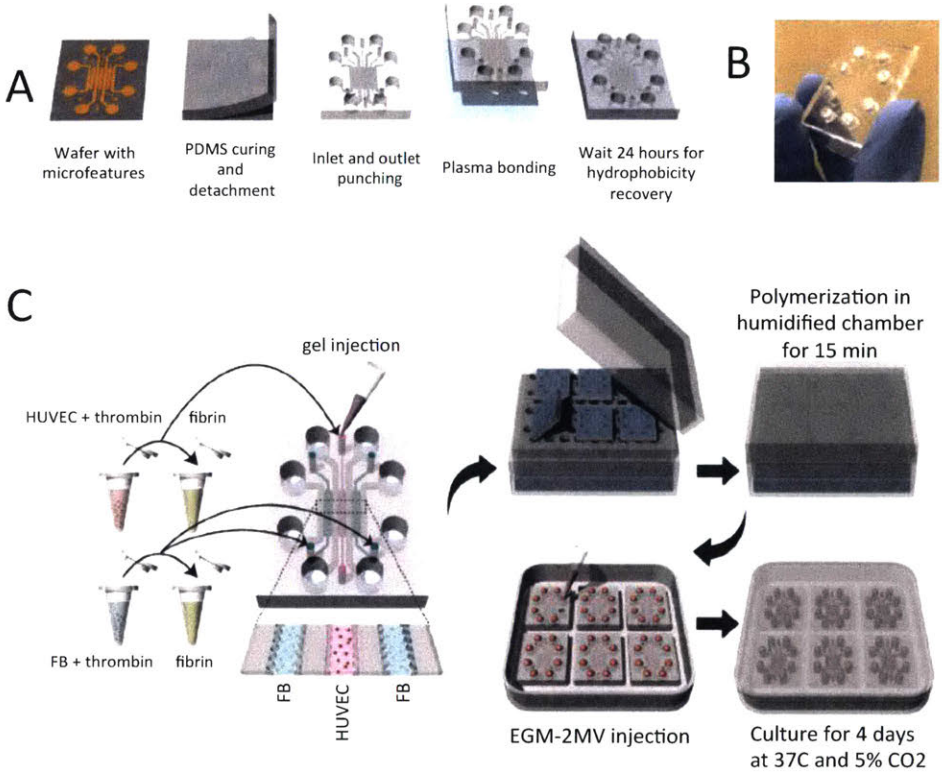

Figure 5. Schematic of assay and cell seeding protocol. (A) SU-8 wafers with micro features are fabricated (design given in Supplementary Materials) and PDMS devices are made via standard lithography techniques. Inlet and outlet holes are cored and PDMS channels are bonded to no. 1 coverslips. (B) Photograph of finished microdevice prior to cell seeding. (C) HUVECs and FBs are suspended in fibrin gel and are microinjected into separate gel regions. Upon gel polymerization, media channels are are filled with EGM-2MV growth media and incubated for 4 days to allow for lumen formation.

Tumor cell perfusion

Vasculogenesis-like tube formation in 3D hydrogels has long been demonstrated in a variety of assays, including gel droplets and endothelial cell spheroids [52,53]. However, while micro-vessels form, most systems remain un-perfusable to small particles due to the lack of accessible entry points into the vasculature. In our assay, the device is designed such that the μVNs form open lumens that connect with the media channels via the gel between micro posts, after 4-5 days of culture (**Figure 6B**). Similar designs in microfluidics have been robustly employed to allow vascular network formation followed by perfusion to study endothelial barrier function[47,49,54]. In this set-up, tumor cells suspended in medium can be perfused into μVNs by applying a hydrostatic pressure drop (~ 5mm H_2O) across the HUVEC gel region, which results in physiologically relevant fluid shear stresses (~1 Pa). During 10 minutes of perfusion via a hydrostatic pressure drop, both single and aggregates of tumor cells physically lodge and/or adhere to the endothelium in the microvessels (**Figure 6C**). At times, single tumor cells lodge and dislodge multiple times throughout the network before permanently arresting, similar to *in vivo* observations [42]. In the case of tumor cells with diameters of ~15-20 μm, >80% of tumor cells arrested in the networks are physically lodged, rather than purely adhered. The number of arrested tumor cells per device generally ranges between 40 to 100 cells. This depends on several factors including average vessel diameter, tumor cell diameter, duration of perfusion and degree of perfusability of the μVN.

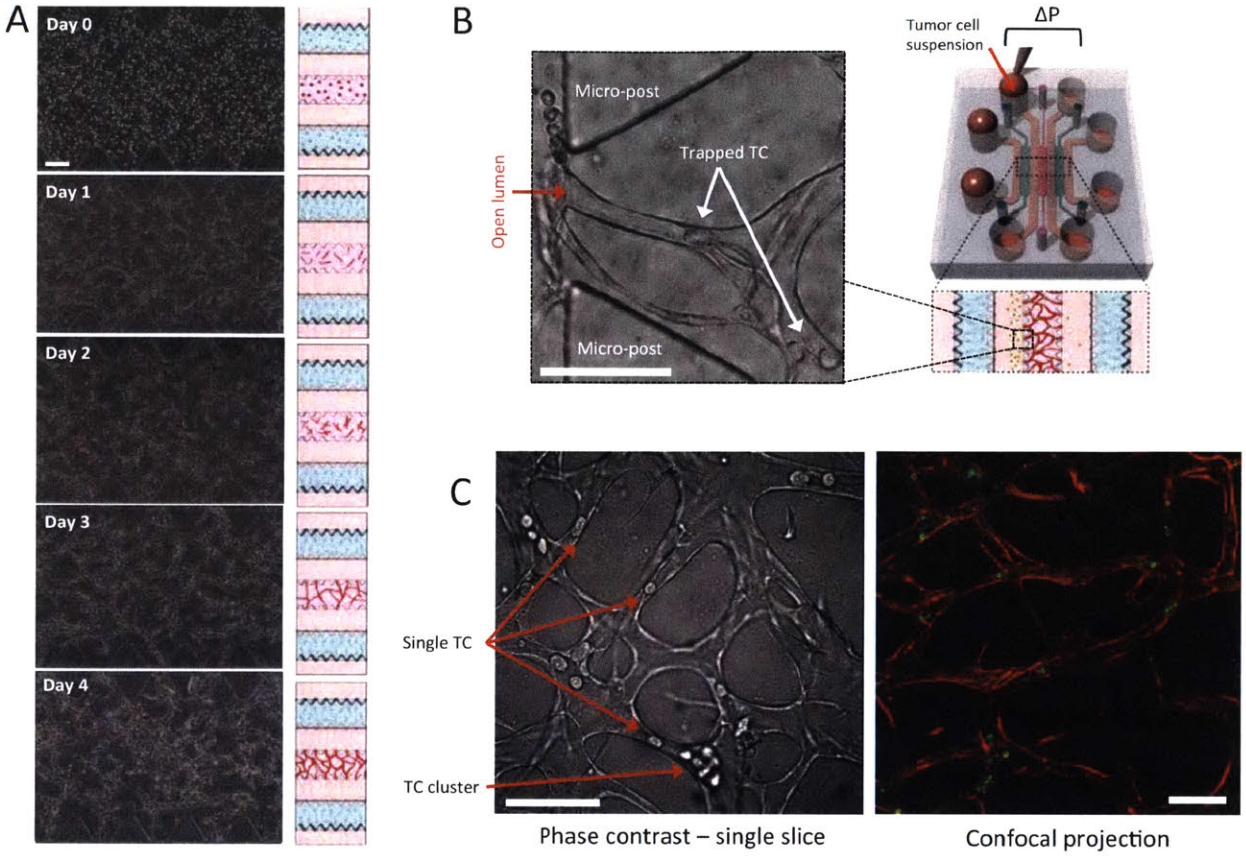

Figure 6. Vessel formation and tumor cell perfusion procedure. (A) Single HUVECS elongate, form vacuoles and subsequently self-assemble into interconnected lumenized vascular networks over the course of 4 days. (B) Triangular PDMS micro posts spaced 100 μm apart allow cell-laden fibrin gels to be spatially contained, but also serve as a connection between the cells and media sources. Uniquely, lumens form openings which connect the microvascular network to the media ports, allowing tumor cells to be perfused via a hydrostatic pressure drop. (C) Flowing tumor cells become physically trapped in networks due to size restriction. Trapped tumor cells (TC) can be clearly identified via phase contrast and fluorescent microscopy. Scale bars = 100 μm.

Briefly, MDA-MB-231, HT-1080 (from Dr. Frank Gertler, MIT) cultured in DMEM (Sigma, MO) supplemented with 10% FBS and 1% Pen-Strep (Invitrogen, CA), and MCF-10A cells (from the Brugge Lab) were trypsinized and resuspended at a final concentration of 0.4 M cells/mL in EGM. Media from the reservoirs of the two channels flanking the HUVEC channel were aspirated and 40 μL of the tumor cell suspension was introduced into one of the reservoirs of the central media channel. This creates a pressure drop of 5.2 mmH_2O across the vascular network, drawing the tumor cells into the vasculature, and corresponds to estimated shear stress values in the range of ~1 Pa during cell seeding, comparable to

the range of wall shear stresses found in venular microvessels, (< 1 Pa)[55]. Devices were placed in an incubator immediately after seeding and left to equilibrate for 30 min, after which devices were washed by applying fresh media via a pressure drop in the same direction as the tumor cell seeding to remove any non-adherent cells.

Cells were seeded at a density low enough to prevent clogging of the lumen openings and be reflective of the low cell density *in vivo*[56], yet high enough to observe at least one extravasation event per region of interest (ROI). After varying tumor seeding densities, we selected 0.4 million MDA-MB-231 cells/mL, which produced an average of 21.2 ±8.7 tumor cells per ROI (24 ROIs over 3 devices). This corresponds to an estimated 0.63 million cells/mL of vascular volume.

Quantification of extravasation efficiency and live tracking of extravasation kinetics

To quantify extravasation events, HUVECs were imaged live or fixed at the final time point to visualize the position of the tumor cell relative to the endothelial barrier. Confocal images were obtained each microvascular bed at 20X magnification and assessed in Imaris Bitplane or ImageJ using the built-in functions for "orthogonal views." Cells are scored as extravasated if the entire tumor cell body is found outside of the lumen. These can be clearly differentiated from mid-transmigrating and fully intravascular cells. The thin height of the hydrogel region causes μVNs to be confined largely to a single plane, greatly increasing the speed of imaging and enabling robust extravasation scoring (**Figure 7**). Tumor cells are typically found to initiate the extravasation cascade within 2 to 6 h p.i., and a fraction of these can complete transmigration anywhere between 4 to 48 hours depending on the tumor cell type and/or treatments applied. If desired, the user can impose constant flow of media through the μVNs to simulate the flow condition *in vivo,* throughout the entire extravasation process. This can be achieved via hydrostatic pressures generated from integrated reservoirs (typically for <6 hours before significant equilibration), or syringe pumps. Extravasation efficiency can be assessed over time via live confocal microscopy *in situ.* At 20X magnification, imaging of an entire device typically takes 6 to 8 minutes, depending on the optimal imaging configurations and number of regions of interest. Images are later reconstructed in 3D using standard software packages such as Imaris Bitplane (Belfast, UK) for analysis.

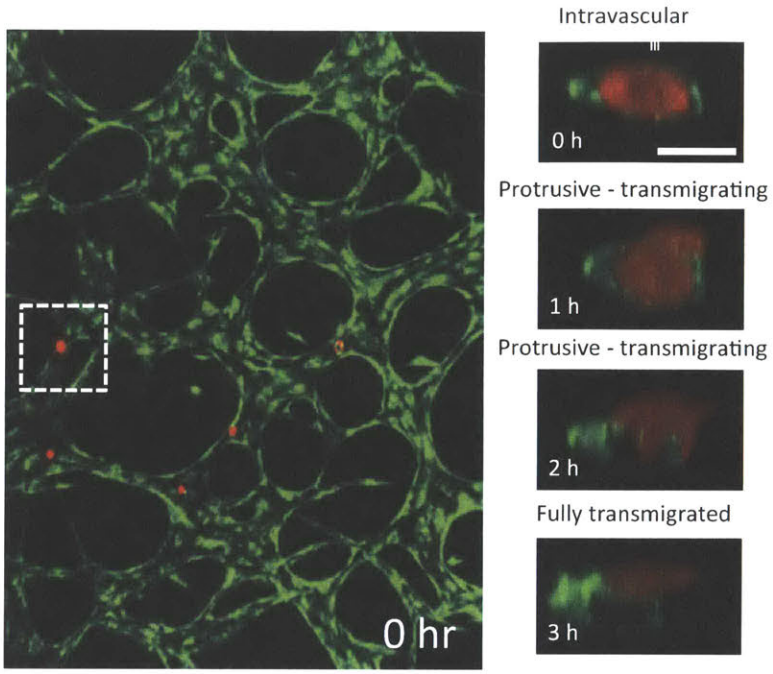

Figure 7. Scoring and quantification of extravasation efficiency. (A) Confocal projection of a representative region of tumor perfused (red) microvascular network (green) at 20X. Tumor cells can be robustly scored as intravascular, mid-transmigrating, or fully transmigrated by reconstructing the cross section at 20X (scale bar = 10 μm).

If desired, kinetic data from single or clusters of extravasating cells can be quantified in a moderate throughput manner via time-lapse imaging. The user can observe detailed morphological dynamics such as the time to initial endothelial penetration, and speed of translocation across the vascular wall. Generally, a magnification of ~20X is sufficient to visualize these details, with time intervals as small as 5 minutes, depending on the number of cells to be imaged. Such imaging is facilitated by the short distance (between 170 to 210 μm) between the outer bottom surface of the device and the plane of the μVNs. In addition, temporal and spatial organization of intracellular or extracellular proteins can be resolved, provided that proteins of interest are fluorescently labeled prior to imaging. Depending on the desired level of discrimination between discrete elements, imaging of some cellular proteins (e.g. F-actin, VE-cadherin, focal adhesion proteins) may require higher magnification (>30X), at the cost of increased imaging duration.

2.3 Biological characterization of engineered microvasculature and tumor cell extravasation events

Characterization of endothelial barrier function

To confirm the integrity of the endothelial barrier, staining of the networks at 96 h with anti-VE-cadherin showed the presence of continuous cell-cell junctions spanning the entire circumference of the lumen (**Figure 8**). To assess EC barrier function quantitatively, we employ the method used to quantify vessel permeability based on that described previously[57]. Briefly, background fluorescence images of the vascular network were obtained (I_b). The media in all reservoirs were aspirated and the three reservoirs on one side were injected with 45 μL of 10 μM 70 kDa MW Texas red dextran solution (Invitrogen, CA) simultaneously. Devices were placed in an incubator for 20 min, and then transferred to the microscope environmental chamber for another 10 min, to account for time required for dextran diffusion into the vessels and recovery from agitation during transfer. Once equilibrium was established (i.e. intensity inside the vessels remained constant), fluorescent images were captured every 5 min for 60 min. The permeability coefficient was calculated by obtaining the average intensity in a measuring window containing both the vessel segment and surrounding gel, at the initial and final time points. Individual sections of the vessel network of length ~80 μm each (2 sections/ROI, 4 ROI/device, n=3) were selected for analysis. The length of each section varied slightly, in order to capture a segment that was relatively uniform in diameter. Care was taken to select vessel segments in the central region of the channel, which was far enough from the media-gel boundary. Permeability coefficients were computed as:

$$P_d = \frac{1}{I_i - I_b}\left(\frac{I_f - I_i}{\Delta t}\right) \times \frac{d}{4}$$

where I_i, I_f and I_b are the initial, final and background average intensities, Δt is the time between the two captured images, and d is the average diameter of the vessel segment. All imaging was performed using a confocal microscope (Olympus, Japan).

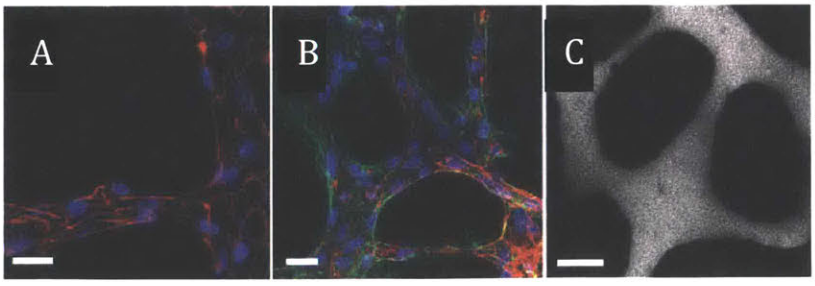

Figure 8. Characterization of microvascular networks. (A) Visualization of VE-cadherin (red) at 60X reveals continuous cell-cell junctions. (B) Collagen IV basement membrane deposition (green) around the lumen (red) and in the perivascular space suggests vessel maturation. (C) Perfusion of vessels with 70 kDa dextran reveals patent lumens void of local leaks. Scale bars are 20 μm.

Perfusion of the vasculature with 70 kDa dextran revealed patent lumens that were void of local leaks (**Figure 8C**) and exhibited a diffusive permeability of $(8.92 \pm 1.47) \times 10^{-7}$ cm/s (n=24 vessel segments over 3 devices) at 96 h after HUVEC seeding. These values were comparable to that of *in vivo* venules [58]and similar to existing *in vitro* *u*VN platforms produced via angiogenic sprouting[49] suggesting a strong and more physiologically relevant barrier compared to those reported in *in vitro* EC monolayers[21,46,57]. Moreover, the relative quiescence of these microvessels allows us to justify the decoupling of vessel remodeling and extravasation occurring within the time frame in which the events are studied.

Characterization of perivascular basement membrane proteins

Immunostaining revealed that the abluminal sides of microvessels were positive for basement membrane proteins collagen IV, laminin, and fibronectin (**Figure 9**), further confirming the level of maturity and physiological relevance of the vasculature. It is important to note one key advantage of our micro devices is the low volume of reagents required (<30 μl) of diluted antibody solutions per device, rendering it a much more economical choice, especially when a large number of proteins or samples are involved and/or when antibodies are particularly costly or rare. High spatial resolution can be achieved – in particular, staining for basement membrane proteins such as collagen IV and laminin allows precise localization of the tumor cells at various stages of extravasation. The ability to generate these data may be valuable, as it has recently been found that protease-localizing invadopodia can mediate extravasation, suggesting that basement membrane degradation may be required for complete transmigration.

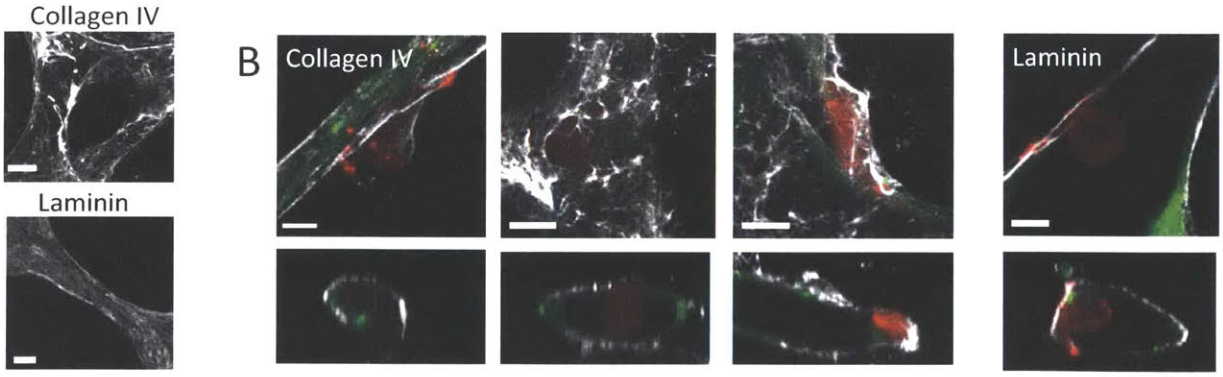

Figure 9. Interaction with the endothelial basement membrane. (A) In vitro endothelial networks deposit a layer of collagen IV and laminin on the abluminal side, constituting the vascular basement membrane (BM). (B) Fixed immunostaining at various time points for collagen IV and laminin reveal the close association of extravasating tumor cells to the basement membrane, suggesting that tumor-BM interactions are involved in the transmigration process. Scale bars are 10 μm.

2.4 Characterization of extravasation rates, kinetics and cell morphological dynamics

Extravasation rates

In untreated microvascular HUVEC networks (RFP transfected, Angioprotemie), we quantified an MDA-MB-231 extravasation efficiency of $12.3 \pm 3.4\%$ after 6 h and $23.6 \pm 4.5\%$ after 24 h. Extravasation could be observed as early as 30 min after tumor cell introduction into the vasculature, while the number of extravasated cells plateaued at around 24 h, with no significant difference in the number of extravasated cells at 48 h ($p=0.298$). The average number of tumor cells found in each ROI exhibited a slight yet insignificant ($p=0.37$) increase between 0 h and 24 h. These results suggest that most extravasation events occur in the first 24 h, which is similar to the time scales witnessed *in vivo*[27] and in other *in vitro* platforms[21]. Cell viability was $95.2 \pm 3.7\%$ at 24 h, suggesting that the adhered yet non-migratory and/or circular cells were likely not due to tumor cell apoptosis. Lastly, 10 μm fluorescent beads introduced into the vasculature were lodged but never extravasated, confirming that extravasation from within the vessels is not a passive process inherent to the platform.

Tumor cell morphology during TEM

Analysis of a sequence of images of a transmigrating MDA-MB-231 cell revealed that (1) transmigrating tumor cells first penetrate the EC barrier by extending thin fillipodial protrusions (<1 μm in width) into the subendothelial matrix, (2) protrusions continue to increase and branch out while the remaining body on the apical side of the lumen maintains its sphericity (3), the spherical body decreases in diameter as more of the cell and the nucleus clears the barrier (4), the tumor cell undergoes significant shape changes as it adopts a final spread morphology upon exiting the lumen (**Figure 10**). Interestingly, during mid-transmigration, the remaining portion of the cell body on the apical side remains spherical, even after transmigration of the nucleus, suggesting that the sphericity is not due to that of the nucleus. Furthermore, live nuclear staining at 40X reveals that transmigration of the nucleus occurs within a relatively short time frame (~15 min) compared to the total time required for complete tumor cell TEM. Microscopy at 90X revealed a thin segment of the tumor cell joining the two parts of the cell body on each side of the lumen, suggesting that TEM of most of the cell body occurs via extrusion through a gap of sub nuclear dimensions.

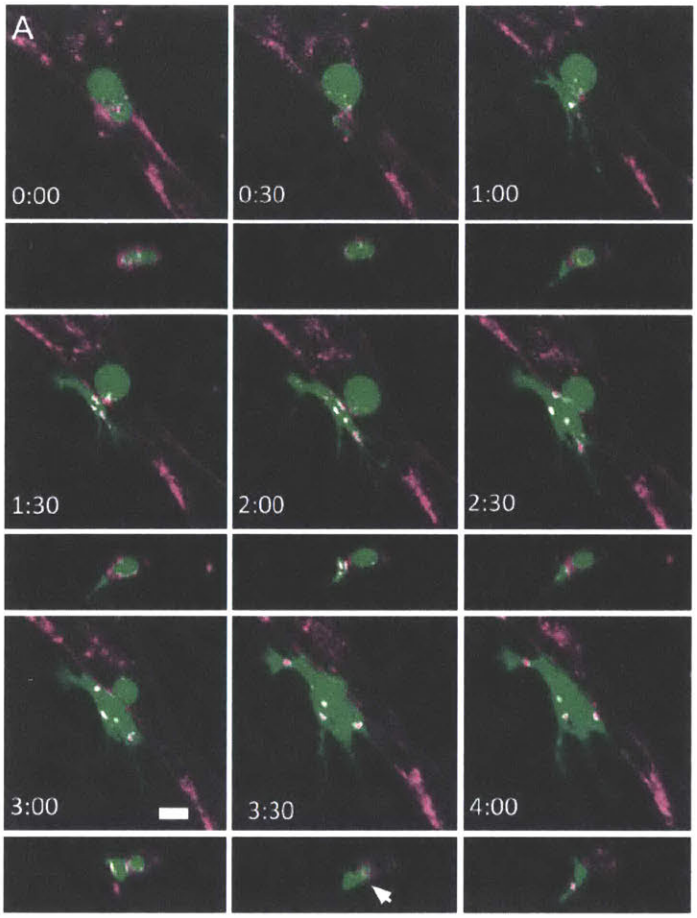

Figure 10. Visualization of extravasation dynamics. High-resolution time-lapse confocal microscopy (40X) of an extravasating entrapped MDA-MB-231 (green). Lumens were labeled with a far-red plasma membrane stain (purple). Tumor cells transmigrate through the endothelium and into the 3D matrix over a period of 4 h. The white arrow at 3:30 h indicates the location of a vessel opening at the site of tumor cell TEM.

In addition to dynamic tracking of extravasation rates, time-lapse microscopy (at 20X or 30X) allows the collection of other insightful kinetic data such as the time to initiation of tumor cell protrusions and the total time required for complete translocation past the EC barrier. Assessment of images at each time point via Imaris Bitplane allows the categorization of each individual tumor cell as intravascular, protruding or fully extravasated (**Figure 11A**). For instance, when time lapses of MDA-MB-231 and MDA-MB-231 incubated with anti-VE-cadherin were compared, the endpoint extravasation rates at 11 hours post-injection were greater with anti-VE-cadherin treatment. When data from earlier time points was analyzed, it revealed that TC protrusions were initiated at earlier times and formed at a faster rate. When MDA-MB-231 were compared with its highly metastatic variant LM2, not only were extravasation rates significantly lower at 11 hours, events appear to plateau while non-extravasating LM2 cells

continued to initiate protrusions (**Figure 11B**). Such kinetic morphological data can valuable as clues into the mechanisms at which cells arrive at their endpoint extravasated state. For instance, depending on the experimental condition, faster protrusion rate can possibly indicate a more permissive endothelium or increased ability for the tumor cell to initiate adhesion to the subendothelial ECM. Thus, insightful information may be lost if only end-point measurements are made.

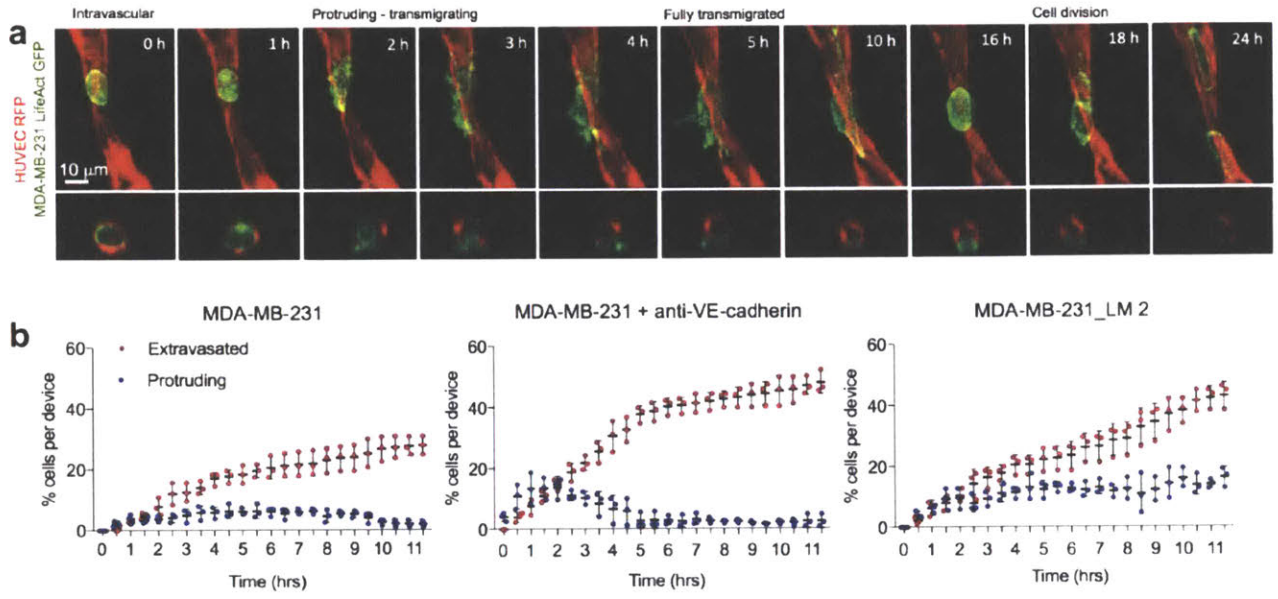

Figure 11. Tracking and quantification of extravasation kinetics. (A) Time lapse sequence of a trapped tumor cell extravasating from a lumen and subsequently undergoing cell division over 24 hours (scale bar = 10 μm). **(B)** Kinetics of the speed of tumor protrusion formation and time for total transmigration can be readily quantified by following single cells. Sample data of the percentage of tumor cells in either a "protrusive" state (blue) or "fully transmigrated" state (red) is calculated for MDA-MB-231 with and without the presence of a VE-cadherin antibody to enhance endothelial permissiveness, and LM2 cells (highly metastatic variant of MDA-MB-231). Each graph represents data from 1 device (between 80 to 160 tumor cells per device).

Endothelial barrier during TEM

Live time-lapse microscopy at 40X did not reveal a discernable gap in the endothelial plasma membrane at the site of transmigration, suggesting that the area through which tumor cell protrusions penetrate is relatively small, and likely paracellular rather than transcellular. A definitive opening in the barrier was only observed near the end of the extravasation events, which was presumably larger to allow the transmigration of the nucleus. This was confirmed via higher resolution imaging at 60X of endothelial F-actin, which revealed small gaps (~2 μm) in the endothelial barrier during the initial stages of

transmigration (**Figure 12**). Gaps then gradually increased in size to form holes ~8-10 μm in diameter. Furthermore, live imaging of endothelial VE-cadherin during the process of transmigration confirmed that tumor cells protrusions initiate at the cell junctions and that the disrupted junction "re-seals" after completion of tumor extravasation (**Figure 12**). Perfusion of the live vessels with 70-kDa dextran also revealed no apparent leaks at the sites of complete TEM.

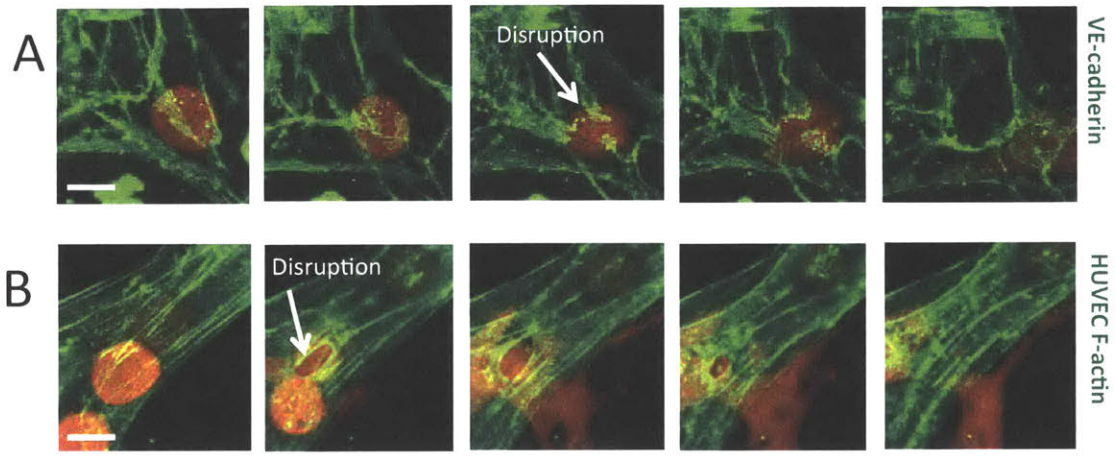

Figure 12. Endothelial disruption and re-sealing during tumor TEM. Time lapse sequence depicting the dynamics of (A) endothelial VE-cadherin (arrow depicts junctional disruption) and (B) endothelial F-actin (arrow depicts EC disruption) throughout an extravasation event.

Tracking tumor cell proliferation and early micrometastasis formation

Lastly, the assay can potentially be used to study early micrometastases formation via prolonged culture of microdevices (e.g. >24 hours). We have found that μVNs can remain relatively stable between days 1-6 post tumor cell seeding, such that the morphological changes of the μVNs (i.e. vessel diameter, interconnectivity) are small enough that the same vessel segments can be recognized and tracked as culture progresses[51]. This is partly due to paracrine factors secreted by supporting FBs which enhance μVN stability compared to HUVEC monoculture, where vessel regression can be evident as little as 3 days post endothelial seeding[51]. Tumor cells can also be tracked after extravasation by continued culture of the endothelial-tumor cell system for periods up to 5-6 days post tumor seeding (**Figure 13**). Via time-lapse microscopy or time point imaging, the number of tumor cells can be quantified when tumor cell nuclei are labeled with fluorescent tags (e.g, mCherry H2B) or when the tumor cell cytoplasm is labeled with nuclear excluded markers. Cell nuclei can be counted with conventional imaging software such as

ImageJ or Imaris Bitplane (Belfast, UK) to assess the level of tumor cell proliferation in both extravasated and intravascular subpopulations.

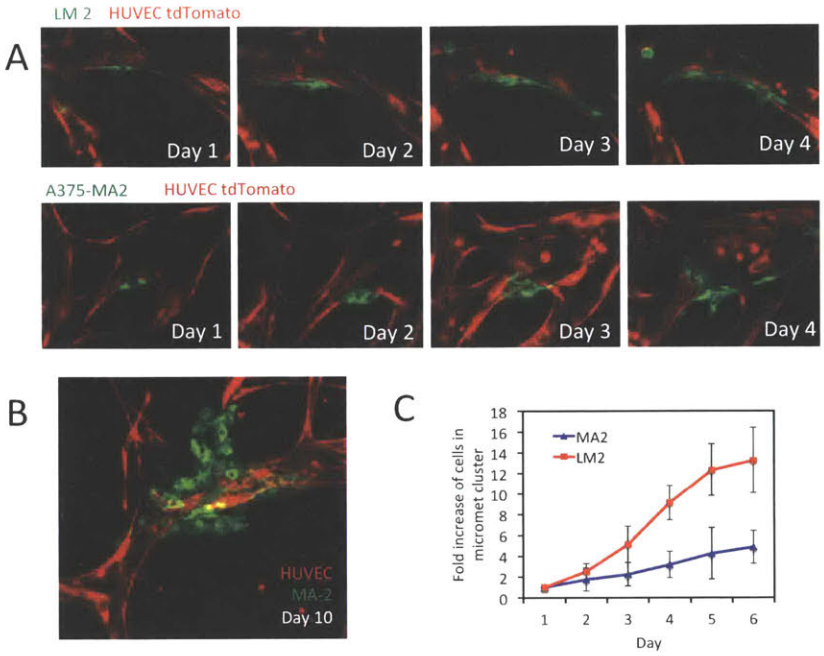

Figure 13. Tracking tumor cell proliferation and early micrometastases formation. (A) Time lapse of single extravasated LM2 (breast) and A375-MA2 (melanoma) cells proliferating in close association to the abluminal side of the lumen over 4 days (B) Example of an A375-MA2 micrometastases after 10 days of culture. (C) Quantification of the average fold increase in initial cell number at the cell "cluster" over 6 days.

2.5 Identification of factors that modulate tumor cell extravasation rate

Endothelial barrier function is correlated with TEM efficiency

Although progress has been made in identifying critical regulators of endothelial-tumor interactions in the context of intravasation[59,60] it remains unclear whether impaired barrier function is a necessary precursor to TEM in extravasation. Physiological conditions which affect vascular permeability include inflammation, which can play a mediating role in cancer progression and metastasis[61]. For instance, elevated levels of pro-inflammatory cytokines including IL-1B, TNF-α and IL-6 have been found in the circulation of cancer patients, and may upregulate the expression of adhesion molecules on the endothelium or in target organs[61]. Here, we investigated the response endothelial barrier function and tumor cell TEM rates to TNF-α. HUVECs were stimulated with 2, 5 or 10 ng/mL of TNF-α (R&D systems, MI), at 96 h after endothelial seeding, for 12 h. To ensure that the results observed were not due to the direct modulation of TNF-α on tumor cell migration, devices were washed and incubated in normal

media for 30 min prior to tumor cell seeding. Treatment of μVNs with 2 ng/mL TNF-α for 12 h resulted in a 2.1-fold increase in HUVEC permeability ((18.4 ± 1.1) $\times 10^{-7}$ cm/s compared to (8.68 ± 0.6) $\times 10^{-7}$ cm/s) to 70 kDa dextran, with no significant difference in cell viability. Stimulation with 10 ng/mL TNF-α led to a 4.6-fold increase in permeability ((41.5 ± 7.21) $\times 10^{-7}$ cm/s). The high standard deviation in the 10 ng/mL treatment was investigated; upon closer inspection, we observed what appeared to be focal leaks, and cell viability was found to be significantly lower compared to the control, indicating that such a high concentration of TNF-α led to endothelial cell-death induced ruptures in the lumen. Consistent with this, in TNF-α stimulated (2 ng/mL) HUVECs, tumor cell TEM rates increased 2.3-fold (32.3±5.1% compared to 13.1±2.12%) (**Figure 14**). The positive correlations observed between extravasation rates and vessel permeability have also been observed in *in vivo* rat tail-vein and transparent zebrafish[28] models subject to VEGF overexpressing tumor cells, which induced endothelial barrier disruption. Combined with our results, it is likely impaired endothelial function may enhance transendothelial migration dynamics.

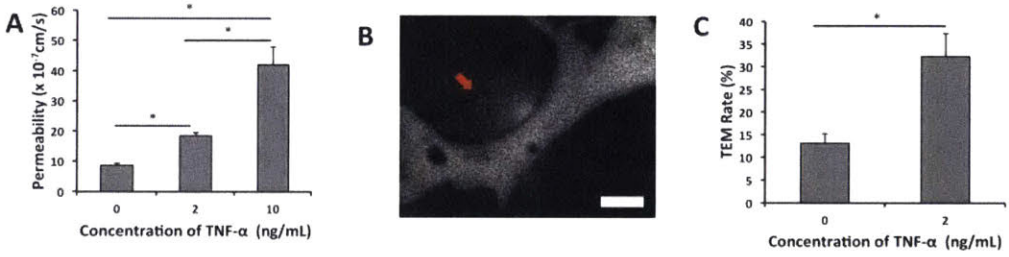

Figure 14. The effect of TNF-α on barrier function and TEM. (A) Graded response of vessel permeability to TNF-α perturbation. (B) High concentrations of TNF-α (10 ng/mL) results in cell-death induced ruptures and focal leaks (red arrow) seen by 70 kDa dextran (white). (C) Effect of TNF-α stimulation on TEM efficiency of MDA-MB-321. Data is represented as mean ± SD, with 9 total devices over 3 experiments for each condition. Statistical significance was tested with one-way ANOVA and Tukey's Test (*$p<0.05$). Scale bars are 20 μm.

Tumor cell metastatic potential correlates with extravasation capabilities

Although the metastatic potentials of different tumor cell lines are well characterized in various *in vivo* models[28,62] the dependence of extravasation efficiency on metastatic abilities remains unclear. Koop et al demonstrated similar extravasation kinetics of highly metastatic PAP2, non-metastatic NIH3T3 and primary fibroblast cells from mouse embryos, suggesting that extravasation is independent of metastatic potential in chick CAM models[38]. Contrarily, Stoletov et al showed a clear positive correlation between the metastatic potentials of different tumor cell lines and their extravasation abilities (HT1080>MDA-MB-231>MDA-MB-435) in an *in vivo* zebrafish model[28]. In our model with untreated HUVECs, we

tested several tumor cell lines with varying origins, and observed that the extravasation potential can be a function of tumor cell type, a behavior which may be interdependent with endothelial barrier function. Highly invasive breast cancer cell lines MDA-MB-231, SUM-159 or prostate PC-3 exhibited TEM rates of 25-35% 6 h after tumor cell seeding, while the non-metastatic normal epithelial cell line MCF-10A exhibited ~6% extravasation rate. In order to determine whether these differences could be due to the varying tumor tissue origins of the cell lines, we compared the extravasation rates of MDA-MB-231 versus LM2 (the highly metastatic variant of adenosarcoma MDA-MB-231), and A-375 versus MA2 (highly metastatic variant of melanoma A-375). In both cases, highly metastatic variants of the same cell line resulted in significantly higher transmigration rates (**Figure 15**). These results indicate that human tumor cells exhibiting different tumor origins or metastatic potentials exit the vascular system with different efficiencies and that our platform possesses the sensitivity to detect such variations.

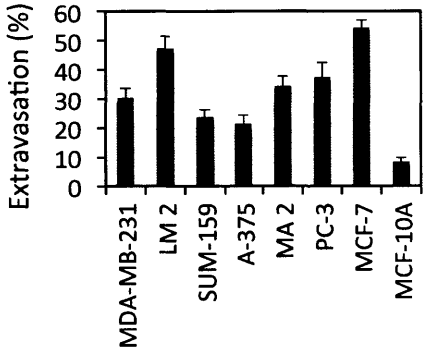

Figure 15. Examples of extravasation efficiencies of a panel of tumor cell lines with varying extravasation potentials at 6 hours post-injection into in vitro microvascular networks.

Different tumor cell subpopulations within the same device exhibit different TEM capabilities

We are able to observe arrested cells on the endothelium that are either mechanically trapped, or adhered and non-trapped. Non-trapped cells remained adhered onto the luminal side of the endothelium in vessels with diameters larger than that of the tumor cell, even after vessel perfusion. This suggests the presence of purely adhesive interactions with the endothelium in contrast to cells lodged mechanically in narrow constrictions. Analysis of each subpopulation revealed that trapped cells exhibited a significantly higher rate of TEM (47.8±4.67%) compared to arrested non-trapped cells (9.8±3.3%) (**Figure 16 A-C**). This may be attributed to the fact that lodged cells have access to more adhesion sites on the endothelium, as the area of TC-EC contact is greater.

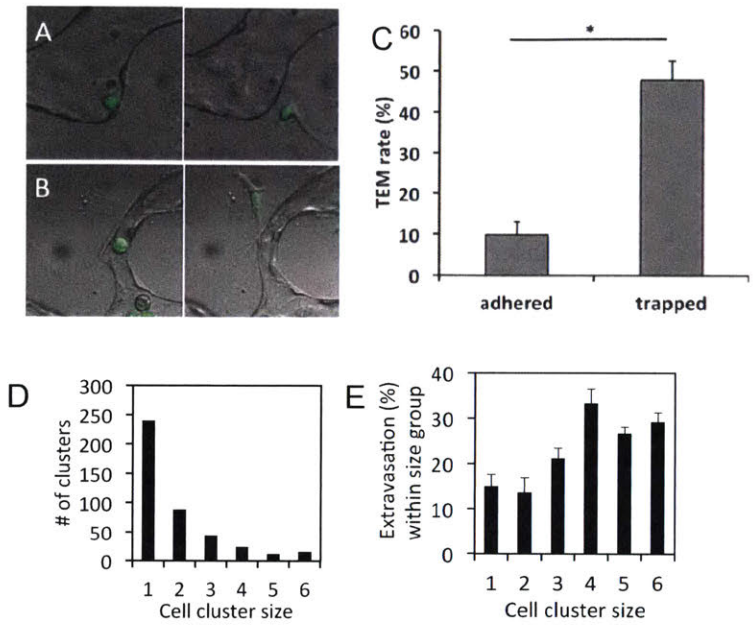

Figure 16. TEM efficiencies of different tumor cell subpopulations. (A) Non-trapped adhered tumor cell at 30 min and 4 h after seeding. (B) Entrapped tumor cell at 30 min and 4 h after seeding. (C) TEM efficiency of adhered non-trapped and trapped subpopulations. (D) Frequency of various tumor cluster sizes found lodged in microvascular networks (over 5 devices). (E) Extravasation efficiencies of tumor cells within each cluster size subpopulation. Data are represented as mean ± SD, with 9 total devices over 3 independent experiments for each condition. Statistical significance was tested with one-way ANOVA and Tukey's Test (*$p<0.001$). All scale bars are 20 μm.

Tumor cell clusters are of particular interest because it has been suggested that CTCs that travel in clusters exhibit a higher survival rate, either from shear stress protection, and/or localized increase concentration of secreted factors that facilitate TEM. Using our assay, we are able to visualize TEM events of both single tumor cells and a heterogeneous distribution of tumor cell clusters ranging from 2-6 tumor cells (**Figure 16 D-E**). Interestingly, we find that an increase in tumor cell cluster size roughly correlates with an increase in the percentage of cells extravasated in the same subpopulation. This may be attributed to several mechanisms including, but not limited to (1) an increase in the local concentration of tumor-secreted biochemical factors that regulate endothelial permeability, (2) access to the subendothelial matrix provided by a previously transmigrated cell, and (3) the inability to repair the endothelial damage before the transmigration of another tumor cell in the cluster. In particular, tumor paracrine factors can contribute to increased TEM efficiency via the modulation of endothelial permeability, such as impairment of the endothelial barrier function by tumor secreted VEGF[60]. Together, our data suggests that

beyond "macro scale" properties such as tumor cell metastatic potential and endothelial barrier function which can be modulated between independent devices, there exists heterogeneities in extravasation potentials even within the same condition, depending on physical and spatial parameters such method of arrest and separation distances between tumor cells themselves.

2.6 Advantages and limitations of on-chip microvasculature extravasation assay

The key advantageous features of this device can be summarized as follows: **(1)** Arrest of tumor cells and extravasation from small diameter (ranging from 8-70 micron) vessels represents greater physiological relevance than conventional monolayer based assays. **(2)** Human cells (endothelial, tumor, stromal, immune) can be exclusively used in this model, decreasing the uncertainty of "species incompatibility." **(3)** Tumor cells interact and invade past a HUVEC -deposited basement membrane and into 3D ECM, all of which can be visualized in considerable detail via standard immunofluorescent techniques. **(4)** Extravasated or mid-extravasating cells are clearly distinct from intravascular cells and extravasation efficiency can be evaluated at lower power magnifications (20X), enabling both greater speed of data acquisition and robustness of extravasation scoring. **(5)** Regions of interest with tumor cells are easily identified due to the fact that the μVN lie largely in the same plane of focus. **(6)** This feature also enables tumor/endothelial cell morphological dynamics to be resolved with relatively high spatiotemporal resolution and throughput (~30 cells per time-lapse at 30X-60X, taken at 10 minutes intervals) due to the applicability of high magnification objectives (which have shorter working distances). This provides novel metrics on extravasation kinetics such as protrusion initiation rate and speed of complete transmigration. **(7)** The technical expertise required to form microvascular networks is low compared to techniques such as pin pull-out, sacrificial gels or 3D scaffold printing techniques. **(8)** Tumor cell injection into μVNs only requires basic pipetting maneuvers instead of acquired animal intravenous injection skills. **(9)** The material cost of each device is low (<$0.40 per device) compared to most *in vivo* alternatives, and is easily fabricated via standard soft lithography techniques that are now prevalent amongst most bioengineering laboratories. **(10)** Required reagent volumes and cell numbers can be orders of magnitude lower than most other extravasation assays (< 4000 tumor cells/device and <80 μL of media/device) due to miniaturized features and low dead volume, greatly reducing costs associated with expensive or rare cells (e.g. CTCs), drugs, or antibodies.

One of the limitations is the general inability of *in vitro* systems to fully recapitulate the *in vivo* scenario. In reality, the early metastatic seeding and extravasation microenvironment is characterized by a range of host cells and factors such as platelets and leukocytes, with which tumor cells have been found to

interact during transit *in vivo* [42,63,64]. However, the devices are flexible enough to accommodate increased complexity of the microenvironment in order to achieve greater realism. For instance, tumor-immune cell interactions can be studied via isolation of platelets or leukocytes from whole human blood followed by perfusion in conjunction with tumor cells, which we demonstrate in Chapter 4. In fact, the reductionist nature of such an *in vitro* system can be highly beneficial when one is required to parse out specific interactions independent of the effect of other cell types; this would be more difficult *in vivo* as it requires either complete ablation or loss of function of endogenous cells. Another limitation is that while soft lithography techniques are widespread amongst bioengineering labs, there are fewer biology/cancer research labs that preform soft lithography on a routine basis. However, protocols of PDMS-based device fabrication are now well established and robust, and only require several pieces of easily accessible equipment such as a degasser, 80°C oven and plasma etcher. The photo-mask of the device design is accessible through this article (Supplementary Materials) and fabrication of molds can be easily outsourced to specialized SU-8 fabrication companies (e.g. FlowGEM, etc.) if in-house fabrication is not available.

2.7 Conclusions

We have presented a microfluidic extravasation assay consisting of self-organized perfusable 3D vasculature that allows for the study of tumor extravasation from within *in vitro* μVNs. We demonstrate the effect of inflammatory cytokine stimulation on endothelial barrier function and TEM efficiency, and the positive correlation between metastatic potentials of different cell lines and their extravasation capabilities. We characterize the morphological dynamics of tumor cell and endotheliail cells during extravasation in high spatiotemporal resolution from within *in vitro* μVNs, and observe the TEM patterns of different tumor cell subpopulations, including mechanically trapped tumor cells, single adhered cells and tumor clusters. The ability to enable high-throughput parametric studies in a tightly controlled environment coupled with increased physiological relevance compared to 2D and 3D planar monolayer models will give rise to new insights regarding the complex endothelial-tumor cell interactions in extravasation and facilitate the identification of factors to target this crucial step in cancer metastasis.

Chapter 3

Dynamic roles of tumor integrins in tumor-endothelial-ECM interactions during extravasation*

3.1 Introduction

Tumor cell extravasation is thought to be a complex series of cell-cell and cell-matrix interactions is thought to involve integrins, the family of heterodimeric transmembrane receptors that mediate cellular interactions with the extracellular matrix (ECM). Integrins are widely known to regulate a variety of tumor cell functions including adhesion, migration, invasion, proliferation and survival [41]. In particular, the β1 subunit forms heterodimers with at least 18 different alpha subunits, and has been shown to bind via its extracellular domain to a substantial number of ECM proteins, and via its intracellular domain to recruit many signaling and cytoskeletal proteins [65]. In the context of cancer, β1 is up-regulated in highly invasive breast carcinoma cells *in vivo* [66,67], and plays crucial roles in the context of primary tumor formation and metastasis in breast, ovarian, pancreas and skin cancers [10,68-81]. Further *in vitro* studies report that β1 strongly mediates adhesion of pancreatic and ovarian cancer cells to matrix proteins including collagen 1, collagen IV, fibronectin and laminin on 2D substrates [10,82], and promotes the degradation of gelatin at the whole cell level and localizes at invadopodia [83]. In addition to its effects on adhesion, knockdown of β1 inhibits cell migration and proliferation on numerous ECM substrates [10,84]. Collectively, these studies suggest the importance of β1 in mediating growth and migration in the primary tumor stroma.

The precise roles of β1 during tumor cell extravasation, however, are less explored. Although the molecular players in extravasation (e.g. ECM molecules, endothelium) are likely similar to those in invasion and intravasation, the mechanics and sequence of the cell-cell and cell-matrix interactions are different. Furthermore, the roles and degree of requirement of specific adhesion molecules may differ

*Sections of this chapter have been published previously. See Reference 26.

depending on the context of the migration event. Thus, results obtained in these contexts may not directly translate to extravasation. In terms of metastasis, it has been shown that inhibition of β1 significantly reduces seeding and formation of metastatic foci after several weeks, suggesting a possible defect in a preceding step of the metastatic cascade, such as extravasation [10,70,78,80,85,86]. However, except for a study by Stoletov et al, which demonstrated the necessity of β1 for TEM in a zebrafish model, to our knowledge no other groups have explored in depth the role of β1 and the associated alpha subunits in distinct steps of extravasation.[28] Furthermore, it remains unclear whether the defects lie in adhesion, tumor-endothelial interactions, ECM/BM interactions or even post-extravasation proliferation and survival. This is often difficult to dissect due to relatively low throughput and low spatio-temporal resolution of single cell TEM events in most *in vivo* assays.

In this Chapter, we employ the microfluidic vasculature model developed in Chapter 2 to probe the role of integrins during extravasation. We demonstrate that, with the help of other conventional in vitro methods, we can successfully isolate and recapitulate the sequential steps in the extravasation cascade. Much is currently known about the cell adhesion molecules and proteases required by cancer cells to invade their microenvironment, but whether these same players are required for tumor cell extravasation are unclear. First, we find that β1 expression in human tumor cells lines is necessary for efficient TEM in an *in vitro* model of human microvasculature. High-resolution imaging further reveals the requirement of activated β1 integrin for protrusion maintenance via engagement with the sub endothelial ECM, which enables recruitment of F-actin to the protrusion tip, followed by translocation of the cell past the endothelial layer, likely via acto-myosin contractility. Specifically, adhesion onto vascular laminin via α3β1 and α6β1 integrins is involved in this process. Additionally, after clearing the endothelial barrier, β1 is required for invasion past the BM. Finally, we show that β1 depletion reduces extravasation *in vivo* and inhibits metastatic colonization, suggesting that the cumulative defects in the extravasation cascade due to β1 depletion ultimately impairs metastasis formation.

3.2 Methods for investigating the role of beta-1 integrin during extravasation

Cell culture

GFP or RFP expressing human umbilical vein endothelial cells (HUVECs) (Angioprotemie) were cultured in EGM-2MV medium (Lonza) and used at passage 4. Normal human lung fibroblasts (NHLF) (Lonza) were cultured in complete FGM (Lonza) and used between passages 4 to 8. MDA-MB-231, A-375 MA2 and 4T1 cells (parental, control and stable knockdowns) were cultured in DMEM supplemented with 10% FBS and 1% penicillin/streptomycin and 1% L-glutamate while SUM159 cells were cultured in

Ham F12 supplemented with 5% FBS, 1% penicillin/streptomycin, 5 μg/ml insulin, 1 μg/ml Hydrocortisone, and 20ng/ml EGF. All cells were incubated at 5% CO_2 at 37°C.

DNA constructs, RNA interference and transfection

To generate miR30-based shRNAs targeting human and mouse integrins, 97-bp shRNAs were designed (Supplemental Table 1), synthesized (IDT, Coralville, Iowa) and PCR amplified to add XhoI and EcoRI sites. shRNAs were then cloned into barcoded versions of the MSCV-ZSG-2A-Puro-miR30 vector [87] using standard molecular biology techniques. Packaging of retrovirus and transduction of cells was done as described previously [88]. Efficient knockdown was then confirmed using western blotting, qPCR or flow cytometry as described below. Antibodies for immunoblots include integrin β1 (MEM 101-A, Abcam), β3 (Cell Signaling), GAPDH (Cell Signaling) and beta-actin (Millipore). For mouse cell lines, rabbit polyclonal anti-mouse integrin α3, anti-mouse integrin αV (BD Pharmigen), and mouse anti-GAPDH (Millipore) were used. Quantitative PCR (qPCR) was performed for integrin β1 as described previously [87] using the MyiQ real-time PCR detection system (Bio-Rad). Flow cytometry was performed using the following primary antibodies: biotin conjugated anti-human β1 integrin (P5D1, Abcam), biotin-conjugated anti-mouse integrins αV, β1, β2, β3 (BD Pharmigen), or unconjugated rat anti-mouse integrin α1, α2, α4, α6, α8, β4 (BD Pharmigen). Secondary antibodies were either Streptavidin-APC, or APC-conjugated anti-Rat IgG.

For siRNA-mediated knockdown of α3, α6 and β4 integrins, cells were plated on six well plates and transfected with 25 pmol of α3, α6 or β4 integrin Silencer Select siRNA (Thermo Fischer) using Lipofectamine RNAiMax reagent (treated twice over 48 h) before trypsinization and perfusion into microvascular networks. Knockdown was confirmed via western blotting using antibodies for α3 (Thermo Scientific), α6 (Cell Signaling) and β4 (Cell Signaling). For visualization F-actin in transmigrating tumor cells, MDA-MB-231 were transduced with LifeAct mCherry (Ibidi) via standard lentiviral techniques.

Blocking of integrins, MMPs and ECM protein binding

For functional blocking of individual alpha subunits, azide-free antibodies for α1 (FB12), α2 (P1E6), α3 (P1B5), α4 (P4C2), α5 (P1D6), β4 (ASC-6), β1 (P4C10) and associated IgG_1 or IgG_3 controls from Millipore, and α6 (GoH3) and IgG_{2a} from Santa Cruz were incubated at 5ug/mL with tumor cells suspended in serum free DMEM at 0.5 million cells/mL for 30 min, prior to perfusion into microvascular devices. For neutralization of MMPs, anti-MT1-MMP catalytic domain (LEM-2/63.1, Abcam) and anti-MMP-9 (IM09-L, Calbiochem) were incubated at 15 μg/mL with tumor cells suspended in serum free

DMEM at 0.5 million cells/mL for 30 min prior to perfusion. To block laminin function, anti-laminin alpha 3 chain (P3H9-2, R&D Systems) or IgG_1 at 10 μg/mL in EGM was perfused into the microvascular devices 10 minutes prior to tumor perfusion.

Immunofluorescence and imaging analysis

Devices were fixed and immunostained as previously described[89]. Primary antibodies used include human CD31, vinculin at 1:100 (Sigma Aldrich), Tks-5 at 1:50 (Santa Cruz), human collagen IV, laminin, fibronectin, or β1 integrin activated conformation (clone 12G10) at 1:100 (from Abcam). Lungs were processed and stained as previously described [27]. Briefly, lobes were cut into smaller pieces and blocked for 1 h (10% goat serum and 0.3% Triton-X), followed by incubation in mouse anti-CD 31 (BD Biosciences) at 1:100 overnight at 4°C. Lungs were washed in wash buffer and incubated in secondary antibody (Alexa Fluor 568 goat anti-rat, Invitrogen) at 1:500 overnight at 4°C.

Microfluidics-based vertical endothelial monolayer extravasation assay

In some experiments, a microfluidic device featuring an endothelial monolayer is used instead of the microvascular network assay presented in Chapter 2. Using the exact same PDMS device, a single lumen is modeled by forming a confluent monolayer on the hydrogel and micro-post surfaces (SI Fig. 1A), as described previously[21]. Tumor cells at 0.1 million cells/mL were perfused into one media channel and tilted at a 90-degree angle at 37°C for 30 min in a humidified chamber, and transferred to a confocal microscope (Olympus FV1000) for observation.

Adhesion assay

To test the degree of tumor-endothelial adhesion without the added factor of physical trapping, rectangular PDMS micro-channels were fabricated (0.3 cm wide by 110 μm high by 5 cm long). Three inlet holes were punched (two on both ends and one in the middle). HUVECs (2 million cells/mL) were seeded into micro-channels. At the formation of a confluent monolayer, tumor cells at 1 million cells/mL in serum-free endothelial basal medium (EBM) were perfused from the outer inlet port (while keeping the center port plugged) and allowed to settle and adhere 10, 30 or 60 min. EBM is then perfused into the middle port via a syringe pump to obtain a shear rate of 5 dynes/cm^2 for 15 min, after which tumor cells are recounted.

In vivo mouse extravasation assay

One hundred microliters of cell suspension in PBS (0.5 million cells) were injected via lateral tail vein of female NOD/SCID/gamma mice. Mice were euthanized and lungs were collected after inflation with 4% formaldehyde, 0.3% Triton X-100 at 3, 16 and 24 h.

In vivo metastasis assay

miR-30 based shRNAs targeting each integrin subunit were designed and cloned into uniquely barcoded versions of the MSCV-ZSG-2A-Puro-miR30 vector [87] as described above, and then used to stably transduce 4T1 cells. Once integrin knockdown was confirmed via FACs, individual 4T1 cell populations were mixed in equal numbers and injected into the lateral tail veins of mice. Lungs were isolated for analysis after 17 days. A starting population was also collected at the time the mixed cell populations were injected and was used for normalization of subsequent samples. Luminex-based analysis of metastasis burden was performed as described previously[87].

Quantification of extravasation and statistics

In all *in vitro* experiments (unless otherwise indicated), the average TEM efficiency is the average of the mean of 3 devices per condition and 3 independent experiments (total 9 devices). "Extravasated" cells are scored as ones that have completely cleared the endothelial barrier. The value of each device was calculated as an average of 6 fields of view (microvascular networks) or 10 fields of view (monolayer device). Statistical analysis was performed with SigmaPlot using Student's two-tailed *t*-test when comparing two conditions, or ANOVA with Tukey's post-hoc analysis when applicable. Unless otherwise indicated, "n" represents one independent experiment with at least 3 devices per condition.

3.3 β1 integrins are required for efficient transendothelial migration from *in vitro* microvascular networks and *in vivo* mouse lung extravasation assays

We stably expressed shRNAs targeting either control firefly luciferase (control) or integrin β1 (*β1KD)* in human metastatic human breast cancer (MDA-MB-231, SUM-159), highly metastatic human melanoma (A-375 MA2) and mouse mammary carcinoma (4T1) cell lines (**Figure 17** B). Cells were perfused into *in vitro* microvascular networks and TEM events were tracked via live confocal microscopy. Reduction of β1 via shRNA and blocking antibodies in MDA-MB-231 significantly abrogated TEM in microdevices at 6 h, while knockdown of β3 integrin had no significant effects, indicating that the observed attenuation of TEM may be specific to β1 (**Fig 17 C**). The β1-4 shRNA, with

an intermediate level of knockdown (66% mRNA inhibition), exhibited an intermediate TEM rate at 6 h, suggesting a graded response with decreasing β1 expression. Longer-term kinetics of transmigration were tested in all cell lines revealing that the decrease in TEM is likely not cell line specific. Furthermore, TEM rates reach a plateau at ~ 12 h in all conditions (**Figure 17 E**), indicating that the defects in transmigration are not simply due to a delay in the progression of extravasation. Additionally, proliferation assays reveal no significant differences between control and β1KD cells in the span of 48 h, thus the number of TEM events is likely not influenced by differences in cell proliferation throughout the duration of the assay.

To validate our findings in an *in vivo* context, MDA-MB-231 control and β1KD cells were injected into Nod/Scid/gamma mice via the lateral tail vein. Close inspection via confocal microscopy and 3D rendering at 60X allowed visualization of individual tumor cells near the tissue surface (**Figure 17 F**). Tumor cells surrounded by a continuous and distinct border of CD31 staining were scored as intravascular, while all other cells were counted as transmigrated, even if partly surrounded by vascular staining. Both control and β1KD cells were mainly contained within blood vessels at 3 h post injection. At 16 h there was a significant (~5 fold) difference in the number of transmigrated control cells versus β1KD, with the difference increasing at 24 h (**Figure 17 G**).

Combined, these results confirm that tumor integrin β1 is essential for TEM. However, the role of β1 in other distinct steps of extravasation both preceding and subsequent to TEM remains unclear. These steps include tumor-endothelial adhesion, tumor cell protrusion initiation and formation into the sub-endothelial matrix, interaction with the endothelial BM, and migration through the parenchyma. Due to the challenges associated high resolution and dynamic imaging *in vivo,* we capitalized on the unique capabilities of our *in vitro* microvasculature assay.

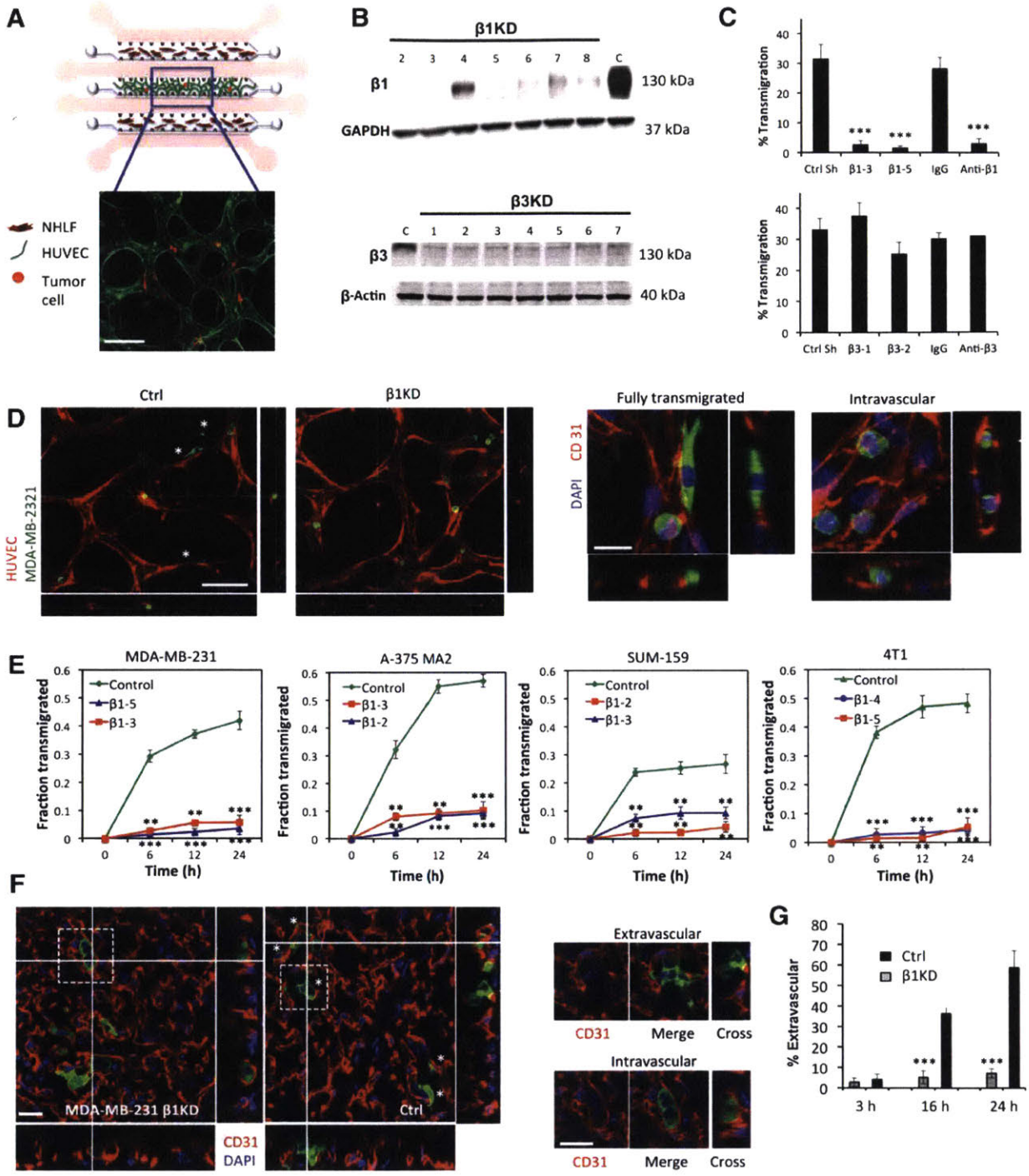

Figure 17. Knockdown of β 1 integrin inhibits tumor-cell transendothelial migration in *in vitro* microvascular networks and *in vivo* extravasation assays. **(A)** Schematic of device presented in Chapter 2. Representative fluorescence image of a single field of view of the device at 20X (HUVEC LifeAct; green, MDA-MB 231; red, scale bar = 100 μm). **(B)** Western blot of β 1 and β 3 integrin expression after suppression via shRNA (C=control shRNA targeting firefly luciferase). **(C)** Effect of β 1 and β 3 knockdowns and integrin function-blocking antibodies on the TEM efficiency of MDA-MB 231 in *in vitro* microvascular

networks at 6 hours (***p<0.001). **(D)** Representative field of views (20X) of live microvascular networks at 12 hr after seeding of control or β 1 KD MDA-MB-231 cells (HUVEC; red, MDA-MB 231; green). Asterisks indicate fully transmigrated cells (scale bar = 100 μm). Immunostaining for CD31 show distinctions between transmigrated and non-transmigrated cells (scale bar = 20 μm). **(E)** Differences in kinetics of TEM between β 1 KD and control shRNA cells were assessed for MDA-MB-231, A375 MA2, SUM-159 and 4T1 cells lines. Fraction transmigrated in human microvascular network devices is determined at the same field of view for time points of 0, 6, 12 and 24 hr (n=3, **p<0.01, ***p<0.001, bars represent mean +/- SEM). **(F)** Immunostaining for CD31 (red) in mouse lungs 24 hours after injection of 0.5 million MDA-MB 231 control or β 1 KD cells (green). Asterisks indicate cells scored as transmigrated (scale bars = 20 μm). Cells in white dotted boxes are zoomed in to indicate examples of intravascular and extravascular cells. **(G)** Percentage of transmigrated control and β 1 KD MDA-MB 231 cells in mice lungs 3hr, 16 hr and 24 hr after tail vein injection (n=8 mice per condition at 3 hr and 24 hr, 4 mice per condition at 16 hr, 100 randomly selected tumor cells analyzed per mouse) (**p<0.001, bars represent mean +/- SEM).

3.4 β1 integrin does not mediate adhesion to endothelium but adhesion to sub-endothelial matrix, under flow conditions

We further investigated whether β1 integrin plays a role in heterotypic endothelial-tumor adhesion, a possible precursor to TEM. It is believed that since tumor cells that are rapidly cleared from the circulation *in vivo*, cells that quickly arrest in the vasculature and extravasate may have a selective advantage toward establishing new colonies [30,86].

To isolate the effect of adhesion, tumor cells were seeded into endothelial-lined chambers and allowed to settle and adhere for 10, 30 or 60 min. This is followed by continuous perfusion of media for 15 min at 5 dynes/cm^2. With 30 or 60 min of settling time, more control cells remained adherent than β1KD cells post-perfusion, with the greatest difference being at 60 min (**Figure 18B**). In contrast, 10 min of settling time resulted in no significant differences. Upon closer inspection, more than half of all adherent cells in 30 or 60 min control samples had gained access to the subendothelial ECM, as identified by short (1-4 μm) tumor cell protrusions extending past the plane of the endothelium (**Figure 18A**). In contrast, the few adherent β1KD cells did not exhibit protrusions. This suggests that β1 mediates adhesion to the underlying matrix, rather than the endothelium, thereby providing the force necessary to resist detachment under flow. We also note that adherent cells at the 10 min time point do not exhibit discernable protrusions, suggesting that early tumor-endothelial adhesion exists, but is likely mediated by other adhesion molecules such as selectins (CD62) or glycoproteins like CD44[12], rather than integrins.

In vivo, we observed similar numbers of control and β1KD cells in lungs at early time points (3 and 16 h post-injection) and only a slight difference at 24 h (**Figure 18C**). This lack of β1 dependence

compared to *in vitro* findings could be due to a tendency for physical trapping to dominate over adherence in vivo, since narrow capillaries are not recapitulated in the *in vitro* flow channel. That is, while we find that β1 can mediate adhesion under flow due to subendothelial matrix anchorage, physical trapping of cells may be the rate-controlling factor in retention *in vivo*.

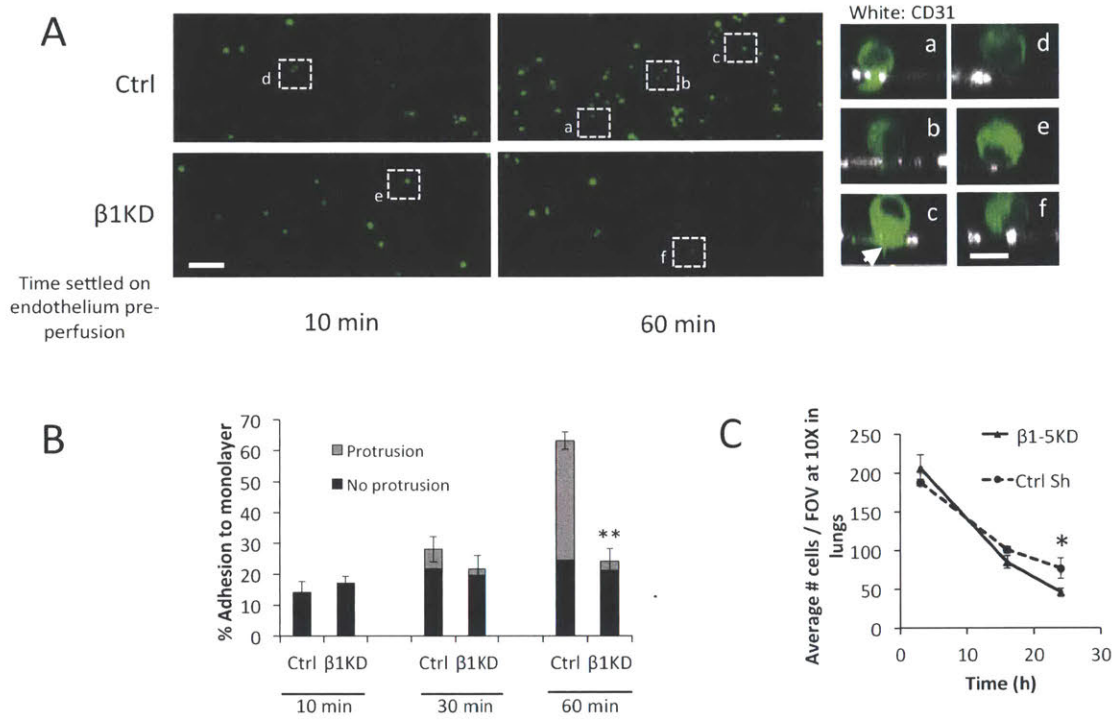

Figure 18. Analysis of adhesion rate in an endothelial monolayer microfluidic flow assay. (A) Confocal imaging of remaining adhered control or β1KD MDA-MB-231 on a confluent endothelium after 15 minutes of flow (0.5 dynes/cm^2 shear stress, scale bar=100 μm). Cells were allowed to settle on the endothelium for 10, 30 or 60 min prior to perfusion. Confocal stacks of individual tumor cells (in white dotted boxes) relative to the endothelium are shown (CD31: white, scale bar=10 μm). **(B)** Quantification of the percentage of adhered control or β1KD MDA-MB-231 and the percentage of adhered cells which have formed protrusions across the endothelium into the subendothelial matrix, after 10, 30 or 60 min of tumor cell settling. **(C)** Numbers of tumor cells in the lung of mice at 3 hr, 16 hr and 24 hr after tail-vein injection of control or β1 KD MDA-MB-231 cells in NOD/SCID/γ mice. Each point represents the mean +/- SEM of cells/field of view (FOV) (10X) (n=7 mice per condition) (*p<0.05).

3.5 Activated β1 and actin-rich protrusion formation precede and are required for complete transmigration

Previously, it has been suggested that tumor cells form invadopodia-type processes past the endothelium[36,90] and that abrogating these structures prevents extravasation in chick chorioallantoic membrane assays (CAM)[36]. Thus, we sought to understand the role of β1 in protrusion formation and

endothelial barrier breaching. We employ an alternate "vertical monolayer device" consisting of microchannels connected by 3D ECM hydrogels, where tumor cells are seeded in one channel, arrest onto and extravasate across an endothelial monolayer into a fibrin-type 1 collagen matrix [21,46]. In this assay, migration across and through the monolayer and subendothelial matrix occurs in the plane of view; thus, protrusion formation and dynamics during extravasation can be observed in high detail. Time-lapse confocal images taken over 6 h reveal that transmigrating control cells extend numerous thin filipodial-like protrusions past a gap in the endothelial barrier as early as 20 min post-perfusion (**Figure 19A**). In contrast, β1KD cells remained largely spherical and lacked protrusions in nearly all cells sampled (**Figure 19B**). Surprisingly, while β1KD tumor cells do not transmigrate, there is still discernable endothelial gap formation at the site of tumor arrest, suggesting that β1 does not significantly hinder the ability for endothelial disruption.

Immunostaining for the active conformation of β1 showed localized punctates at the tips of the protrusions extending into the sub-endothelial matrix in transmigrating control cells only (**Figure 19C**), suggesting that β1 mediated protrusion formation and ECM engagement is required for complete TEM. Dynamic tracking of tumor cell protrusions embedded in 3D collagen 1-fibrin mixed matrices reveal that control cells quickly extend protrusions that often persist (>30 min), and subsequently take on an elongated morphology. In contrast, β1KD cells exhibit small, short-lived transient protrusions and typically retain a more spherical shape. Thus, it is likely that β1 is not required for protrusion initiation, but for protrusion stabilization via β1 mediated anchorage onto vascular BM, which is supported by previous findings, in a 2D context[83]. Furthermore, live imaging of tumor F-actin during TEM reveals actin-rich punctates at the tips of protrusions extending past the endothelium (**Figure 19D**). At times, these actin-rich protrusions are also diffusely marked by the focal adhesion protein vinculin (**Figure 19E**), which is generally diffuse in tumor cells embedded in 3D collagen gels (data not shown). There has recently been growing evidence that integrins play important roles in invadopodia formation and function, in particular $\alpha v\beta 3$ and β1 integrins; however, whether invadopodia form during extravasation is unclear. Indeed, immunofluorescent imaging showed Tks5 punctates specifically in protrusions, suggesting the presence of functional and degradatory invadopodia during TEM (**Figure 19F**). Together our results suggest that β1 mediates tumor cell protrusion stabilization by facilitating anchorage vascular BM, followed by recruitment of actin and possibly focal adhesion proteins, at the protruding-edge. Subsequent actomyosin-mediated contractions then likely pull the remaining cell body past the endothelium.

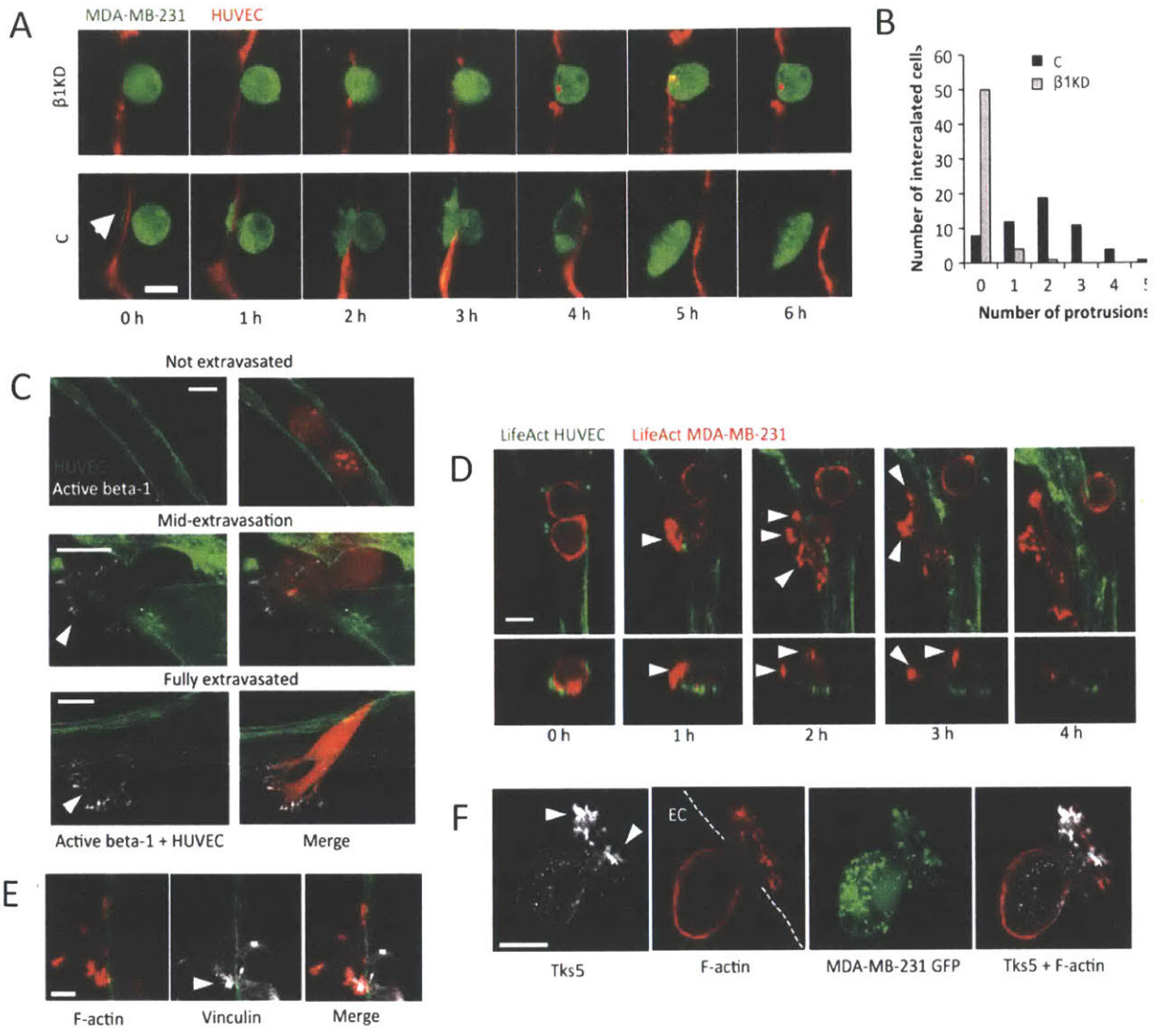

Figure 19. (A) Time-lapse confocal microscopy of representative transmigrating control and β 1-5 KD cells (single plane) over a period of 6 hours (HUVEC cell tracker; red, MDA-MB 231; green, scale bar=15 μm). Arrow indicates the formation of initial protrusions into the subendothelial matrix in control cells. **(C)** Differences between control and β 1-5 KD cells in the frequency of protrusion formation in single cells during TEM at 3 hours (55 intercalated cells over 3 devices per condition were chosen randomly and scored). Protrusion number (that was definable at 30X magnification) was quantified via 3D reconstructions of single transmigrating cells. **(D)** Immunostaining with an antibody against the activated conformation of β 1 integrin (clone 12G10, white) in microvascular networks (green) (scale bar = 10 μm). Arrows indicate localization at protrusion tips. **(E)** Time-lapse imaging depicting spatial organization of tumor F-actin (red) during TEM in microvascular network devices. Arrows indicates areas in protrusions where F-actin appears as punctates (scale bar = 10 μm). **(F-G)** Immunostaining of vinculin and Tks-5 in tumor cells during mid-transmigration past the endothelium. Arrows indicate localization of indicated proteins at the protrusion tips (scale bars = 10 μm).

3.6 β1 integrins mediate invasion across the basement membrane

Upon closer inspection of fixed images in both microvascular network and monolayer assays, fully transmigrated cells were observed in 3 distinct "positions" relative to the endothelium: (1) directly adjacent to the abluminal surface, (2) adjacent but elongated perpendicular to the lumen, and (3) migrated away from the abluminal surface. At 4 h control cells were found in all three positions while of the few (<6%) β1KD cells that had transmigrated, almost all were exclusively confined to "position 1" (**Figure 20A**). Not only were transmigration distances significantly reduced in knockdown cells, few protrusions were observed, consistent with their rounded and non-protrusive morphology (**Figure 20B**).

Since β1KDs are unable to migrate away from the endothelium, we hypothesized that tumor cells were unable to invade past the endothelium BM, due to the inability to attach to and/or degrade it. During the formation of microvasculature, endothelial cells forming the *in vitro* microvessels deposit a continuous layer of BM proteins including collagen IV, laminin and fibronectin similar to *in vivo* vasculature (see Chapter 2). Staining for laminin revealed tumor cells in four "states" relative to the BM and endothelium: (1) breaching the endothelium but not the BM, (2) fully transmigrated but intercalated between the endothelium and BM, (3) breaching the BM, and (4) completely cleared of endothelium and BM (**Figure 20C**). At 2 h, out of the subpopulation of transendothelial migrating cells, both control and β1KD cells were mostly found in state (1). Subsequently, at 9 h, most transmigrating control cells were in states (3) and (4), breaching both the endothelium and laminin (**Figure 20D**). This suggests that the formation of stable protrusions requires sequentially adhesive interactions with the underlying BM, followed by degradation and invasion past it. Conversely, nearly all transmigrating β1KD cells remained in state (1).

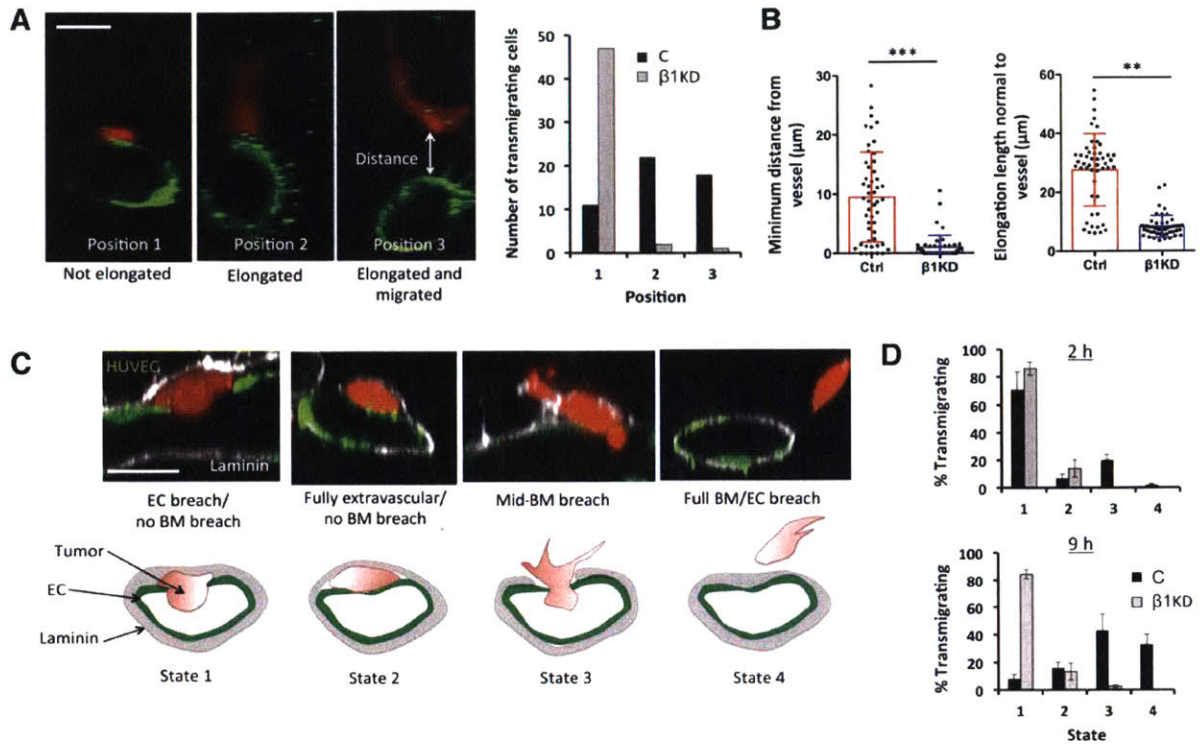

Figure 20. β 1 integrins mediate invasion past the basement membrane. **(A)** Representative cross sections of lumens in microvascular devices (scale bars = 10 μm) depicting the 3 distinct states in which a transmigrated tumor cell can be found relative to the endothelium after 6 hours (Position 1: directly adjacent to abluminal surface, Position 2: adjacent and elongated normal to vessel wall, Position 3: migrated away from the endothelium) (scale bars = 10 μm). Quantification of the number of fully transmigrated β 1KD or control cells found in each "state" (50 cells analyzed per condition). **(B)** Quantification of the migration distance of extravasated tumor cells away from the endothelium. Distance is defined as the shortest length between the endothelium (at the point where transmigration occurred) and the nearest point on the transmigrated tumor cell body. Elongation length of the same transmigrated tumor cells is defined as the maximum length of the cell normal (perpendicular) to the vessel wall at the point of transmigration (n=50 transmigrated cells per condition, ***p<0.001, bars represent mean +/- standard deviation). **(C)** Representative immunofluorescence staining depicting the possible position of transmigrated tumor cells relative to the sub-endothelial laminin layer (LN: white, HUVEC LifeAct: green, MDA-MB 231: red, scale bars=10 μm). State 1: breached ECs but not laminin, State 2: fully transmigrated but no breaching of laminin, State 3: simultaneously breaching EC and laminin layer, State 4: fully breached EC and laminin layers. **(D)** Percentage of total fully transmigrated control or total β 1-5 KD cells that are found in states 1 to 4 relative to the laminin layer (n=2 experiments, 4 devices per condition).

Due to the inability of β1KD cells to invade past the BM, we hypothesized that MMPs are required to digest BM proteins, and that β1KD cells may exhibit a defect in MMP activity. We tested the effect of anti-MT1-MMP and anti-MMP-9 (two major MMPs implicated in BM degradation) on TEM efficiency in microvascular networks at 6 h. Both anti-MT1-MMP and anti-MMP-9 slightly reduce TEM efficiency ($p=0.046$ and $p=0.089$, respectively) (although not comparable to knocking down β1 integrins) suggesting that initial crossing of the EC barrier is only weakly dependent on these proteases (**Figure 21**). Further immunostaining for laminin on the same devices revealed that transmigrating cells treated with either anti-MT1-MMP or anti-MMP-9 were both less likely to breach the laminin layer upon exiting the endothelium ($p=0.026$ and $p=0.008$, respectively). Together, this suggests that MT1-MMP and MMP-9 are involved in matrix degradation once the cell has transmigrated, while playing a smaller role in the initial crossing of the endothelium. However, when MMP secretion levels were tested via an MMP antibody array, no discernable differences were found between β1KD and control shRNA MDA-MB-231 in secreted levels of MMP-1, 2, 3, 8, 9, 10 and TIMP-1, 2, and 4. Further testing of MMP-9 and MMP-2 levels via zymography also revealed no differences (data not shown). Despite these results, we cannot completely rule out the possibility of β1KD-induced defects in MMP localization and/or activation in the specific context of TEM, since conventional conditioned medium collection techniques (cells mono-cultured on a 2-D culture dish) do not recapitulate the specific context of TEM and MMP localization.

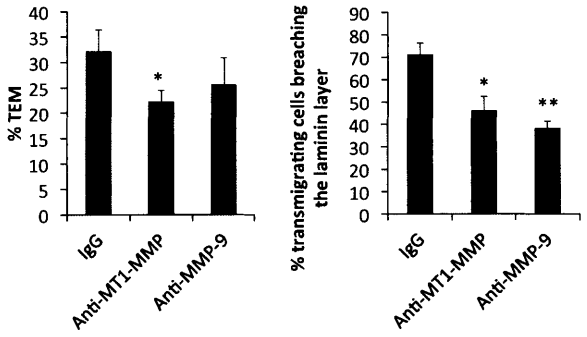

Figure 21. The effect of anti-MT1-MMP and anti-MMP-9 on transendothelial migration rate and efficiency of breaching the laminin layer, in microvascular networks (n=3, *p<0.05, **p<0.01).

3.7 Transendothelial migration is mediated by α3β1 and α6β1 integrins via interactions with sub-endothelial laminin

Our results suggest that TEM is facilitated by the formation of activated β1 and actin-rich protrusions, which then form stable adhesions onto the subendothelial matrix, and likely followed by contraction at the protruding edge. Because we demonstrated that tumor cell protrusions associate closely

with the BM during the initial hours of TEM, we hypothesized that the defects induced by β1 depletion are partly due to the inability of protrusions to bind to specific underlying BM proteins. To determine which alpha subunits and corresponding ECM ligands are important for TEM, we first employed function blocking antibodies for integrins α 1, 2, 3, 4, 5, 6, v, β1 and β4 to tumor cells prior to, and during the *in vitro* microvasculature assay. Reduction of integrin(s) function was verified via adhesion assays to collagen I, collagen IV, fibronection and laminin. At 6 h post tumor cell seeding, TEM efficiencies for most individually blocked alpha subunits (α 1, 2, 3, 4 and 5) and β4 were not significantly different, while there were slight attenuations when α6 and αv were blocked, and when αv/α5 and α1/α2 were co-blocked (**Figure 22A**). The most striking decrease occurred when laminin-binding integrins α3 and α6 were co-blocked (p=0.0059), indicating that adhesion to subendothelial laminin is critical for efficient TEM. To further confirm our results, we silenced α3 and α6 via siRNA (**Figure 22B**) and carried out longer-term (~24 h) kinetics experiments. At 24 h post tumor seeding, co-silencing of α3 and α6 continues to yield a significantly lower TEM rate compared to silencing α3 or α6 alone (**Figure 22C**). Furthermore, silencing of β4 integrin did not result in significant changes in TEM over 24 h, indicating that α6β1, and not α6β4 (which also bind to laminin), is likely at play.

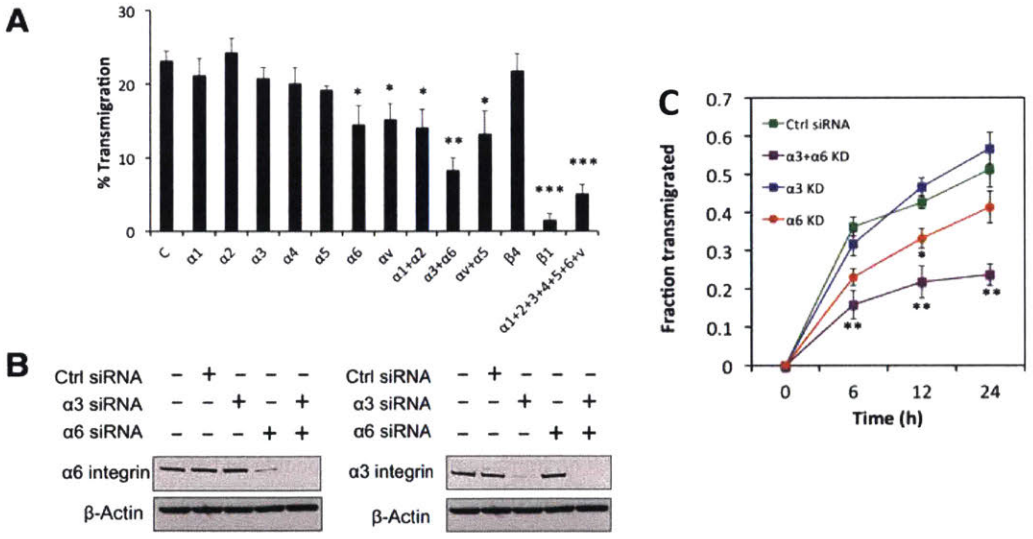

Figure 22. Transendothelial migration is mediated by α3β1 and α6β1 integrins via interactions with laminin. (A) Percentage transendothelial migration in microvascular network devices at 6 hours when tumor cells are treated with function-blocking antibodies for various α and β subunits (n=3 experiments, 3 devices per condition, *p<0.05, **p<0.01, ***p<0.001, bars represent mean +/- SEM). **(B)** Western blot analysis of alpha 3 and alpha 6-integrin individual knockdowns and co-knockdowns in MDA-MB-231 via siRNA. **(C)** Kinetics of TEM in microvascular networks following the same regions at 0, 6, 12 and 24 hr after tumor cell seeding.

Dynamic tracking of TEM on individual tumor cells revealed that the time required to reach a state of discernable stable protrusion formation past the endothelium was longer in $\alpha 3/\alpha 6$ co-knockdown cells compared to controls (**Figure 23A**). Furthermore, blocking of microvascular devices with anti-laminin antibodies prior to tumor cell perfusion resulted in a significantly lower percentage of cells exhibiting protrusions at early time points of 1 and 4 h, strongly suggesting that the ability to adhere to BM laminin is important in the specific context of extravasation (**Figure 23B**). However, while co-blocking α3 and α6 significantly decreases TEM efficiency, it does not reach the levels associated with blocking β1. Combined with the finding that blocking of most individual alpha subunits only yields small or insignificant changes, it is highly likely that multiple alpha subunits function simultaneously to facilitate TEM.

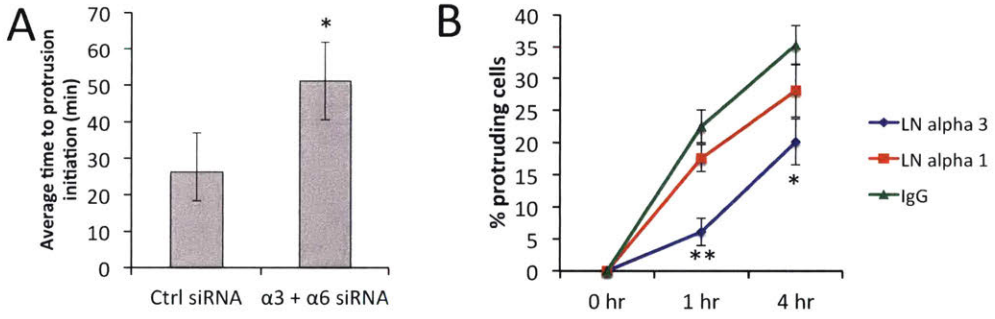

Figure 23. Dependence of tumor cell protrusion rates on adhesion to laminin. (A) The average time required for initial protrusion formation in control siRNA or α3/α6 co-knockdown MDA-MB-231 (n=50 cells/condition, p=0.013**). (B)** Percentage of MDA-MB-231 forming protrusions past the endothelium (in microvascular networks assay) at 1 and 4 hours when microvessels were treated with anti-laminin antibodies immediately prior to tumor cell perfusion (n=3, **p<0.01).

3.8 β1 integrin is required for metastatic colony formation *in vivo*

Our results show that loss of β1 integrins significantly impairs tumor cell extravasation by influencing multiple processes during extravasation, which is widely believed to be a rate-limiting step in metastatic colonization of distant organs. Therefore, we tested whether β1 knockdown impairs metastatic colonization. Since several cell types in the immune system are known to influence metastatic colonization[42,91], we performed these experiments using the highly metastatic mouse mammary carcinoma cell line 4T1 which is syngeneic in Balb/C mice. These 4T1 β1KDs were confirmed to impair extravasation in our microvascular network assay (**Figure 17 F-G**).

To test the effect of knocking down individual integrin subunits, we utilized a previously developed a Luminex-based, multiplexed assay for metastatic colonization (**Figure 24A**), as described

previously[87]. 4T1 cells stably expressing uniquely DNA-barcoded vectors with shRNAs targeting each integrin subunit were individually generated and efficient knockdown of each integrin subunit was confirmed by flow cytometry. Cells expressing shRNAs targeting β1 were significantly reduced in the lungs relative to control shRNAs (**Figure 24B**), indicating the loss of β1 significantly impairs metastatic colonization. In contrast, targeting other beta subunits or individual alpha subunits did not significantly reduced in the lungs relative to control shRNAs, suggesting that the functions of individual alpha subunits are dispensable for metastatic colonization. This finding is strongly correlated with the earlier results presented, showing that blocking of individual alphas and other beta subunits does not significantly impair TEM in *in vitro* microvasculature. Together these findings suggest that the ability to successfully extravasate is strongly correlated with the ability to form metastasis, and that β1 integrin is required for metastatic formation.

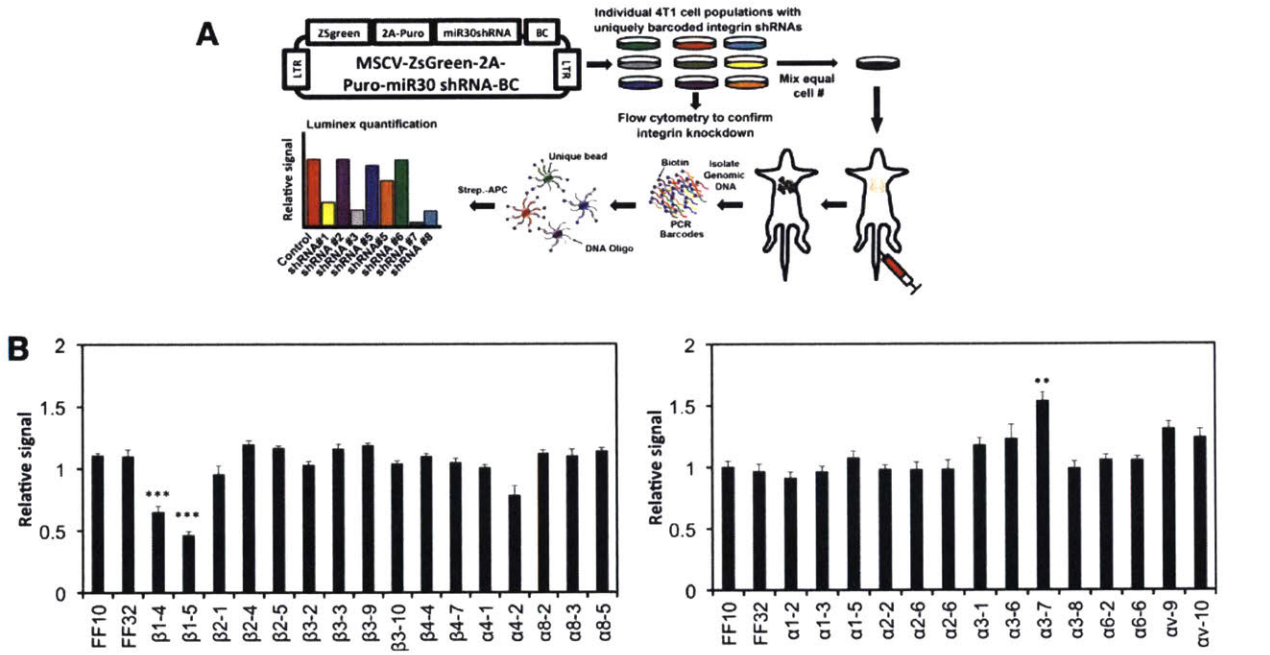

Figure 24. Knockdown of β 1 integrin in 4T1 cells inhibits metastatic colonization.

(A) Schematic of our Luminex-based approach for multiplexing tail vein metastasis assays (see Methods). 4T1 cells were stably transduced with uniquely barcoded *(BC)* vectors expressing miR30-based shRNAs targeting one integrin subunit per cell population, and knock down was confirmed by flow cytometry (see Table 1). Uniquely barcoded 4T1 integrin knockdown cell populations were then mixed in equal numbers and injected into the tail veins of syngeneic Balb/C mice. After 17 days, Genomic DNA was isolated from the metastasis-containing lungs, and the relative amount of each barcode (i.e. the relative number cells expressing each shRNA) was quantified using streptavidin-conjugated APC *(Strep-APC)* and the Luminex FlexMap 3D system. **(B)** Luminex-based quantification of the relative metastatic burden of each 4T1 integrin knockdown cell population. Graphs show the relative signal ± S.E.M. from each shRNA relative to the signal for that shRNA in the starting mixed population (n=10 mice / mix analyzed in duplicate).

3.9 Discussion

Tumor cell extravasation is a key step during cancer metastasis, yet the precise mechanisms that regulate this process remain unclear. This is partly due to the difficulty of most *in vivo* assays in isolating the effect of different perturbations on discrete steps during extravasation. Furthermore, *in vivo* models are often hindered by relatively low spatio-temporal resolution of extravasation events and the tortuosity of *in vivo* vasculature presents challenges in scoring extravascular and intravascular cells, rendering the analysis subjective. To address this need, we have recently developed *in vitro* microvascular platforms capable of observing multiple steps of the extravasation cascade as well as tumor cell morphological dynamics in high detail. Uniquely, vessels largely lie in the same plane of view and distances between the cells and microscope objective is <300 microns. The assay also recapitulates tumor cell arrest via trapping in small capillaries, which is generally not achievable in other *in vitro* platforms of extravasation. Thus, despite the essential role that *in vivo* extravasation models play in recapitulating physiological conditions, the *in vitro* assays used in this study are more suitable for discerning the spatial organization of tumor-endothelial cell interactions. Using our assays, we are able to pinpoint the distinct roles of tumor β1 integrin in tumor-endothelial and tumor-BM interactions during extravasation. First, β1 integrin is activated at the tip of leading protrusions penetrating the endothelium, allowing adhesion to subendothelial ECM, in particular, BM laminin via $\alpha 3\beta 1$ and $\alpha 6\beta 1$ integrins. Engagement of these integrins with their ligand allows stabilization and growth of these protrusions, which is followed by recruitment of F-actin at the protruding edge. This then enables the cell to translocate by pulling itself past the gap formed in the endothelium (**Figure 25**).

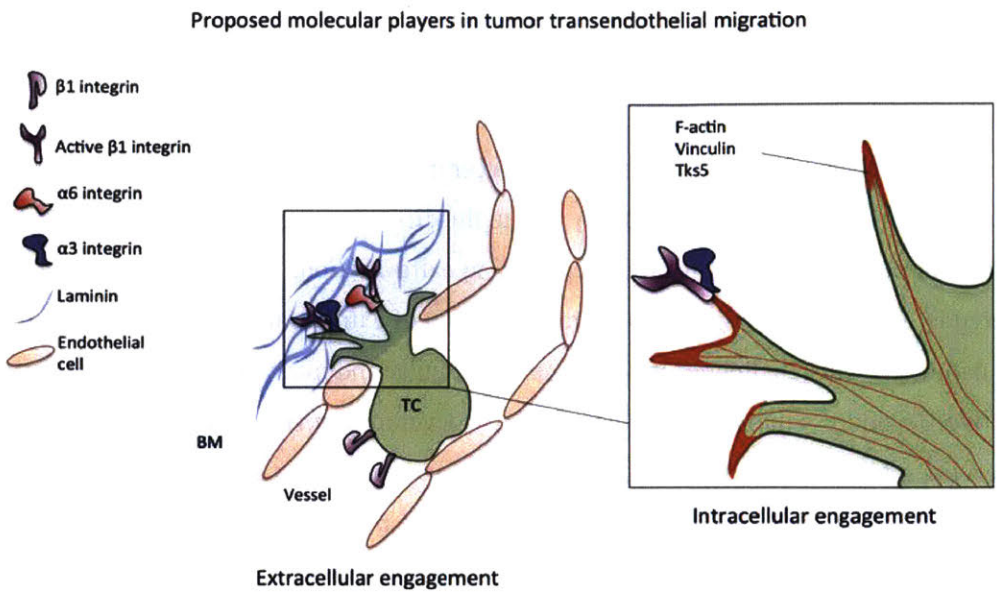

Figure 25. Proposed molecular players involved in tumor transendothelial migration.

Extracellular engagement: activation of β 1 integrin facilitates protrusion maintenance past retracted endothelium, via engagement to subendothelial ECM. Specifically, integrins $\alpha 3\beta 1$ and $\alpha 6\beta 1$ are both required for adhesion to vascular basement membrane laminin. Intracellular engagement: β 1integrin-rich extracellular adhesions maintain protrusions, allowing focal adhesion proteins (e.g. vinculin) and F-actin to be recruited to the tips of protrusions, resulting in transmigration via acto-myosin contraction at the protruding edge.

The lack of discernable tumor cell protrusions during transmigration in β1KD cells suggests that the extension of cytoplasmic projections is required for complete extravasation. Cells transmigrating in our microvascular networks exhibit invadopodial-like extensions into the sub endothelial matrix during transmigration. Furthermore, these protrusions are marked by co-localized punctate regions of F-actin, activated β1 integrin, vinculin and Tks5 at the tips of the protrusion. In contrast, these proteins are only weakly diffuse in the intravascular portion of transmigrating cells, as well as in non-transmigrating cells. In support of this, it has been shown that invadopodia formation is associated with β1 and β3 integrins [92], and that pharmacological inhibition of invadopodia maturation (Tks5) and function (Tks4) results in an abrogation of extravasation in CAM models and metastatic colony formation *in vivo* [36].

During the initial stages of TEM (20 min to 1 h) tumor cells begin by extending small actin rich protrusions (~1-3 μm deep) into the extravascular space. Combined with the observation that these initial protrusions do not breach but rather associate closely with the subendothelial BM, we hypothesized that β1 integrins facilitate the engagement of these protrusions to specific underlying BM proteins via specific alpha integrin subunits. In support of this, *in vivo* studies have shown that tumor cells extend processes

past the endothelium, contacting the basal lamina [31,35,60]. The integrin profile of MDA-MB-231 has previously been characterized and shown to express a variety of alpha subunits (including $\alpha 1$ to $\alpha 6$ and v) [93], however whether all or only a specific subset of these are required in extravasation is unclear. Numerous studies have demonstrated the importance of various alpha integrins in the context of 3D invasion and contribution to metastatic formation[70,74,77,81,82,86,94]. However, while similar ECM components may be present in both the primary site and extravasation microenvironments, their spatial distributions and abundance may differ. Additionally, the necessity of engagement to specific ECM components may also differ depending on the context of migration. Using our assays, we find that co-knockdown of $\alpha 3$ and $\alpha 6$ integrins results in the most significant defect in TEM, indicating that adhesion to BM laminin is required in the context of TEM, and likely facilitates maintenance of tumor cell projections past the endothelium. In fact, it has been found that the ability to adhere onto vascular laminin may involved in the extravasation step, which is suggested by the requirement of $\alpha 3\beta 1$ for adhesion to exposed regions of pulmonary vascular LN-5 and subsequent metastatic foci formation in a mouse model [86]. In support of this, our dynamic imaging reveals co-blocking $\alpha 3$ and $\alpha 6$ integrins results in a slower rate of protrusion formation into the subendothelial matrix. In an *in vivo* context, it may be advantageous for tumor cells to form stable anchorage into the matrix faster, in order to gain better chances of escaping the hostile intravascular environment. In contrast, blocking integrin receptors αv and $\alpha 5$ for fibronection do not yield significant results, despite the fact that fibronectin is present on the abluminal surface of the vessels. This further suggests that the inability to adhere to laminin cannot be fully compensated via adhesion to other available ECMs during extravasation.

The BM scaffold is a tight covalently cross-linked mesh formed by laminin and type IV collagen that is bridged by nidogens on which other components are bound. It seems highly unlikely that a cell could squeeze through pores on the order of 50 nm; however, tumor cells constantly migrate across basement membranes[95]. Thus, the process has long been thought to require local degradation of the BM with matrix metalloproteinases (especially MT- MMPs), which may be recruited via integrin engagement to the ECM. These proteases are well characterized in the context of invasion, but whether the same factors are involved in vascular BM invasion are largely unclear. Because we observe the inability of $\beta 1$KDs to migrate away from the endothelium post-transmigration, we hypothesized that $\beta 1$ mediates the localization and production of MMPs that are required to degrade the vascular BM. In support of this hypothesis, studies show that $\beta 1$ is required for invadopodia formation and matrix degradation in both 2D and 3D ECM scenarios[96,97 83]. Indeed, immunostaining of laminin in our devices revealed that while control cells begin to breach the laminin layer within the first 6 to 9 h of TEM, few transmigrating $\beta 1$KD cells were able to invade the laminin layer, remaining trapped between the endothelium and BM.

Furthermore, blocking of MMP-9 and MT1-MMP pheno-copied this behavior, suggesting that localization and activation of MMPs are involved in BM breaching.

In vivo metastasis assays show a clear role of β1 in dissemination [10,70,77,78,80,85,86]; however, whether and how the defects lie in extravasation or even post-extravasation micro-metastatic growth remained unclear . In this Chapter, we demonstrate that the tumor β1 subunit is an indispensible player in the tumor cell extravasation cascade, and that its depletion contributes to an overall decrease in formation of metastases *in vivo.* Using the high-resolution *in vitro* extravasation assay developed in Chapter 2, we find that tumor cells first send activated β1-rich protrusions past the endothelium, which engages with subendothelial matrix, in particular laminin, via $\alpha 3\beta 1$ and $\alpha 6\beta 1$ integrins. This is followed by protrusion stabilization, F-actin recruitment, translocation of the tumor cell into the parenchyma, and subsequently, β1-mediated invasion past the vascular basement membrane.

Chapter 4

Tumor-host cell interactions and modulation of tumor cell extravasation

4.1 Introduction

The metastatic potential of tumor cells has been shown to be significantly modulated by the host microenvironmental conditions and host cells, such macrophages and fibroblasts at the primary tumor site. Similarly, during hematogenous dissemination, circulating tumor cells encounter a variety of host cells such as platelets and bone marrow-derived cells (BMDCs) at distant metastatic sites. In fact, it is now widely believed that the metastatic potential of disseminated tumor cells can be modulated by both cooperative and antagonistic interactions between host microenvironment and tumor cells[42]. However, tumor-host cell interactions during the steps of circulatory transit, arrest and extravasation are less understood due to the technical challenges associated with imaging, isolation and analysis of single disseminated tumor cells at secondary sites. In this Chapter, we increase the complexity of the device presented in Chapter 2 and apply it to probe the dynamic interactions between non-cancer host cells and tumor cells in the circulation. Our assay allows the observation of host cell interactions during extravasation with high spatio-temporal resolution, revealing details that are challenging to resolve in vivo. In a modular fashion, we first focus on the role of a single class of host immune cells, neutrophils, the pre-dominant circulating granulocyte in humans.

Currently, the roles of neutrophils in metastatic seeding are controversial. Clinical studies have shown that in cancer patients, neutrophilia often predicts worsened metastasis-specific survival[98]. In support of this, experimental mouse models reveal that neutrophils can enhance metastatic foci formation, as seen by the decrease in metastatic burden upon their depletion via anti-Ly6G [27,99-101], or increase when exogenous human neutrophils are added[102,103]. Various mechanisms have been proposed for this pro-metastatic effect, such as the increase in tumor cell retention in the vasculature via tumor-neutrophil

adhesions through integrins[102]. Neutrophil derived factors have also been implicated, such as LTB4 which enhances colonization by selectively expanding the sub-pool of cancer cells with high tumorigenic potential[99]. Conversely, neutrophils have been shown to accumulate in the pre-metastatic lung and inhibit metastatic seeding by generating H_2O_2, an effect that is mediated by tumor secreted CCL2[104,105]. Thus, neutrophil-tumor cell interactions may not be uniformly pro-metastatic.

Because neutrophils are the first line of defense for infectious insults, attention has recently focused on the link between systemic infection and metastatic seeding. In particular, cancer patients undergoing tumor resection surgeries often encounter post-surgical infection, which is followed by the activation of the immune response fundamental for the reparative process[106]. However, a disturbing feature of systemic infection in cancer patients is the association of neutrophilia and activation with adverse metastatic outcomes independent of the morbidity associated with the infection itself [107-109]. Animal models of injury such as cecal ligation and ischemia reperfusion have shown to induce the formation of neutrophil extracellular traps (NETs) which trap circulating tumor cells and enhance metastasis[110,111]. Similarly, pre-stimulation of neutrophils with lipopolysaccharide (LPS) increased tumor cell retention in hepatic sinusoids and gross metastases [103]. Thus, tumor-PMN interactions can play an important role in linking infection, inflammation, and metastasis. Combined with the finding that tumor resection often sheds cancer cells into the circulation[112,113], it has become imperative to clearly elucidate the cellular and molecular players underlying these observations.

In this Chapter, we make improvements to the microvasculature model developed in Chapter 2 in order to address issues of throughput and robustness. Using this improved assay combined with LPS-stimulated neutrophils to recapitulate an inflamed state, we probed the dynamic interactions between tumor and host cells during hematogenous dissemination. We show that various tumor cell types can co-localize with neutrophils and arrest intraluminally in heterogeneous TC-PMN clusters. Aggregation is dependent on PMN adhesive interactions, particularly with endothelial ICAM-1 that is up regulated only upon tumor cell contact. Following initial arrest in clusters, PMNs are further confined and sequestered via autologous chemotaxis towards PMN derived IL-8 and tumor-derived CXCL-1, a response which is enhanced via immobilization and maintenance of chemokines on the intraluminal endothelial heparan sulfate (HS) groups. PMN sequestration at tumor clusters results in the spatial localization and hence effectiveness of PMN-derived IL-8, which, above threshold concentrations, disrupts the adjacent endothelial barrier and facilitates invasion of PMN-associated tumor cells through the vascular wall.

4.2 Methods for investigating the role of PMNs during tumor extravasation

Design and fabrication of a multiplexed extravasation assay

In order to address the technical challenges associated with assay throughput and reproducibility, the device presented in Chapter 2 was modified. A single gel injection port allows the parallel distribution of cells into 8 independent vascular beds through a branching network (**Figure 26A**). Wider channels (500 μm wide by 130 μm high) in the branching network leading to the entrance of each gel region, combined with a narrow channel (120 μm wide) downstream of the gel region prevents premature leakage of hydrogel into the side channels if any other is prematurely filled. Since fibrinogen polymerizes rapidly once in contact with thrombin, the branching network length and channel width were designed to reduce the tendency for premature polymerization before all 8 devices have been filled. Although the gel regions are all connected via a the same branching network, they can be considered to be independent since the characteristic diffusion time scale is on the order of days for a small proteins in water ($D \sim 10^{-6}$ cm^2/s), even when media flow is introduced to the system. This is negligible compared to the time span of a typical extravasation experiment in our assay (8-12 hours).

Constant media perfusion is achieved via a ~5 mm passive hydrostatic pressure head using a large integrated reservoir attached to the top of the device after introduction of the tumor cells into each microvascular bed (**Figure 26B**). The reservoir and channels are separated by a dual-purpose "ports and plugs" layer, which simultaneously provides access to and restricts flow in a manner that allows formation of identical pressure drops across all 8 regions in the direction orthogonal to that in the reservoir. Using this simple pump-free method, physiologically relevant shear stresses ranging from 0.1-1 Pa can be robustly maintained for ~ 6 hours before significant changes (>10%) in the pressure drop occurs. In cases were the experiment was longer, fluid was replenished in reservoirs to restore the original hydrostatic pressure drop, and the reservoir was carefully secured to the chip to prevent delamination over time.

In addition, the larger gel-cell mixing volume decreases variations in cell densities between hydrogel regions in one entire chip, which greatly improves the percentage of perfusable vascular beds in each experiment. Furthermore, with no changes to the volume of perfusable networks and the number of starting HUVECs and FBs, the number of independent devices that can be filled is increased at least 4-fold (>56). This is partly due to the significant reduction in the dead-volume by replacing 8 gel injection ports with one, while parallel seeding significantly reduces the time required to seed a "single" hydrogel region independently. Preparation of cells for device injection is similar to that described in Chapter 2 and the step-by-step modified protocol can be found in **Appendix B.**

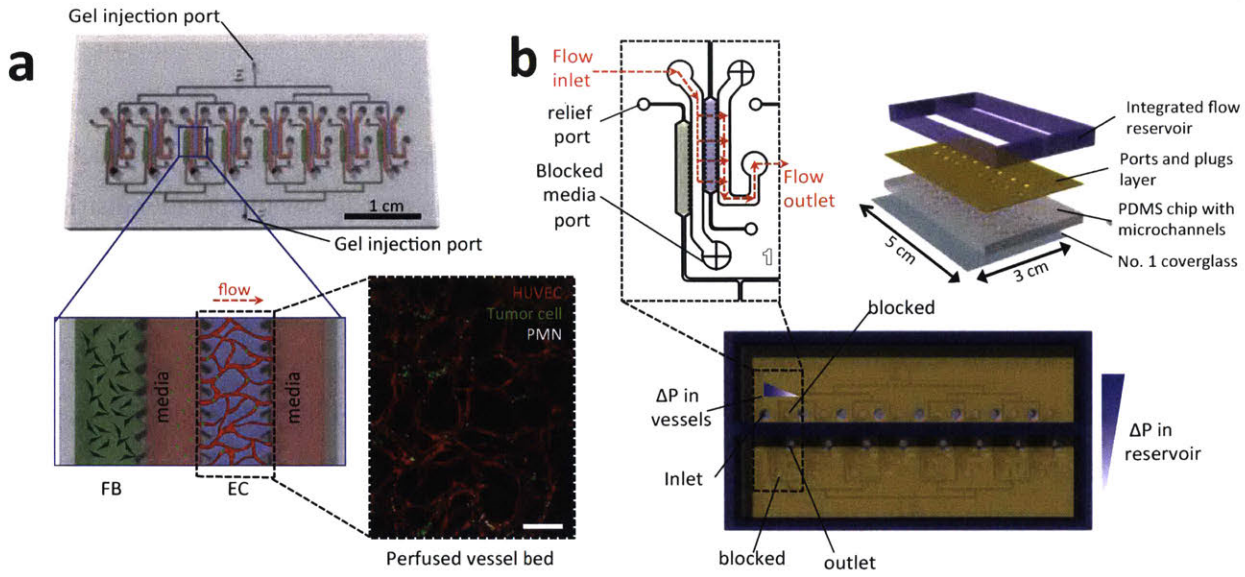

Figure 26. Multiplexed microfluidic chip allows higher throughput and robust formation of microvascular beds and quantification of TC extravasation. (A) Each chip houses 8 independent hydrogel regions for the formation of microvessel beds. 8 gel regions are connected by branching channels on each side to facilitate parallel injection of HUVEC or FB suspensions. Gels are prevented from bursting via the use of relief ports downstream of the hydrogel region. After 4 days of culture, perfusable vascular beds form in the HUVEC chamber with the help of paracrine signaling from suppor8ng fibroblasts (green region). TCs/PMNs are introduced into the flow inlets and travel across vascular bed via a short (~ 1 min) pressure drop across each individual gel region. Fluorescence inset depicts a confocal projec8on of one perfused vascular network. (B) To induce continuous media flow over ~6 hrs after cell perfusion, a large integrated reservoir sustaining a hydrostatic pressure drop of ~5mm water is secured on top of the PDMS chip. The media in the reservoir is connected to the flow inlets and outlets on the PDMS chip via an acrylic layer that that blocks reservoirs at required positions (diagonal).

Human neutrophil isolation

Human neutrophils were obtained from fresh human blood (diluted 1:1 in HBSS (Invitrogen)) collected from healthy donors (Research Blood Components, Cambridge, MA), at most 3 hours before perfusion. Briefly, blood anti-coagulated with sodium citrate was layered onto Histopaque 1077 (Sigma), centrifuged (without brake at 1400 rpm), and plasma and PMBC layers were removed. PMNs were further separated using a density gradient with 2% dextran (Sigma) for 30 minutes at 1400 rpm, followed by red blood cell lysis with cold water. All procedures were done at room temperature. Isolated cells were resuspended at 6M/mL in HBSS and stained with Cell Tracker Deep Red™ (Invitrogen) at 0.5 μM for 10 minutes and washed twice with HBSS. In experiments requiring inflamed PMNs, cells were further incubated with 30 ng/mL of LPS (Sigma) for 25 minutes at 37°C, and washed 3 times with HBSS. The full protocol for PMN isolation can be found in **Appendix C.**

Cytokine array

MA2 were plated onto 6 well plates in EGM-2MV until 60% confluence, after which media was replaced and incubated for 4 hours before collection conditioned media. In some cases, freshly isolated PMNs were also incubated on 6 well plates, or co-incubated with MA2 cells, for 4 hours in EGM-2MV. Conditioned media was centrifuged at 800g for 10 minutes to remove debris and stored at -20C until use. Undiluted conditioned media and EGM-2MV control media was assayed using a human 80-cytokine array (Cat #. AAH-CYT-5, Raybiotech), following the manufacturer's protocol.

Cell culture and treatments

Pooled human umbilical vein ECs (HUVECs) (Lonza) were transduced with a mCherry LifeAct plasmid (Addgene), and cultured in EGM-2MV supplemented with Singlequots™ (Lonza, Walkersville) on collagen-1 coated plates and used at passage <6. Normal human lung fibroblasts (Lonza) were cultured in FGM-3 supplemented with Singlequots™ (Lonza, Walkersville) and used at passage <12. Human GFP expressing melanoma A-375 and A-375 MA2 (gift from the Hynes Lab, MIT) and MDA-MB-231 (ATCC) were maintained in DMEM supplemented with 10% FBS and 1% penicillin/streptomycin. For tumor cell and PMN perfusion, cells were trypsinized and resuspended at 1.2 M/mL and mixed with PMNs to achieve a final density of 0.6 M/mL (tumor) and 3 M/mL (PMN).

Antibodies and reagents

For blocking of neutrophil surface CD11b after LPS activation, cells were incubated with anti-CD11b (1:200 in HBSS) (Cat #. 301319, Biolegend) for 30 minutes at 4°C, followed by an HBSS wash. Tumor ICAM-1 was blocked by a 30-minute incubation with anti-ICAM-1 diluted 1:200 in DMEM (Cat #. BBA9, R&D) at 4°C. HUVEC ICAM-1 was blocked by perfusing vascular networks with anti-ICAM-1 (1:200 in EGM-2MV) and devices were incubated for 30 minutes at 37°C followed by 2 washes with EGM-2MV before perfusion of cells. At times, HUVEC microvessels were stimulated with recombinant human IL-8 (Cat #. 208-IL, R&D) diluted at various concentrations in EGM-2MV for 3 hours at 37C prior to cell perfusion. To degrade the endothelial heparan sulfate layer, microvascular networks were pre-incubated with heparinase III from flavobacterium heparinum (Cat #. H88891, Sigma) at 3U/mL for 2 hours prior to tumor cell perfusion. At times, HUVEC vessels were pre-treated with undiluted conditioned media (collected as described above) from tumor cells or PMNs for 3 hours prior to cell perfusion with the same media.

To test the influences of various cytokines on PMN dispersion and TC extravasation, tumor cells mixed with LPS activated PMNs (at final perfusion densities) were incubated with anti-CXCL at 15

μg/mL (Cat #. MAB275), anti-IL-8 at 1 μg/mL (Cat #. MAB208), anti-CCL-4 at 5 μg/mL (Cat #. MAB271), anti-CXCL-7 at 20 μg/mL (Cat #. MAB393), anti-IL-6 at 0.2 μg/mL (Cat #. MAB206), or control isotypes, all from R&D. Cells suspension were incubated with antibodies for 20 minutes on ice followed immediately by perfusion into microvascular networks (without washing).

For siRNA mediate knockdown of IL-8 and CXCL-1 in MA2, cells were plated on six well plates and transfected with 25 pmol of IL-8 (Cat #. s7327) and/or CXCL-1 (Cat #. 215133) Silencer Select siRNA (Thermo Fischer) using Lipofectamine RNAiMax reagent (Thermo Fischer) (treated twice over 48 h), before trypsinization and perfusion into microvessels. Knockdown on secreted proteins was confirmed via ELISA (Cat #. D8000C, R&D).

Immunostaining

Microfluidic chips were fixed with 4% paraformaldehyde for 10 min, not permeabilized (to stain for cell surface proteins only), and blocked with 3% BSA and 10% normal goat serum in PBS for 5 h. Samples were then incubated in primary antibodies against active conformation of CD11b (1:200) (Cat #. 301407, Biolegend), ICAM-1 (1:100) (Cat #. 322702, Biolegend), and heparan sulfate (1:100) (Cat #. 370255-S, Amsbio) overnight at 4C in blocking buffer. Devices were washed with PBS for 5 hours and incubated with secondary antibody (Alexa Fluor 647 or Alexa Fluor 568, Invitrogen) at 1:200 for 4 h.

Confocal and epifluorescent time-lapse imaging. Devices were imaged with a laser scanning confocal microscope (Olympus FV-1000) at 10X (N.A. 0.45) at 4-micron z-steps with 800X800 pixel resolution, every 20 minutes. For epifluorescent time lapses (Carl Zeiss), devices were imaged at 10X (N.A. 0.45) on one focal plane with 486 X 468 pixel resolution, every 40-50 seconds. In both set-ups, devices were maintained at 37C and 5%CO_2 for the duration of the time lapse. Time-lapse sequences were analyzed via Imaris Bitplane (for 3D confocal projections) and ImageJ (for 2D epifluorescent images).

Quantification of tumor cell or PMN extravasation

In all experiments quantifying extravasation in microvascular networks, the transmigration rate of one device is calculated from 6 random fields of view via confocal microscopy at 20X (NA 0.75) with 1.26-micron z-steps and 800 X 800 pixel size. 3D projections were reconstructed in Imaris Bitplane. All tumor cells or PMNs that were observed to partially cross or completely clear the endothelial barrier were classified as "extravasated."

Image segmentation, determination of TC-PMN clusters, cluster-associated or free PMNs/TCs

Because TC-PMN clusters are heterogeneous in cell numbers, area coverage, cell-cell ratios, and cell-cell separation distances, we defined a "TC-PMN cluster" as any aggregate of cells with at least 1 tumor cell and 6 PMNs, each of which must be no more than 10 μm away from nearest cell in the cluster (determined from images at t=0). Relative distances between all cells were determined beforehand by segmentation of TCs into surfaces (thresholded) and PMNs (into 3 μm radius spots), using the "Surfaces" and "Spots" functions, followed by the "Distance Transformation" function on Imaris Bitplane (**Figure 27A**). Furthermore, the cluster must be at least 150 μm away from other defined clusters (see **Figure 27B** for examples). PMNs lying within TC-PMN clusters were categorized as "cluster-associated," while those free from clusters within a 150 μm radius of the cluster boundary were classified as "free."

To determine the fractions of PMNs remaining over time, the periphery of each TC-PMN cluster defined at t=0 was delineated by generating a minimum bounding sphere around the cluster, using Image J. At each 20-minute time frame, that stayed within a 50 μm radius from the defined periphery was considered to be "remaining," while those outside of the 50 μm radius was deemed "lost." The fraction remaining was determined by taking the fraction of the total PMNs remaining over the 5 analyzed clusters in one device. The mean of at least 5 devices per condition is presented.

Conversely, to categorize "PMN-associated" TCs or "PMN-free" TCs, a similar metric was applied. If a tumor cell has at least 6 PMNs within a 40 μm radius from the tumor cell periphery, it was categorized as "PMN-associated." If the tumor cell has less than 2 PMNs within a 100 μm radius is deemed "PMN-free." Tumor cells do not fall into either category is "undefined" and not used for this specific analysis (see **Figure 27C** for examples). The extravasation rate of each subpopulation is determined by taking the fraction of the total number of PMN-associated TCs or free-TCs extravasated in a single device, and the average of at least 5 devices is presented.

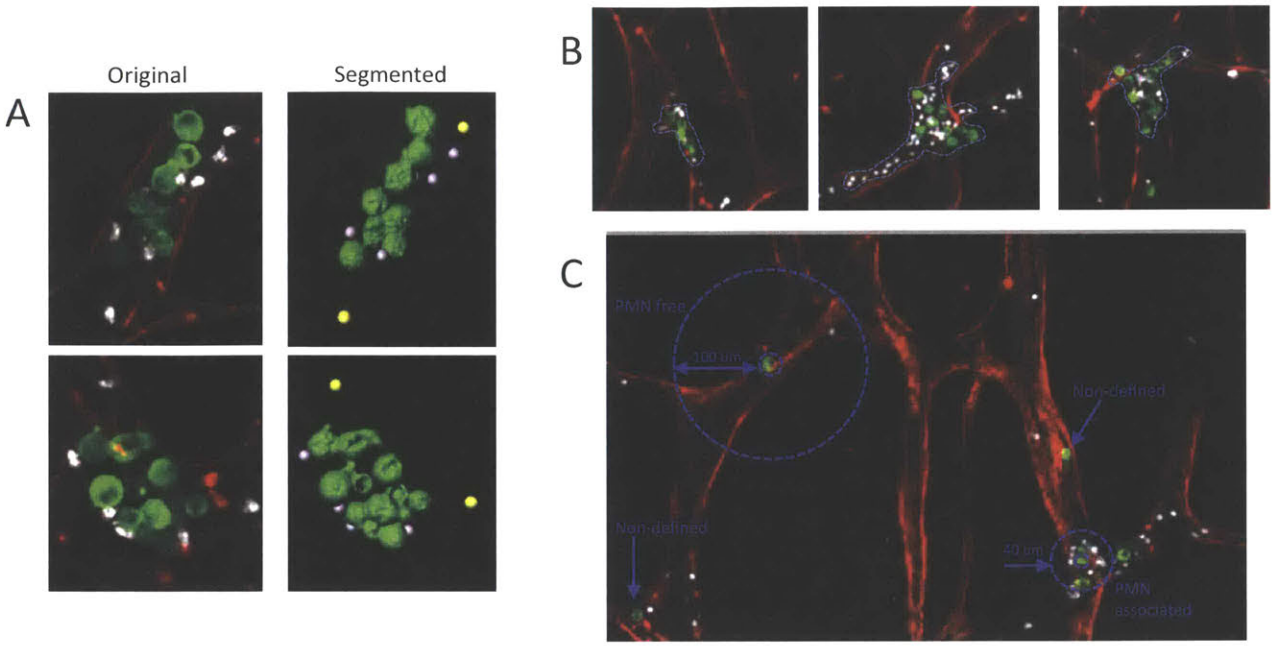

Figure 27. (A) Examples of original (maximum intensity projection) and segmented TCs and PMNs. PMNs are represented as 3 micron radius spheres. White spheres denote "cluster-associated" PMNS, while yellow spheres denote PMNs that are >10 micron any other cells in the cluster, and hence are not part of the cluster (for definitions, see Methods). (C) Further examples of defined "TC-PMN clusters." PMNs within the blue dotted boundary are classified as "cluster-associated" PMNs. PMNs that are not part of TC-PMN clusters are are at least 150 away from any other clusters are defined as "free" PMNs. All other PMNs that do satisfy either criteria are categorized as "undefined" to order to clearly discretize each population. (D) Examples of "PMN-associated" tumor cells and "free" tumor cells.

Tracking of PMN migration

To determine migration tracks of PMNs, epifluorescent images taken every 40-50 s were segmented (via ImageJ) to clearly delineate individual PMNs. PMNs were manually tracked using the "Manual Tracking" algorithm and paths were plotted on MATLAB.

To determine the migration speeds and euclidian distances of cluster-associated PMNs or free PMNs, representative cells were randomly chosen based and their categorization was based on their position at the first time point of imaging ("t=0"), despite the fact that their association with clusters may change over time. Each point represents one PMN, and statistics are determined by averaging speeds of analyzed PMNs in one device, with n=5 devices per condition.

Statistics

Statistical analysis was performed with SigmaPlot using the student's two-tailed t-test when comparing two conditions, or one-way ANOVA with Tukey's post-hoc analysis when applicable.

4.3 TC-PMN aggregation is dependent on the up-regulation of endothelial ICAM-1 upon TC contact, combined with passive trapping

To recapitulate the inflamed phenotype of neutrophils found during post-surgical infections often occurring from primary tumor resections, neutrophils were first stimulated with LPS (30 ng/mL) for 30 minutes and washed 3 times, followed by co-perfusion with A375-MA2 melanoma cells into *in vitro* vascular beds. Immediately after intraluminal arrest, the two cell types were frequently found clustered together either in direct physical contact or close proximity to one another (**Figure 28A-B**). Approximately 60% of PMNs in a microvascular bed are found to be associated with TCs (within 40 microns to closest TC surface). Live video analysis revealed that while some neutrophils appear to make direct adhesive contact with tumor cells during transit, the clustering becomes most apparent when tumor cells begin to decelerate and plug or partially obstruct a narrow capillary, causing adjacent neutrophils to also decelerate and arrest. Upon closer inspection, many clustered neutrophils exhibited a spread morphology directly on the surface of the trapped tumor cell and on adjacent endothelial cells, and were frequently positive for the activated conformation of CD11b suggesting engagement of neutrophil CD11b with ligands on the tumor and endothelial surfaces (**Figure 28 C-D)**.

To understand whether intravascular TC-PMN clustering is dependent on adhesive interactions or passive trapping, quiescent or LPS treated neutrophils were incubated with anti-CD11b prior to perfusion. LPS stimulation upregulated surface CD11b expression and increased the percentage of trapped TC aggregates associated with PMNs. In contrast, addition of anti-CD11b attenuated this association. To understand whether CD11b is interacting with tumor and/or endothelial cell ligands, either the endothelium or TCs were pre-treated with anti-ICAM-1, a known ligand for CD11b. Both conditions resulted in significantly less TC-PMN clustering, with blocking of EC-ICAM-1 giving a stronger reduction. Notably, replacement of PMNs with 4-micron beads still resulted in ~18% of association, indicating an inherent level of pure physical trapping in TC-PMN clustering (**Figure 28E-F)**.

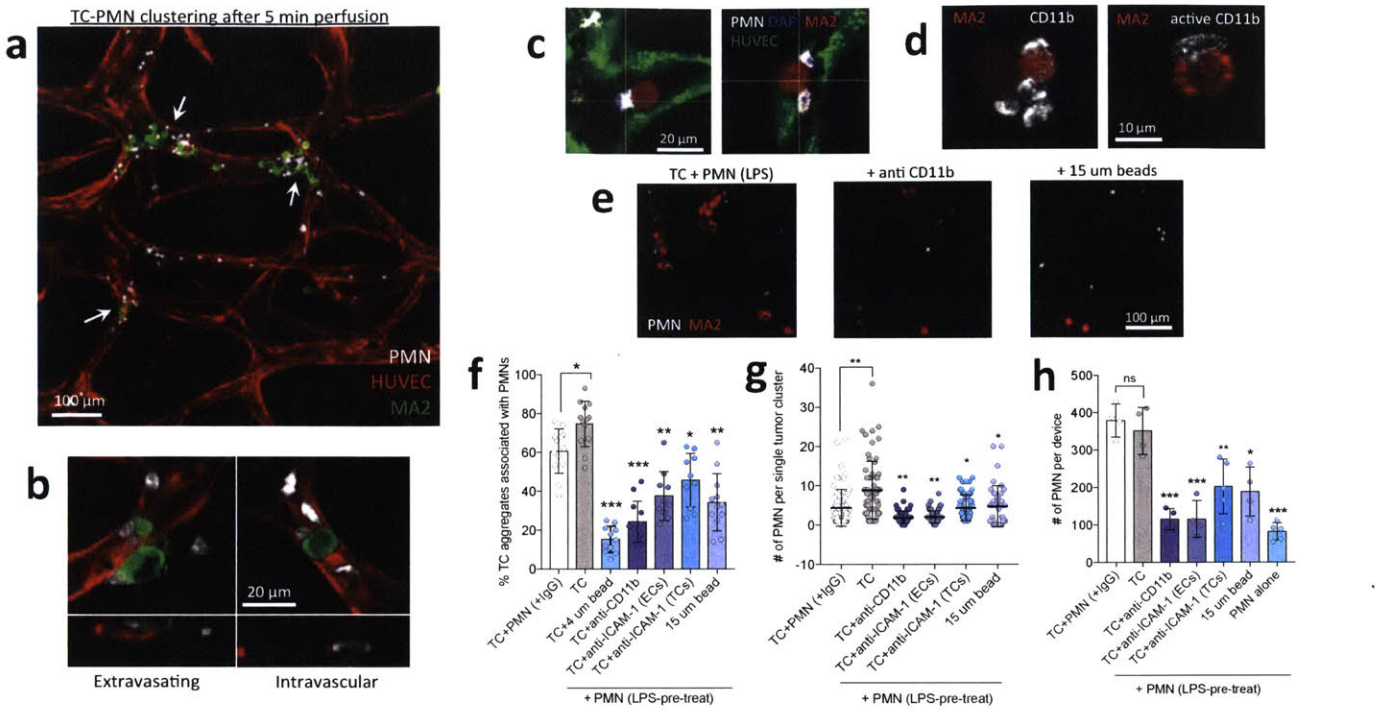

Figure 28. TCs and PMNs arrest in heterogeneous clusters during co-perfusion in vascular networks, and this behavior is modulated by PMN-TC-EC adhesive interactions. (A) Representative images of arrested TC-PMN clusters in microvessels. White arrows depict TC-PMN clusters . (B) Examples of extravasating and non-extravasated MA2 cells from within TC-PMN clusters. (C) Confocal images depicting the close association between PMNs and TCs intraluminally. (D) PMNs clustered near the surface of TCs are often positive for the activated conformation of CD11b. (E) Representative 10X images showing overall level of PMN-TC intraluminal clustering under flow in the presence of control IgG, anti-CD11b or when tumor cells are replaced with 15 µm diameter beads. (F) Percentage of arrested TC aggregates per device that are found associated with PMNs, in presence of neutralizing antibodies for CD11b, ICAM-1 , or when PMNs/TCs are substituted with similarly sized polystyrene beads, after 30 min of co-perfusion (10-13 devices per condition). (G) Number of PMNs found in each individual TC-PMN cluster, in the presence of anti-CD11b, anti-ICAM-1, or when TCs are replaced by beads. Each point represents one tumor/bead cluster, with 38-85 clusters over >5 devices/condition. (H) Average number of PMNs arrested in a single device after 1 hr of flow when perfused with TCs in the presence or absence of adhesion neutralizing antibodies, or when PMNs were perfused alone (last bar). Each point represents 1 device with 4-5 devices/condition. In **(f-h)**, statistical significance is generated by comparing to the case of TC + PMN (LPS) (grey). *p<0.01, **p<0.001, ***p<0.0001, and error bars indicate SD.

Immunostaining of ICAM-1 on endothelial cells revealed low levels in quiescent vessels, followed by a significant increase upon MA2 cell perfusion alone, and an even higher increase with MA2 and stimulated PMN co-perfusion (**Figure 29**). When tumor cells were substituted with 15 µm beads, ICAM-1 intensity did not increase, and TC-PMN co-localization was significantly less compared to the case with tumor cell perfusion (**Figure 28F**). Moreover, since blocking TC-ICAM-1 alone showed less clustering attenuation than blocking EC-ICAM-1, this suggests that PMN-CD11b to EC-ICAM-1

interactions may play a more significant role in clustering, and that this adhesion can be strengthened by the up regulation of EC ICAM-1 upon tumor cell contact.

Sequestration of PMNs in the vasculature may be important for effectively exerting their downstream effects. Confocal imaging revealed the total number of PMNs arrested in individual TC-PMN clusters was increased upon LPS treatment, and subsequently decreased when CD11b or endothelial or TC ICAM-1 was blocked (**Figure 28G**). The degree of TC-PMN association was also positively correlated with the number of PMNs remaining in the microvasculature after one hour of flow, while perfusion of stimulated PMNs alone resulted in the least number of PMNs arrested (**Figure 28H**). Altogether, our data suggests that the degree of PMN association with TCs and their overall sequestration in the vasculature is strongly dependent on adhesive interactions between PMN CD11b and endothelial ICAM-1 up regulated upon TC and PMN contact, and partly on physical trapping.

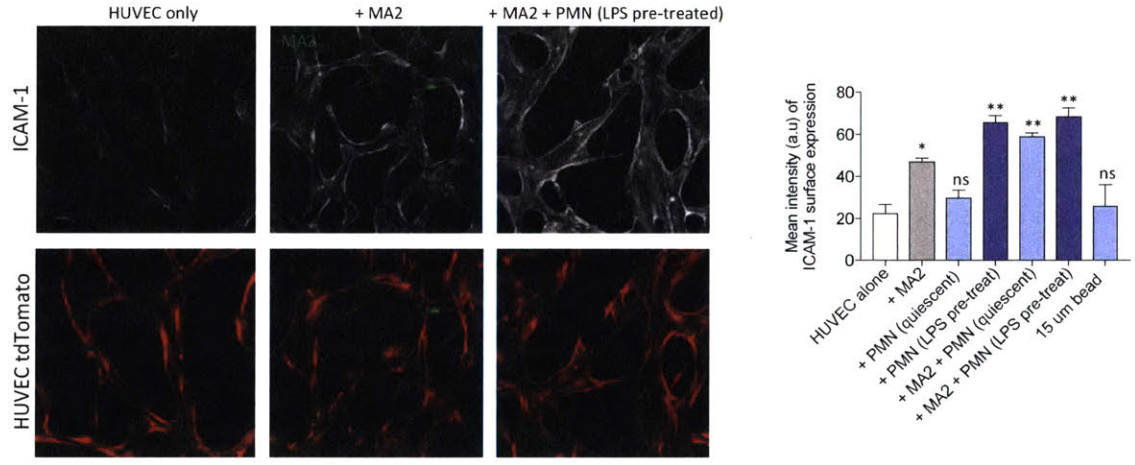

Figure 29. Representative immunostaining images of ICAM-1 in unpermeabilized microvessels. Quantification of mean intensity of ICAM-1 signals normalized to area of vessel coverage (in arbitrary units).

4.4 Clustered PMNs are further confined via autologous chemotaxis to PMN-derived IL-8 and tumor-derived CXCL-1

To probe possible dynamic interactions between tumor cells and PMNs within clusters immediately after their arrest, we performed time-lapse confocal and epifluorescent imaging of individual "TC-PMN clusters" within vessels. We further broke down PMNs into two sub-populations - "cluster-associated" or "free" - based on their proximity to arrested TC-PMN clusters (see **Figure 27** and **Figure 30A** for examples). Approximately 60% of PMNs arrested in a device are classified as "cluster-associated" and ~25% as "free," while the ones which could not fit clearly into either category were "undefined." When

images were acquired at intervals of 40 s, PMNs clustered near TCs were not static, but rather extremely on the surface of the endothelium, with some transmigrating into the surrounding matrix. In particular, the migration behavior of PMNs differed depending on their proximity to trapped TC-PMN clusters.

Cluster-associated PMNs exhibited both decreased migration speeds (0.14 μm/s vs. 0.22 μm/s) and displacement (101 μm vs. 291 μm) compared to free PMNs over a period of 90 min (**Figure 30B**). Since there was a 3-fold difference in displacement and only a 1.5-fold difference in speed, we hypothesized that that cluster-associated PMNs were still highly migratory, but may exhibit some type of confinement behavior. In order to visualize the directionality of PMN movement relative to the cell cluster, we plotted representative migration tracks of cells in either category. Indeed, cluster-associated PMNs remained more confined to their original position, whereas free PMNs exhibited significantly greater dispersion (**Figure 30C**). When individual PMN positions were plotted relative to the cluster boundary rather than their own starting positions, cluster-associated PMNs migrated in a "back and forth" motion while remaining within a ~50-80 μm radius.

We next asked whether the sequestering of PMNs within TC-PMN clusters was simply due to physical confinement (since cluster-associated PMNs may encounter more steric hindrance from adjacent cells compared to free PMNs), or a chemotactic response to chemokines secreted by the cells within the cluster. To identify chemokine candidates, conditioned media was collected from 4 h of culture of adherent MA2 cells alone, quiescent PMNs, MA2-PMN co-culture, and LPS stimulated PMNs alone. The array revealed two highly expressed and potent neutrophil chemotactic factors, IL-8 (from MA2 and inflamed PMNs) and CXCL-1 (from MA2) (**Figure 30D**). We hypothesized that the cells comprising the clusters could behave as a concentrated chemokine source for cluster-associated PMNs. As a preliminary test, we incubated devices with both anti-IL-8 and anti-CXCL-1 and observed the migration patterns of cluster-associated PMNs only. Blocking these chemokines resulted in an increase in PMN dispersion, migration speed and displacement (**Figure 30E-F**), as well as increased separation distance from the periphery of the TC-PMN cluster. This suggests that PMNs initially arrested within the TC-PMN cluster are further sequestered at the site via chemotactic confinement, and that in the absence of these chemokines, PMNs would be free to migrate randomly.

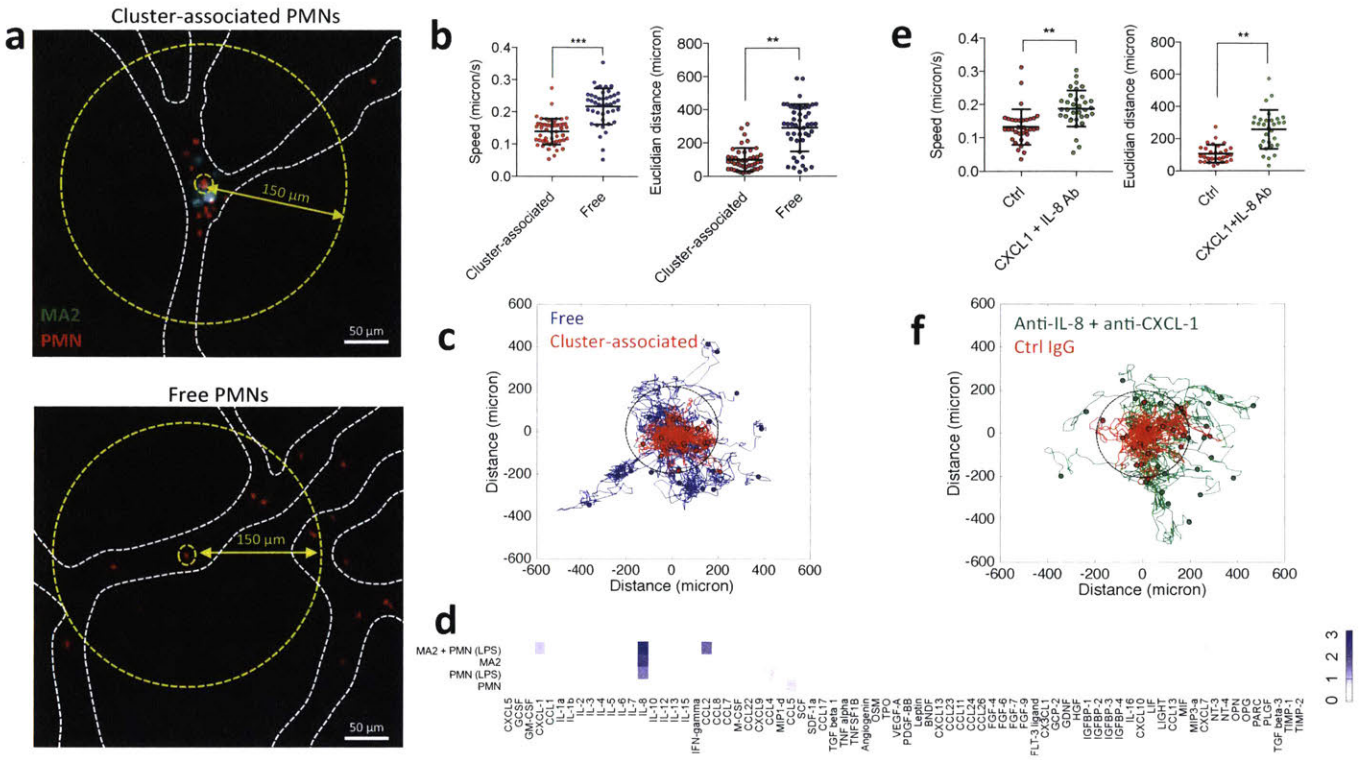

Figure 30. Cluster-associated PMNs exhibit decreased migration speed and increased confinement, which is dependent on TC and PMN secreted factors. (A) Examples of cluster-associated PMNs and free PMNs arrested intraluminally (for criteria to define cluster-associated vs free, see **Methods**). Both associated and free PMNs should be also be free of other TC-PMN clusters within a 150 μm radius. (B) Migration speed and end-to-end distance from original position of cluster-associated vs. free PMNs (43-53 PMNs per condition over 5 devices). (C) Representative migration tracks of free (blue) and cluster-associated associated (red) PMNs over 90 min (40 s time step). Dotted circle delineates the 200 μm radius. (D) Human cytokine array showing relative magnitudes of secreted factors from MA2 alone, PMN alone, LPS-activated PMNs or MA2+PMN co-incubation, after 4 hr of culture. Two highly secreted chemotactic cytokines (CXCL-1 and IL-8) were identified in the system. (E) Migration speed and end-to-end distance from original position of cluster associated PMNs with or without anti-CXCL1+anti-IL-8 (30-34 PMNs per condition, over 5 devices). Error bars indicate SD, **p<0.001, ***p<0.0001, error=stdev. (F) Migration tracks of PMNs incubated with anti-CXCL1+anti-IL-8 (green) or ctrl IgG (red).

Tumor cells are generally not observed to begin extravasation until >2 hours post-arrest in our microvessels[26,114]. Thus, in order to understand whether there exists a correlation between PMN sequestration in clusters and extravasation, we quantified the fraction of PMNs remaining in each cluster after a longer time point of 3 hours, at coarser time steps. As suggested by the dispersion of the migration tracks previously observed, the fraction of original PMNs in TC-PMN clusters remaining at 3 hours was

significantly less when CXCL-1 and IL-8 were co-blocked (**Figure 31A-B**). We next performed a series of experiments to decipher the relative levels of contributions of individual chemokines and their sources. While blocking CXCL-1 alone resulted in a significant reduction in dispersion, blocking IL-8 alone produced dispersion nearly at the same level as co-blocking. This suggests that IL-8 is a more potent chemokine than CXCL-1 in confinement; however, loss of IL-8 may be slightly compensated by the activity of CXCL-1 or other chemokines (**Figure 31B-C**). Additionally, we found that IL-8 is secreted by both stimulated PMNs and MA2s at high levels (and negligible levels from endothelial cells and fibroblasts. Since the IL-8 antibody does not discriminate based on source, we sought to decouple the two sources. Interestingly, ablation of tumor-derived IL-8 via siRNA did not result in changes in PMN sequestration, while co-knockdown of tumor IL-8 and CXCL-1 induced a moderate level of PMN loss, similar to CXCL-1 antibody treatments (**Figure 31C**). Importantly, replacement of TCs with 15 μm beads saw no changes in dispersion, while treatment of beads and PMNs with anti-IL-8 caused high levels of dispersion. Together, this suggests that the presence of tumor cells first promotes intraluminal PMN clustering via up-regulation of EC ICAM-1, and that once aggregated, PMNs are further sequestered by acting as their own chemotactic source. In particular, PMN-derived IL-8 appears to be more critical than tumor secreted factors for confinement.

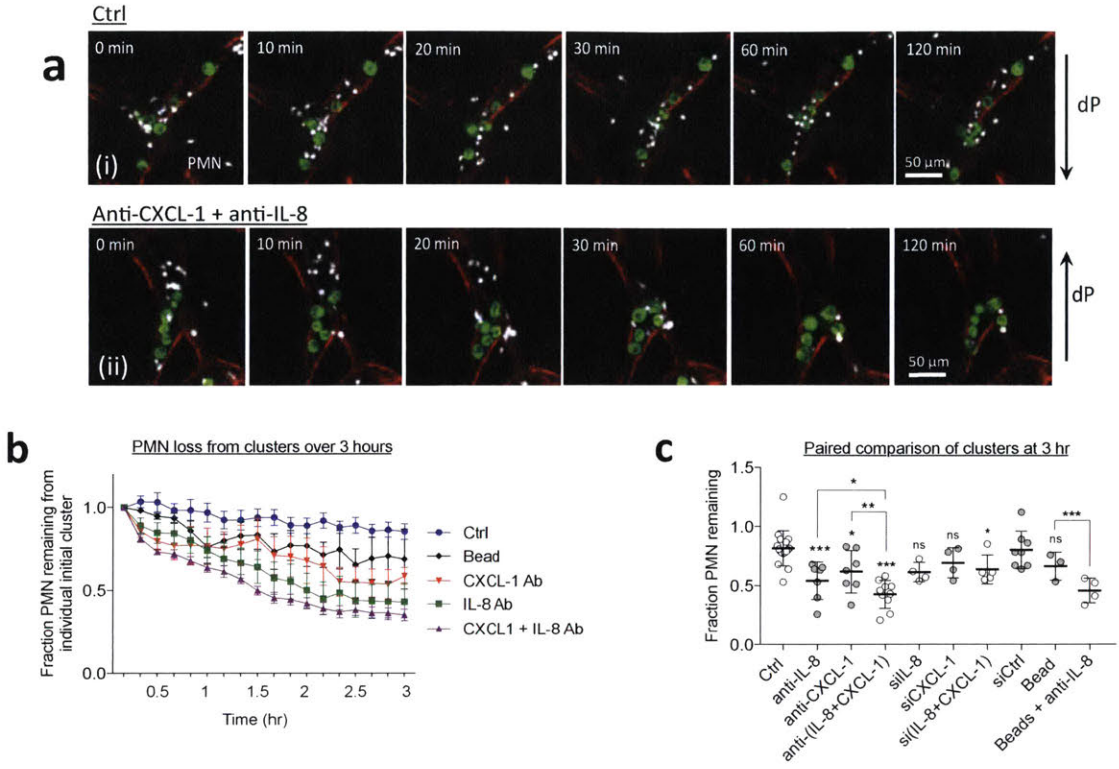

Figure 31. PMN-derived IL-8 and TC-derived CXCL-1 promote PMN sequestration in arrested clusters. (A) Representative images of cluster-associated PMNs (white) and their dispersion from TCs (green) over 2 hours, in the absence and presence of anti-CXCL1 + anti-IL-8. (B) Quantification of PMN dispersion by calculating the fraction of PMNs remaining in individual clusters over 3 hours (every 10 min) when the system is treated with IL-8 and/or CXCL-1 neutralizing antibodies, or when tumor cells are replaced with 15 micron polystyrene beads. (C) Quantification (paired comparison) of the differences between the fraction of PMN remaining at 3 hours. Devices are treated with either ctrl IgG or anti-IL-8 and/or anti-CXCL-1. In some cases, only tumor-derived IL-8 and/or CXCL-1 is ablated via siRNA. Each point represents one device with at least 5 TC-PMN clusters averaged per device (n>5 devices per condition).

Lastly, preliminary simulations showed that it is indeed possible for chemokine gradient (such as IL-8 and CXCL-1) to be established intraluminally with an arrested TC-PMN cluster acting as a chemokine source under fluid flow. The spatial distribution of PMNs around TCs results in higher mean downstream IL-8 concentrations (by one order of magnitude) compared to PMNs and TC lumped in one source or tumor cells alone, and gradients could be established over at least 100 μm from the edge of the TC-PMN cluster (**Figure 32**). Together, this data suggests that PMN confinement at TC-PMN clusters is mediated by self-secreted IL-8 and TC-derived CXCL-1, and possibly via intraluminal chemokine gradient formation.

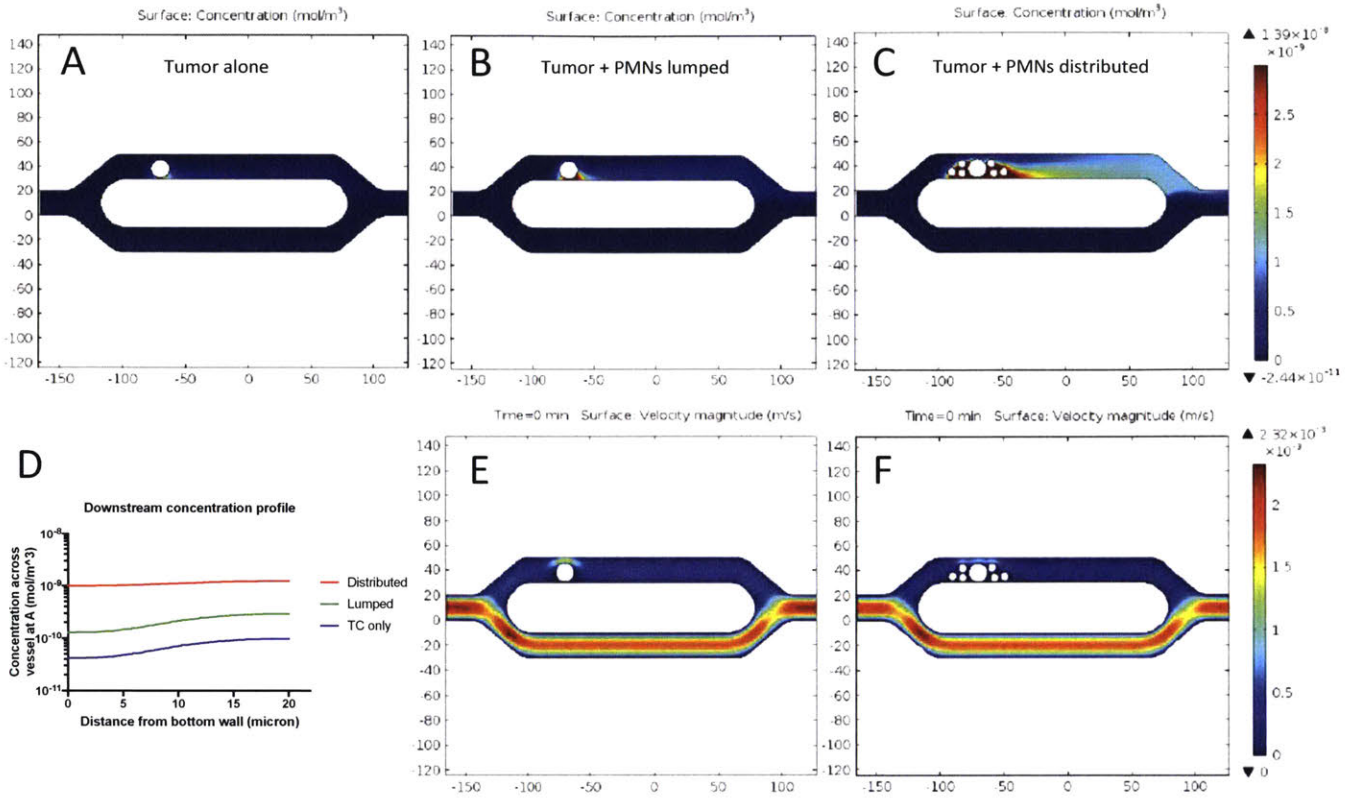

Figure 32. A vessel segment is simulated in 2D using Comsol Multiphysics. IL-8 secretion rates (from both TCs and PMNs), vessel geometry and flow rates were determined empirically. 2D heat maps of the spatial distribution of IL-8 (mol/m^2 s) under physiological flow conditions, assuming constant flux of IL-8 from (A) an arrested tumor cell only, (B) one tumor cell and 6 PMNs lumped in one equivalent source, or (C) distributed. X and Y axes are in microns. (D) The concentration profile across the vessel at the point 100 microns downstream of the tumor cell. Differences in the velocity magnitude and distribution in the case of a single tumor cell (E) versus a cluster of tumor cells and PMNs (F).

Lastly, it is known that the endothelial glycocalyx, specifically heparan sulfate proteoglycans (HSPGs) within syndecan-2, is capable of binding cytokines and growth factors with high affinity[115]. We hypothesized that IL-8 secreted by activated PMNs can be sequestered on the surface of the endothelium and may be critical in maintaining sufficient levels of IL-8 in the presence of fluid flow. To test this, vessels were pre-treated with heparinase III to degrade the HSPG layer and then washed prior to tumor and PMN perfusion. Migration speeds of PMNs alone in microvasculature did not change with heparinase III treatment (**Figure 33A-C**). However, when co-perfused with MA2, PMNs exhibited significant dispersion from their initial cluster over 3 hours, although not comparable to co-blocking IL-8 and CXCL-1 (**Figure 33D**).

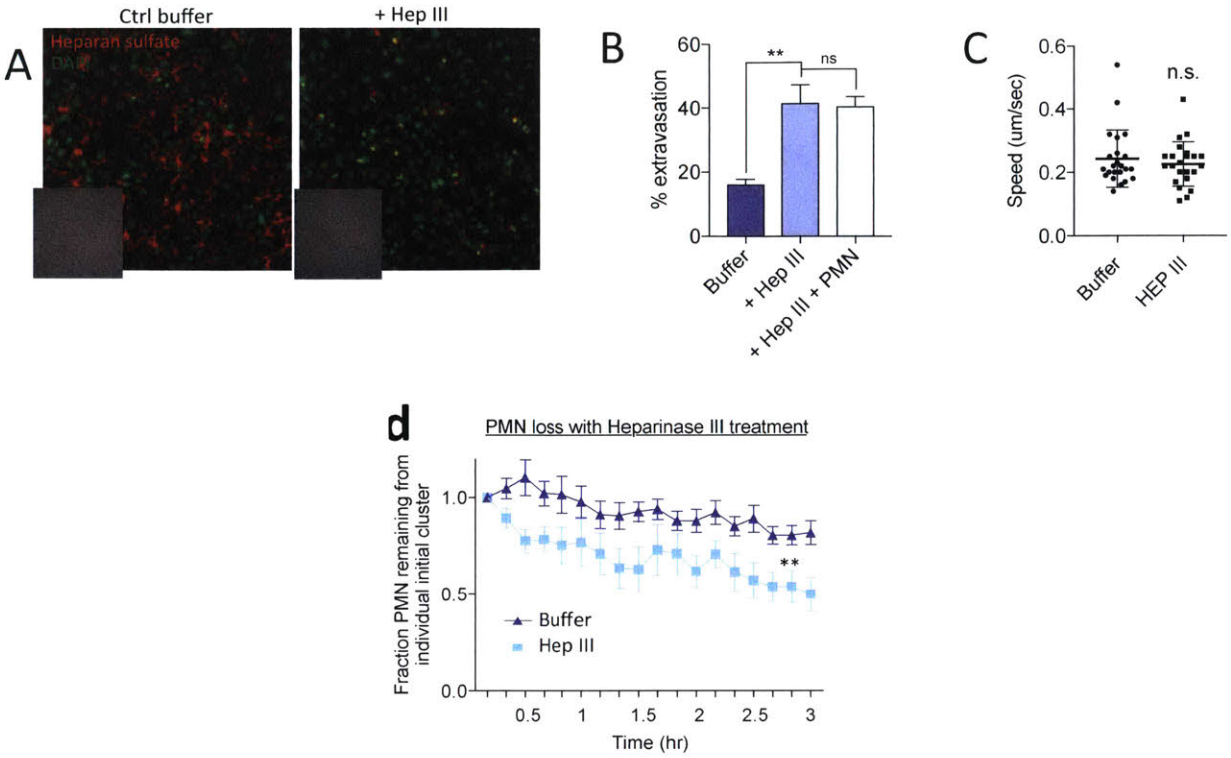

Figure 33. (A) Representative immunostaining (and phase – inset) of heparan sulfate (red) and nucleus (green) on the surface of HUVEC monolayers after 2 hours of treatment with 3U/mL of heparinase III. **(B)** Extravasation rates (at 6 hours) of MA2 alone or MA2 + stimulated PMNs without or without pre-treatment of microvascular heparinase III. **(C)** Migration speed of stimulated PMNs in microvasculature without or without pre-treatment with heparinase III. (**D**) Quantification of fraction of PMNs remaining in TC-PMN clusters over 3 hours (10 min time steps) when the micro-vessels were pre-treated with heparinase III (to degrade the heparan sulfate groups) or buffer and washed prior to MA2-PMN perfusion (n>3 devices/condition, with at least 5 clusters per device). *p<0.05, **p<0.01, ***p<0.001, error=s.e.m.

Lastly, since we observed the ability of tumor and PMN perfusion to up-regulate endothelial ICAM-1, we sought to confirm whether PMN confinement at clusters was due to chemotaxis towards soluble factors, rather than differences in the availability of adhesion receptors on the endothelium. Since PMNs can be found to transmigrate into the extravascular space and migrate within the perivascular space, we analyzed the migration behavior of extravascular PMNs only (**Figure 34**). PMNs were first categorized into "free" and "cluster associated populations. Interestingly, "free" PMNs were much more likely to extravasate compared to "cluster-associated" PMNs, while device treatment with anti-IL-8 and anti-CXCL-1 increased "cluster-associated" PMN extravasation rates only slightly (**Figure 34C**). While extravascular PMN migration speeds were slightly lower than intravascular migration speeds likely due to steric hindrance in the matrix, there were no significant differences in speeds between the extravascular

subpopulations even in the presence of blocking antibodies. However, migration tracks revealed that extravascular PMNs still exhibited similar dispersion patterns to the respective cases where intra- and extravascular PMNs were not distinguished, suggesting that chemotactic confinement is still effective even in the perivascular matrix (**Figure 34D-F**).

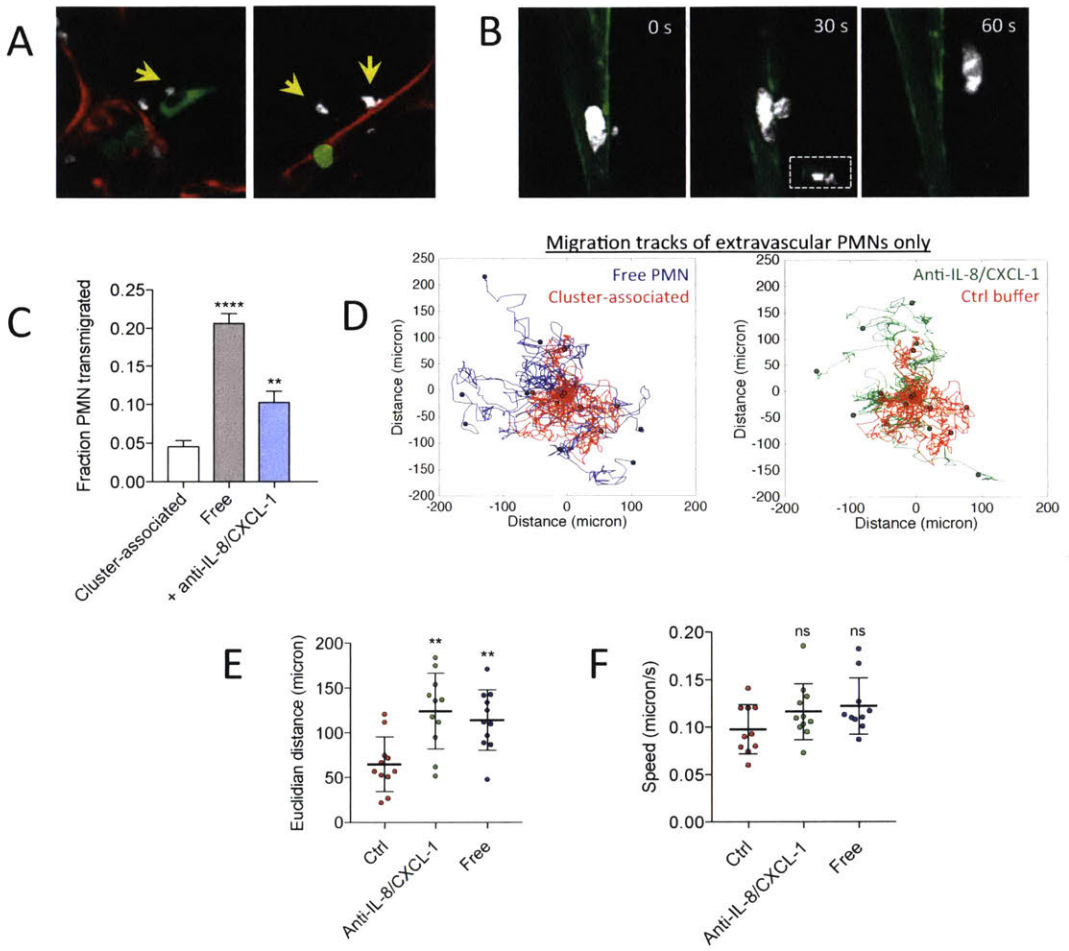

Figure 34. (A) Representative images of both extravasated tumor cells (green) and extravasated PMNs (white) from within microvasculature (red). **(B)** Representative image of a typical transmigrating PMN from microvasculature occurring within 60 s. **(C)** Fraction of PMNs in each subpopulation (cluster-associated, free or associated with antibody treatment) which transmigrate into the extravascular matrix (at least once) over the span of 3 hours post seeding (n=4 devices/condition) **(D)** Migration tracks of extravascular PMNs that are cluster associated, free, or cluster associated and treated with anti-IL-8 and anti-CXCL-1 (8 representative PMN tracks plotted per condition). **(E)** Euclidian distance from original position of extravascular PMNs. **(F)** Migration speed of extravascular PMNs (n=9 cells per condition).

Altogether, our results suggest that PMNs initially associated with TCs are further sequestered at clusters, mainly via an autologous chemotactic response to their own IL-8. Chemokine immobilization on the endothelial glycocalyx further acts to enhance the level of ligand at the cluster vicinity.

4.5 Presence of PMNs enhance TC transendothelial migration rates in addition to attenuating TC loss from shear flow

We next asked whether the sequestration of PMNs at TC-PMN clusters could directly influence the extravasation potential of tumor cells. Sequestration could act to localize pro- or anti- extravasation factors secreted by PMNs, or act as a contact-dependent facilitator (e.g. open the endothelial barrier by transmigrating themselves or act as a protective shield against blood flow) or barrier (e.g. steric hindrance preventing tumor access to the endothelium) for extravasation. We began by deciphering how TC-PMN clustering and PMN confinement could influence both tumor cell retention, and the ability of tumor cells to cross the endothelial barrier.

We found that the numbers of MA2 or MDA-MB-231 arrested in the microvasculature within the first 5 minutes were not significantly different when co-perfused with LPS stimulated PMNs, suggesting little effect on initial TC arrest (**Figure 35A**). However, after 30 minutes of continued media flow (no cells) through the microvascular bed, the percentage of tumor cells retained (out of the number trapped at 5 minutes), was significantly higher for both MA2 and MDA-MB-231 cells with PMNs, and this difference persisted for up to 2.5 hr of flow (**Fig 35B**). We also note that the size of trapped tumor clusters was not significantly different when co-perfused with PMNs, indicating that increased retention is likely due to stronger adhesions of the arrested tumor cell to the surrounding endothelium with PMNs present, rather than differences in the physical size of clusters formed (**Figure 35C**). Thus, PMNs do not promote initial arrest of tumor cells but rather enhance their resistance to intraluminal shear over time, which may be partially due to the CD11b-ICAM-1 interactions we and others[116,117] observed earlier.

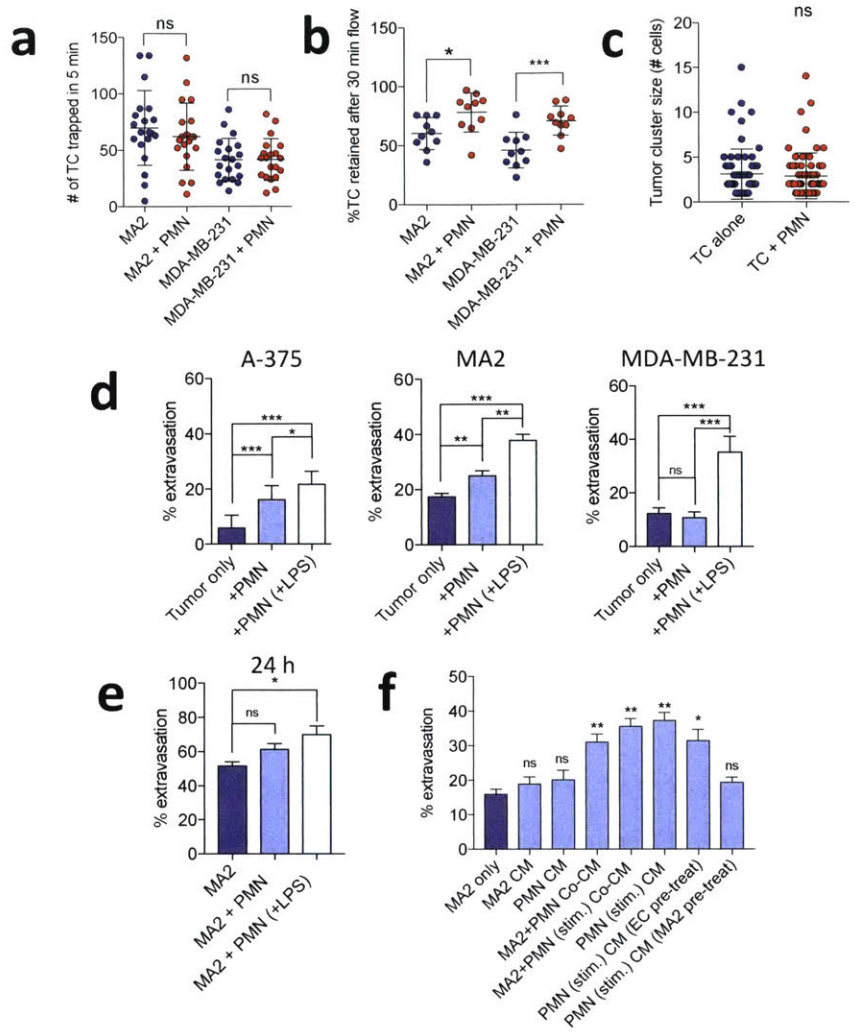

Figure 35. Presence of PMNs enhance TC transendothelial migration rates in addition to attenuating TC loss due to shear flow. (A) Number of tumor cells arrested in microvessels during an initial 5 minute perfusion, with or without PMNs. (B) Percentage of tumor cells retained in devices when flow is continued for 30 minutes (n>10 devices/condition, error bars indicate SD, *p<0.05, ***p<0.001). (C) The number of TCs in individual TC clusters when co-perfused with or without PMNs (n>48 clusters over 5 devices, error bars indicate SD, *p<0.05, ***p<0.001). (D) Extravasation rates at 6 hrs of A375, A-375-MA2 and MDA-MB-231 when co-perfused with quiescent PMNs or LPS activated PMNs at a 1:5 ratio (rates are calculated as the number extravasated over those retained rather than initial numbers arrested, in order to decouple the effects of retention). (E) Extravasation rates of MA2 at 24 hours post TC-PMN perfusion. (F) Extravasation rates of MA2 at 6 hours when co-incubated with conditioned media (CM) generated from various conditions (n>9 devices/condition, error bards indicate SEM, *p<0.01, **p<0.001, ***p<0.0001).

In order to de-couple the effects of PMNs on TC retention and the potential ability of PMNs to directly modulate TC or EC behavior, extravasation rates were determined as the number of transmigrated cells divided by the number retained after 30 minutes of flow. This metric was valid since we observed

tumor cell retention rates to plateau beyond 30 minutes. Melanoma cell lines A375 and A375-MA2 (highly metastatic) and the breast cell line MDA-MB-231 were co-perfused with either quiescent or PMNs pre-stimulated with LPS (then washed). Addition of quiescent PMNs with A375 or MA2 resulted in significant increases in tumor cell transmigration, while addition of inflamed PMNs resulted in even higher levels. Interestingly, transmigration rates of MDA-MB-231 only increased when LPS-stimulated PMNs were perfused (**Figure 35D**). The pro-extravasation effects of inflamed PMNs continued for as long as 24 hours (**Figure 35E**). When the pro-retention effects of PMNs were not decoupled, the differences between extravasation rates (taken over the initial number of cells at t=0 min instead of t=30 min) were even greater. Thus, our results indicate that beyond protecting TC loss from flow, PMNs can additionally enhance the ability of TCs to cross the endothelial barrier.

To determine whether the pro-extravasation effect of PMNs was due to the action of secreted factors or juxtacrine effects, MA2 cells were perfused only in the presence of conditioned media (CM). CM from LPS stimulated neutrophils and MA2-PMN (stimulated) co-culture resulted in significant increases in transmigration compared to quiescent PMN or MA2 CM (**Figure 35F**). Pre-treatment of ECs with the same CM also increased extravasation, while pre-treatment of MA2 cells did not, indicating a stronger effect on ECs. Interestingly, CM from MA2-quiescent PMN co-culture also increased extravasation, suggesting that MA2s alone have the potential to activate PMNs without LPS stimulation. In fact, co-incubation of PMNs with all of our tumor cells lines or their conditioned media resulted in increases in surface CD11b expression, indicating PMN activation. Combined, this suggests that a key mechanism by which PMNs enhance transmigration of tumor cells is via release of cytokines from activated PMNs, rather than contact-dependent mechanisms.

4.6 PMN confinement at the vicinity of TC clusters enhances TC extravasation through sequestration of PMN-derived IL-8

In order to determine the cytokine(s) responsible for the pro-extravasation effect of PMNs, we looked to our cytokine array for factors up-regulated in stimulated PMNs or when co-incubated with MA2s. Upon LPS stimulation, PMNs dramatically increased the secretion of IL-8, IL-6 and CCL4 compared to negligible levels in unstimulated PMNs, and produced CXCL-7 in both unstimulated and stimulated states. Co-incubation of stimulated PMNs with MA2 cells did not induce further production of these cytokines beyond summed levels, nor any other cytokines originally not produced by either cell type alone. To determine whether any of these cytokines affected MA2 extravasation, co-perfused devices were further incubated with antibodies against IL-8, IL-6, CCL4 and CXCL-7 during the entire 6-hr

extravasation assay. Only blocking of IL-8 produced a significant reduction in transmigration, while neutralization of all others showed no appreciable response (**Figure 36A**).

To decipher the target of IL-8, MA2s or HUVEC networks were pre-treated with recombinant human hIL-8 at varying concentrations (0-500 ng/mL) for 3 hours, followed by tumor cell perfusion without PMNs. Extravasation rates increased in a dose dependent manner when HUVECs were pre-treated with IL-8, while no changes were observed with MA2 pre-treatment, consistent with our previous results with conditioned media (**Figure 36B**). Furthermore, permeability to 70kDa dextran begins to increase significantly when HUVECs are treated with > 50 ng/mL of rh-IL-8, suggesting that PMN-derived IL-8 may act to weaken the integrity of the endothelial barrier when present at high enough concentrations.

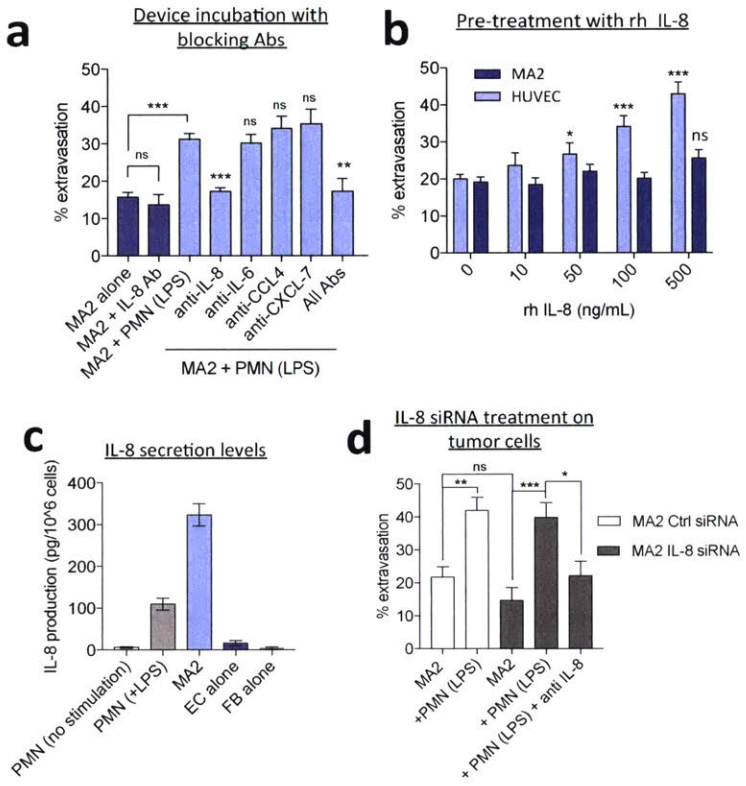

Figure 36. IL-8 released by LPS stimulated neutrophils increases TC transmigration rates. (A) Extravasation rates of MA2 in the presence of neutralizing antibodies at 6 hrs post injection. (B) Effect of micro vessel or MA2 pre-incubation with various concentrations of recombinant IL-8, on MA2 extravasation rates at 6 hrs post injection. (C) Production of IL-8 by LPS stimulated neutrophils compared to MA2 inherent secretion (in pg/million cells). (D) Tumor (MA2) IL-8 secretion was inhibited via siRNA to decouple tumor IL-8 from PMN IL-8. (*p<0.01, **p<0.001, ***p<0.0001, n=3 independent experiments each with 3 devices/condition).

Since MA2 produced IL-8 on the same order of magnitude as stimulated PMNs (300 pg/10^6 cells and 100 pg/10^6 cells, respectively) (**Figure 36C**), we sought to determine whether *additional* levels of IL-8 from PMNs could enhance extravasation independent of MA2 produced IL-8. Tumor cells were again treated with IL-8 siRNA prior to perfusion to attenuate protein secretion during the assay. Co-perfusion of MA2 IL-8si with simulated PMNs still resulted in increases in transmigration rates to levels remarkably similar to MA2 control siRNA with PMNs. Incubation with anti-IL-8 reversed this behavior (**Figure 36D**). Treatment of MA2 with IL-8 siRNA did not affect their own ability to extravasate. Thus, while MA2-derived IL-8 may be below the threshold level to induce appreciable consequences in transmigration, PMN-derived IL-8 alone may be sufficient. Taken together, LPS-stimulated PMNs can enhance extravasation in two ways: (1) increase the absolute number of possible extravasation events by enhancing tumor cell retention, and (2) facilitate tumor transendothelial migration via PMN-derived IL-8, likely via disruption of the endothelial barrier.

Since PMNs can facilitate tumor transmigration via the action of secreted IL-8, we asked whether PMN sequestration at TC-PMN clusters via autologous chemotaxis is indeed critical to the effectiveness of this mechanism. In an attempt to de-couple the effect of PMN-dispersion from the possible direct effect of IL-8 on TC or EC function, we first separated TCs into two sub-populations: PMN-associated and non-associated. Approximately 75% of trapped cells were PMN-associated, ~20% non-associated. Importantly, we found extravasation rates of PMN-associated tumor cells to be significantly higher compared to non-associated cells, strongly suggesting the presence of a proximity-dependent effect of PMNs on neighboring tumor and endothelial cells (**Figure 37A**). Furthermore, neutralizing both IL-8 and CXCL-1 not only abrogates PMN sequestering at clusters, but also causes a significant decrease in the extravasation rates of PMN-associated TCs. Conversely, there is no effect on extravasation rates of the "non-associated" subpopulation, further suggesting a direct correlation between IL-8+CXCL-1-dependent confinement and extravasation (**Figure 37B**). Combined with earlier results showing the ability of both PMN-derived and recombinant IL-8 to enhance extravasation, it is highly likely that PMN sequestration at TC-PMN clusters is critical in the pro-extravasation effect of PMNs by localizing IL-8 to sites of tumor arrest. Without PMN confinement, secreted IL-8 may not reach an effective mean concentration, because the sources are too spatially dispersed.

Importantly, we found that increased dispersion of PMNs from clusters is correlated with an augmented loss of PMNs from the entire microvascular network (**Figure 37B**). It is likely that "free" PMNs are more prone to loss, while PMNs sequestered in clusters benefit from increased protection from shear flow. Indeed, the loss of "free" PMNs was significantly higher compared to the loss of PMNs that were originally "cluster-associated," after 6 hours of flow (**Figure 37C**), despite the fact that "free" PMNs have a higher propensity to extravasate. Taken together, confinement of PMNs in clusters may

enhance the numbers of PMNs arrested in the microvasculature and be necessary for enabling the pro-extravasation effect of PMNs by localizing IL-8 to sites of tumor arrest.

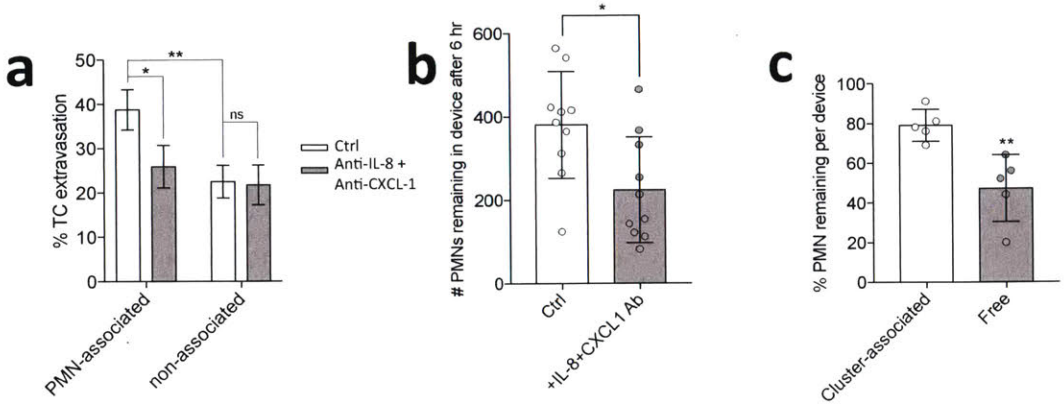

Figure 37. PMN confinement at TC-PMN clusters increases extravasation rates of cluster-associated TCs through sequestration of IL-8 and further prevents PMN loss due to flow (A) Percentage of tumor cells extravasated in the PMN-associated or non-associated subpopulations, either with or without the presence of anti-IL-8 and anti-CXCL-1 to attenuate confinement. Extravasation rates of non-associated TCs do not change in the presence of antibodies (n=6 devices, error bars indicate SEM, *p<0.05, **p<0.01). (B) Percentage of original (at t=0) PMNs remaining in micro-vessel beds after 6 hours of flow in the absence or presence of anti-IL8 + anti-CXCL-1 (n=10 devices, error bars indicate SD, *p<0.05). (C) Percentage of PMNs remaining in cluster-associated or free subpopulations after 6 hours of flow (with MA2 co-perfusion). Each point represents the average of at least 5 clusters across 5 R.O.I, or at least 20 free PMN over 5 R.O.I.

4.7 Discussion

While the roles of neutrophils at the primary tumor site have been extensively studied, whether neutrophils play pro- or anti- metastatic functions during hematogenous dissemination is less clear. Importantly, it has been shown that primary tumor resection surgeries are associated with high rates of infections, and that these complications are correlated with adverse oncological outcomes independent of the morbidity associated with the infectious insult[107–109]. Combined with the fact that resection surgeries often shed tumor cells into the circulation[112,113], it has become apparent that neutrophils, the first line of defense in the body, may play an important role linking infection, inflammation and metastasis. In this study, we aimed to understand the dynamic roles of inflamed neutrophils in the specific steps of tumor cell arrest and extravasation.

To decipher these roles, we employ a unique *in vitro* model of the human microvasculature, which enables us to dynamically visualize tumor-neutrophil-endothelial interactions at spatial and temporal resolutions that would otherwise be challenging in *in vivo* systems. Compared to Transwell assays or parallel flow chambers, we are able to recapitulate key events such as the physical trapping and arrest of tumor cells and neutrophils in vessels with diameters and flow patterns comparable to those of *in vivo* microvasculature[26,114]. This is key since TC-PMN clustering, PMN sequestration and the formation of chemokine gradients (while relevant in the context of *in vivo* vasculature) may not occur in static assays or even those involving flow over an open endothelial monolayer. Furthermore, our vascular beds are embedded within thin (<150 micron) hydrogels, which limit vessels to approximately one plane of view. This facilitates high temporal-resolution tracking of rapidly migrating neutrophils (<30 second per frame) compared to intravital imaging in thicker *in vivo* tissues that are either less optically accessible or require longer imaging times to capture out-of-plane migration events. Importantly, we can easily determine the spatial relationships between tumor, neutrophils and endothelial cells, enabling robust categorization of tumor cells and neutrophils into various sub-populations such as "PMN-associated" tumor cells and "cluster-associated" PMNs. Understanding the minute differences in behavior between cell sub-populations within the same vascular bed was key to our understanding of chemotaxis and sequestration, which would not have been possible if cells were lumped into one category.

It has been previously shown in mouse models of dissemination that arrested tumor cells can co-localize with neutrophils, through integrins[102,103], NETs[110] or even through the attraction of platelets[27]. Huh and colleagues showed that melanoma ICAM-1 and PMN CD11b/beta-2 facilitated the aggregation of the two cell types within a parallel flow chamber. However, realistically, TCs and PMNs interact in narrow capillaries (rather than a flat surface) where physical occlusion and increased contact area with the endothelium may play a more significant role. By coupling both mechanisms in our assay, we show that not only can tumor ICAM-1/PMN CD11b interactions modulate cell clustering, physical trapping under flow can also play a role. Furthermore, we find that up-regulation of endothelial ICAM-1 upon contact with tumor cells and PMNs can greatly enhance co-localization rates, and that this adhesion may play a stronger role than TC ICAM-1. This suggests that aggregation and adhesion of PMNs intraluminally depends strongly on the presence of tumor cells to upregulate endothelial ICAM-1, likely via tumor inflammatory mediators[118].

The initial co-localization of tumor cells and neutrophils via adhesive interactions may be an important pre-requisite for the sequestration of PMNs. We have observed, for the first time, that these cluster-associated neutrophils remain confined to approximately a 70-micron radius of the original TC-

PMN cluster, via an autologous chemotactic mechanism to tumor- and PMN-derived chemokines. This behavior exists even without appreciable neutrophil recruitment from other distant sites, as the initial levels of PMNs in clusters formed during intravascular arrest are sufficient to establish a chemokine source. In particular, we find that the presence of PMN-secreted IL-8 is critical for chemotaxis in this specific context, compared to tumor-secreted IL-8 or CXCL-1.

While neutrophil chemotaxis has generally been well studied in the context of extravascular gradients [119], chemotaxis can also occur intraluminally, such as in the case of MIP-2 generation from an extravascular source[120]. In this instance, gradients are established in spite of blood flow by the immobilization of the chemokine by the endothelial glycoclayx. Hpa-tg mice, which express truncated heparan sulfate chains, exhibited random PMN intraluminal migration[120]. In this study, we show PMN sequestration in tumor clusters may also depend on a similar mechanism of IL-8 binding to heparan sulfate groups on endothelial syndecan-2[115]. Indeed, our numerical simulations suggest that under flow conditions, mean concentrations of IL-8 may be on the lower end of the spectrum required for PMN response[121], and it is possible that IL-8 binding to the endothelial glycocalyx significantly enhances the level of IL-8 available on the luminal surface. It follows that degradation of heparan sulfate groups in our micro-vessels with heparinase III decreased the level of confinement of cluster-associated PMNs. Lastly, it is worth noting that in addition to PMN and TC derived cytokines, other cells in the system can modulate the spatial distribution of chemokines. For instance, we find that HUVECs can also secrete low levels of IL-8 basally, and that this expression is up regulated upon exposure to inflammatory factors such as TNF-a or LPS (but interestingly not by MA2 tumor conditioned media). Thus, it is likely that endothelial cells themselves can produce[122] or even internalize[123] IL-8 or other chemokines, further complicating gradient profiles.

Confinement of PMNs at arrested tumor foci may be a key pre-requisite for the pro-extravasation effect of PMNs to take effect. Direct co-perfusion of tumor cells with stimulated PMNs results in significant increases in extravasation in a paracrine manner. Inflamed PMNs secrete high levels of IL-8, which, in addition to acting as a chemotactic source, can independently disrupt the endothelial barrier, facilitating the invasion of trapped tumor cells into the extravascular matrix. It is likely that the sequestration of PMNs at tumor foci allows IL-8 to be highly localized and act effectively on the adjacent endothelium. The significant increase in the number of co-localized PMNs per tumor cluster upon LPS treatment may further exacerbate this effect. Indeed, the subpopulation of "PMN-associated" tumor cells showed significantly higher transmigration rates than "non-associated" tumor cells, within the same device. Furthermore, extravasation rates in PMN-associated TCs decreased upon neutralization of

chemotactic factors IL-8 and CXCL-1, but not in the non-associated population, strongly suggesting that PMN confinement is critical for the effects of PMN-derived IL-8 to be exerted.

Previous studies have implicated IL-8 in arrest and extravasation in the presence of neutrophils. Specifically, melanoma-derived IL-8 can upregulate CD11b on PMNs, facilitating their aggregation with entrapped tumor cells and promoting retention[102,117]. This leads to an increase in tumor cell transmigration events due to the greater number of tumor cells attached to the endothelial monolayer that are available to extravasate. While we have also found IL-8 to be the key effector in our system, our study is the first to implicate a direct effect of IL-8 and its sequestration near tumor cells on tumor cell transendothelial migration, and that this is not merely a consequence of altered TC retention rate. Furthermore, we show that rather than tumor-derived IL-8, it is PMN-derived IL-8 that is mainly responsible for this specific mechanism.

The phenotypic state of neutrophils in the peripheral blood can be heterogeneous depending on environmental factors such the presence of a primary tumor or systemic inflammation. For instance, in the presence of a growing tumor, subclinical changes in leukocyte compositions and numbers can occur at distant sites to favor metastatic growth[124,125]. In the present study, we primarily focused on deciphering the link between systemic inflammation and hematogenous dissemination. As such, most of our experiments were performed with LPS-pre-stimulated neutrophils to mimic the inflamed phenotype that would be typically found during severe infection. Interestingly, we find that even without pre-stimulation, initially non-stimulated PMNs are still capable of elevating extravasation when co-perfused with tumor cells in the microvasculature (albeit to a lesser degree than stimulated PMNs). Furthermore, pre-treatment of vascular beds with conditioned media from MA2-PMN (quiescent) co-culture also induces similar effects. This suggests that tumor cells alone can stimulate neutrophils, resulting in an alternate activation pathway that also results in the release of pro-extravasation factors. It has previously been suggested that without exogenous stimulation, melanoma secreted IL-8 can stimulate neutrophils to further produce IL-8 and that this interaction promotes increased tumor-PMN binding and hence metastasis[102]. While we do not find IL-8 secretion in co-culture to be above the summed values of individual sources, we observe that co-incubation of melanoma cells with quiescent PMNs up regulates CD11b.-Furthermore, co-incubation of PMNs with the breast cancer cell line MDA-MB-231 does not produce pro-extravasation effects, except when PMNs are pre-stimulated. We conclude that the ability of tumor cells to activate PMNs and produce pro-extravasation factors is cell line specific, whereas in the case of systemic infection, PMNs can enhance tumor extravasation without cell-type specificity.

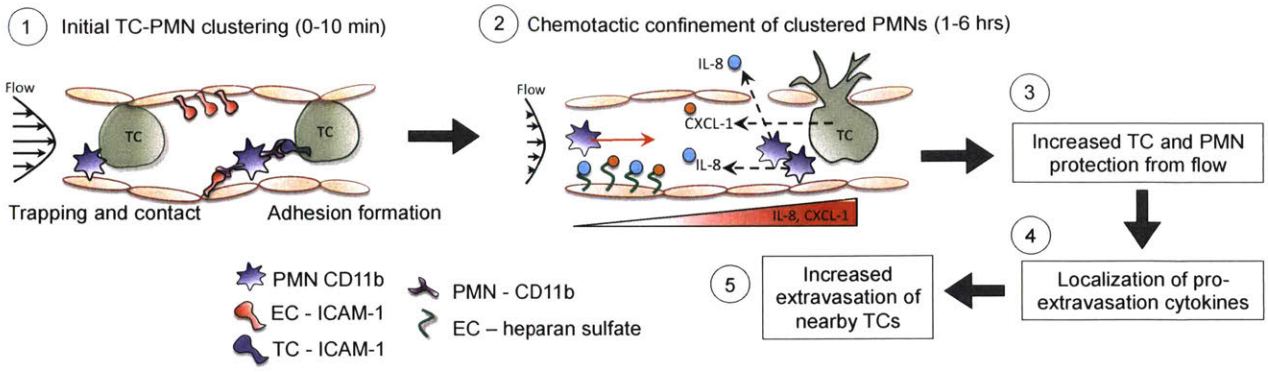

Figure 38. Working hypothesis for PMN-TC interactions during extravasation. (1) PMNs and TCs decelerate and arrest in clusters under flow in narrow capillaries from physical trapping. Increased contact time may facilitate engagement of CD-11b to EC-ICAM-1 and to TC-ICAM-1, enhancing PMN-TC associations. EC-ICAM is further upregulated upon TC contact, which may enhance PMN adhesion. (2) Once clustered, highly migratory PMNs continue to be sequestered in clusters due the action of PMN-derived IL-8 tumor derived CXCL-1. This chemotactic confinement of PMNs is enhanced by immobilization of chemokines on the EC glycocalyx. (3) The the occlusion of vessels by PMN-TC clusters promotes both TC and PMN retention by decreasing levels of flow entering the vessel segment. (4) Confinement of PMNs results in the spatial localization of pro-transmigration cytokines. (5) One of these factors could be IL-8, which plays an additional role of enhancing extravasation potential of tumor cells, such as through the weakening of the endothelial barrier. Dotted arrows indicate chemokine secretion, red arrow indicates migration direction.

In summary, employing an *in vitro* model of human microvasculature, we show that inflamed neutrophils and tumor cells can arrest and co-localize intravascularly to form TC-PMN clusters under flow, and that their formation is dependent on endothelial ICAM-1 up-regulated upon tumor cell contact (**Figure 38**). We show, for the first time, that after initial arrest, "cluster-associated" PMNs are further sequestered within the cell aggregates via autologous chemotaxis to tumor- and PMN-derived CXCL-1 and IL-8 respectively, and that this effect is enhanced via chemokine immobilization to luminal endothelial heparan sulfate groups. Sequestration of PMNs at clusters enables IL-8 to spatially localize and accumulate and facilitating tumor cell extravasation.

Chapter 5

Conclusions and future work

5.1 Conclusions

Despite the fact that metastasis is the leading cause of cancer related deaths, many of the biological mechanisms that drive this key process remain poorly understood. Metastasis is the sequence of events by which cancer spreads from the primary tumor via hematogenous or lymphatic dissemination, resulting in downstream colonization at remote, secondary sites, often the liver, lung, brain or bone marrow[126]. This complex cascade of events is initiated by the invasion of primary tumor cells into surrounding tissues, and entry into the vasculature, followed by transport and intravascular arrest at a distant site, extravasation, and finally, cell proliferation and formation of metastatic foci. In particular, tumor cell extravasation is thought to be an essential and possibly rate-limiting step, as most metastases are found in the extravascular space rather than intraluminal. Thus, it is of utmost importance that we understand the effectors and signaling pathways that regulates the extravasation process. However, these aspects of the metastatic cascade remain less understood, largely due to the technical challenges associated with imaging, throughput, isolation, and analysis of circulating tumor cells that have disseminated into visceral, distance organs. A fundamental understanding of these steps will also likely lead to improved methods for screening of potential therapeutic agents targeted at inhibiting extravasation.

In this thesis, we present the engineering of an *in vitro* model of the human microcirculation with the capability to recapitulate discrete steps of early metastatic seeding, including arrest, transendothelial migration and early micrometastases formation. The microdevice features self-organized human microvascular networks with physiologically relevant microvessel diameters, through which tumor and various host cells can be perfused and easily tracked over time via standard confocal microscopy. Contrary to most *in vivo and ex* vivo extravasation assays, robust and rapid scoring of extravascular cells combined with high-resolution imaging with high magnification (short working distance) objectives can

be easily achieved due to the confinement of the vascular network to one plane close to the surface of the device. This renders extravascular cells clearly distinct and allows tumor cells of interest to be identified quickly compared to those in thick tissues. The ability to generate large numbers of devices per experiment coupled with fast quantitation further allows for highly parametric studies, which is required when testing multiple genetic or pharmacological perturbations. This is coupled with the capability for live tracking of single cell extravasation events allowing both tumor and endothelial morphological dynamics to be observed in high detail with a moderate number of data points.

After biological characterization and functional testing, we applied our extravasation assay to probe a variety of biological questions in order to gain a deeper mechanistic understanding of the process of tumor cell extravasation, in ways that are technically challenge *in vivo*. Harnessing our advantages of increased throughput and higher spatio-temporal resolution, we studied role tumor integrins and how their interactions with endothelial cells and perivascular matrix proteins can modulate extravasation. Results from our assay reveal that tumor beta-1 integrin is critical for successful transendothelial migration in a variety of tumor cell lines and due in part to the inability to maintain filipodial protrusions into the subendothelial matrix via integrin engagement and recruit of F-actin to the protrusion tip. Specifically, adhesion via $\alpha 3\beta 1$ and $\alpha 6\beta 1$ to subendothelial laminin was a critical prerequisite for successful transmigration. Additionally, after clearing the endothelial barrier, $\beta 1$ is required for invasion past the BM and migration away from the abluminal surface. Finally, we show that $\beta 1$ depletion, but not alpha integrin depletion, reduces extravasation *in vivo* and inhibits metastatic colonization, suggesting that the cumulative defects in the extravasation cascade due to $\beta 1$ depletion ultimately impairs metastasis formation. Combined, these novel findings may be useful when designing future therapeutic integrin targets to curtail the progression of the extravasation cascade.

Recently, much attention has been directed to the role of "pre-metastatic" niches, which consist of complex tumor-host cell interactions during circulation, extravasation and re-colonization. For instance, circulating immune cells including platelets and leukocytes have been shown to interact with tumor cells, and can act to enhance metastasis [42,64,127]. To probe the interactions between various circulating cell types, we first demonstrate the ability augment the complexity and relevance of the extravasation microenvironment in our micro-devices and apply it to deduce novel biological insights. In particular, we co-perfuse human leukocytes and tumor cells and monitored their interactions on a single level in the circulation. Results from our assay reveals that PMNs and tumor cells can aggregate together intraluminally in an adhesion dependent manner, which involves PMN-CD11b and endothelial ICAM-1 that is upregulated upon tumor cell contact. Following arrest, PMNs are further confined via an

autologous chemotaxis mechanisms towards PMN-derived IL-8 and tumor derived CXCL-1, chemokines which are immobilized on the surface of the endothelium via heparan sulfate groups. Importantly, sequestration of PMNs with tumor clusters results in the localization PMN-derived IL-8, which acts to increase the extravasation rates of associated tumor cells.

5.2 Future directions

Engineering and Methodology

In vitro platforms should not only offer not only advantages such as low cost and simplicity of application, it should allow for high throughput and highly parametric testing of multiple conditions that is difficult in an *in vivo* set-up. In particular, the increasing popularity, development and robustness of RNAi strategies and genome editing techniques such as CRISPR has allowed high throughput production of knockdown or knockout cell lines targeting genes that could be relevant to metastasis. Thus, it is crucial that the *in vitro* screening technologies are improved to achieve the level of high throughput parametric and even combinatorial testing that is required. Currently, our microfluidic chip has been improved to increase the output of microvascular beds by a factor of ~5, using the same number of starting cells and seeding time. The branching method allows for parallel seeding, cutting down seeding times, dead-volumes, and the variability in cell concentrations from device to device, effectively increasing robustness of device perfusability. Up to 56 independent devices can be generated with 2 million endothelial cells. However, there is still great room for improvement. For instance, automated gel injection using a syringe pump could decrease the user-to –user variability in injection speeds (and hence shear stresses), which can cause differences in polymerized gel architectures. Moreover, while cell-gel injection is parallelized, perfusion of tumor cells and quantification methods currently remain unchanged. Tumor cell suspensions are manually injected into each device, rendering it particularly time consuming when multiple replicates of multiple conditions are required, causing numbers to quickly grow large. This issue may be addressed by designing a modular "tumor cell perfusion" manifold which can be attached onto the top of the PDMS chip after gel injection, and feature a branching channel network capable of delivering tumor cells into multiple devices from a single injection port. Another outstanding issue is one of data acquisition and analysis. Increasing the device throughput also increases the imaging burden, since a minimum number of tumor cells need to be imaged per device to collect sufficient data, and the z-resolution must be fine enough to allow adequate 3D reconstruction for analysis. The most viable solution is to change the imaging modality to epifluorescence microscopy, where multiple stacks can be taken per region of interest at high magnifications, then processed via deconvolution algorithms to achieve the

cross-sectional details of the tumor cells in the z-dimension. Using this imaging mode, the optimal configurations must be determined to give an adequate level of z-resolution for analysis while significantly reducing the speed of acquisition compared to conventional laser-scanning confocal microscopy. Lastly, image analysis can greatly benefit from automation. This requires sequential algorithms to (1) segment the surfaces of the endothelial cell channel and the tumor cell channel, (2) identify then discretize individual tumor cells when present in clusters, (3) extrapolate the cross-sectional data and store as sets of coordinates, (4) determine, based on concavity of the cross-section of vessels, where the intraluminal and extravascular regions are located (4) and last, apply distance transformations to determine the position of the tumor cell surfaces relative to the intra- and extra-vascular regions.

Biological questions

By increasing the level of complexity of the micro device, one can further augment the realism of the extravasation model, and in turn apply the model to answer relevant mechanistic questions. Recently, much attention has been directed to the role of "pre-metastatic" niches, which consist of complex tumor-host cell interactions during circulation, extravasation and re-colonization. For instance, circulating immune cells including platelets and leukocytes have been shown to interact with tumor cells, and can act to enhance metastasis [42,64,127]. We demonstrate that human platelets and/or leukocytes isolated from whole human blood can be perfused with tumor cells and immune-tumor interactions can be monitored in the μVN micro devices and that an effect of co-culture on extravasation efficiency can be detected. Additionally, the contribution of stromal cells such as pericytes can also be investigated by seeding these cells together with HUVECs in the same gel region. There is also increasing evidence favoring the "seed and soil" theory for metastatic cancer cells, which suggest that some cancer cell types display increased propensity to "home" to and/or subsequently colonize certain organs. While the current device cannot be used to model homing processes such as selective arrest (since tumor cells flow into and are physically trapped in the vasculature), it is possible to use the assay to understand how different "organ-microenvironments" influence extravasation and subsequently tumor cell proliferation, beyond extravasation. Such organ-mimicking microenvironments may be achieved by adding relevant cell types to the matrix, allowing either direct physical contact or paracrine communication, depending on the choice of cell arrangement in the various micro-channels. For instance, bone- or muscle-mimicking extravasation microenvironments were recapitulated in our model by co-culturing HUVECs with osteo-differentiated primary hBM-MSCs or C2C12 (myoblasts), respectively. Extravasation rates were significantly different in co-culture and mono-culture environments, suggesting key roles for organ-specific host stromal cells in modulating the factors controlling extravasation [128]. These micro devices can

be very useful tools for studying organ specific microenvironments and metastatic "niches"; they thus complement *in vivo* studies by providing relatively higher throughput and kinetic cell migration data.

Lastly, there is potential, after more development, for the assay to be used to study early micrometastases formation via prolonged culture of microdevices (e.g. >24 hours). We have found that μVNs can remain relatively stable between days 1-6 post tumor cell seeding, such that the morphological changes of the μVNs (i.e. vessel diameter, interconnectivity) are small enough that the same vessel segments can be recognized and tracked as culture progresses[51]. In this time frame, various tumor cell lines can be seen to migrate into the extravascular space as well as proliferate extravascularly. However, the relevance of these results may greatly depend on the stromal microenvironment, thus it may be necessary to consider the presence of stromal cells such as fibroblasts, pericytes, macrophages and others that have been implicated with proliferation and survival in the perivascular niche. Taken together, this assay has the potential to further the understanding of the underlying mechanisms of extravasation, which is critical for the development of therapeutic opportunities at distinct stages of cancer progression.

References

1. Nguyen, D. X., Bos, P. D. & Massagué, J. Metastasis: from dissemination to organ-specific colonization. *Nat. Rev. Cancer* **9,** 274–84 (2009).
2. Hanahan, D. & Weinberg, R. A. Hallmarks of cancer: the next generation. *Cell* **144,** 646–74 (2011).
3. Joyce, J. A. & Pollard, J. W. Microenvironmental regulation of metastasis. *Nat. Rev. Cancer* **9,** 239–52 (2009).
4. Carmeliet, P. & Jain, R. K. Molecular mechanisms and clinical applications of angiogenesis. *Nature* **473,** 298–307 (2011).
5. Psaila, B. & Lyden, D. The metastatic niche: adapting the foreign soil. **9,** 285–293 (2009).
6. Crissman, J. D., Hatfield, J. S., Menter, D. G., Sloane, B. & Honn, K. Y. Morphological Study of the Interaction of Intra vascular Tumor Cells with Endothelial Cells and Subendothelial Matrix1. 4065–4072 (1988).
7. Bussard, K. M., Gay, C. V & Mastro, A. M. The bone microenvironment in metastasis; what is special about bone? *Cancer Metastasis Rev.* **27,** 41–55 (2008).
8. Fidler, I. J. The role of the organ microenvironment in brain metastasis. *Semin. Cancer Biol.* **21,** 107–12 (2011).
9. Miles, F. L., Pruitt, F. L., van Golen, K. L. & Cooper, C. R. Stepping out of the flow: capillary extravasation in cancer metastasis. *Clin. Exp. Metastasis* **25,** 305–24 (2008).
10. Grzesiak, J. J. *et al.* Knockdown of the β(1) integrin subunit reduces primary tumor growth and inhibits pancreatic cancer metastasis. *Int. J. Cancer* **129,** 2905–15 (2011).
11. Imanishi, Y. *et al.* Angiopoietin-2 Stimulates Breast Cancer Metastasis through the 5 1 Integrin-Mediated Pathway. *Cancer Res.* **67,** 4254–4263 (2007).
12. Reymond, N., D'Água, B. B. & Ridley, A. J. Crossing the endothelial barrier during metastasis. *Nat. Rev. Cancer* **13,** 858–70 (2013).
13. Chambers, A. F., Groom, A. C. & MacDonald, I. C. Dissemination and growth of cancer cells in metastatic sites. *Nat. Rev. Cancer* **2,** 563–72 (2002).
14. Shin, Y. *et al.* Microfluidic assay for simultaneous culture of multiple cell types on surfaces or within hydrogels. *Nat. Protoc.* **7,** 1247–59 (2012).
15. Polacheck, W. J., Li, R., Uzel, S. G. M. & Kamm, R. D. Microfluidic platforms for mechanobiology. *Lab Chip* **13,** 2252–67 (2013).
16. Roussos, E. T., Condeelis, J. S. & Patsialou, A. Chemotaxis in cancer. *Nat. Rev. Cancer* **11,** 573–87 (2011).
17. Mierke, C. T. Cancer cells regulate biomechanical properties of human microvascular endothelial cells. *J. Biol. Chem.* **286,** 40025–37 (2011).
18. Roussos, E. T. *et al.* Mena invasive (MenaINV) promotes multicellular streaming motility and transendothelial migration in a mouse model of breast cancer. *J. Cell Sci.* **124,** 2120–31 (2011).
19. Song, J. W. *et al.* Microfluidic endothelium for studying the intravascular adhesion of metastatic breast cancer cells. *PLoS One* **4,** e5756 (2009).
20. Shin, M. K., Kim, S. K. & Jung, H. Integration of intra- and extravasation in one cell-based microfluidic chip for the study of cancer metastasis. *Lab Chip* **11,** 3880–7 (2011).

21. Jeon, J. S., Zervantonakis, I. K., Chung, S., Kamm, R. D. & Charest, J. L. In vitro model of tumor cell extravasation. *PLoS One* **8,** e56910 (2013).

22. Zhang, Q., Liu, T. & Qin, J. A microfluidic-based device for study of transendothelial invasion of tumor aggregates in realtime. *Lab Chip* **12,** 2837–42 (2012).

23. Chaw, K. C., Manimaran, M., Tay, E. H. & Swaminathan, S. Multi-step microfluidic device for studying cancer metastasis. *Lab Chip* **7,** 1041–7 (2007).

24. Zheng, Y. *et al.* In vitro microvessels for the study of angiogenesis and thrombosis. *Proc. Natl. Acad. Sci. U. S. A.* **109,** 9342–7 (2012).

25. Kim, Y. *et al.* Quantification of cancer cell extravasation in vivo. *Nat. Protoc.* **11,** 937–948 (2016).

26. Chen, M. B., Lamar, J. M., Li, R., Hynes, R. O. & Kamm, R. D. Elucidation of the roles of tumor integrin ss1 in the extravasation stage of the metastasis cascade. *Cancer Res.* 1–13 (2016). doi:10.1158/0008-5472.CAN-15-1325

27. Labelle, M., Begum, S. & Hynes, R. O. Platelets guide the formation of early metastatic niches. *Proc. Natl. Acad. Sci. U. S. A.* **111,** E3053-61 (2014).

28. Stoletov, K. *et al.* Visualizing extravasation dynamics of metastatic tumor cells. *J. Cell Sci.* **123,** 2332–41 (2010).

29. Song, J. W. *et al.* Microfluidic endothelium for studying the intravascular adhesion of metastatic breast cancer cells. *PLoS One* **4,** e5756 (2009).

30. Labelle, M., Begum, S. & Hynes, R. O. Direct signaling between platelets and cancer cells induces an epithelial-mesenchymal-like transition and promotes metastasis. *Cancer Cell* **20,** 576–90 (2011).

31. Kienast, Y. *et al.* Real-time imaging reveals the single steps of brain metastasis formation. *Nat. Med.* **16,** 116–22 (2010).

32. Francia, G., Cruz-munoz, W., Man, S., Xu, P. & Kerbel, R. S. Mouse models of advanced spontaneous metastasis for experimental therapeutics. **11,** 135–141 (2011).

33. Kitamura, T. *et al.* CCL2-induced chemokine cascade promotes breast cancer metastasis by enhancing retention of metastasis-associated macrophages. *J. Exp. Med.* **212,** 1043–1059 (2015).

34. Qian, B. *et al.* A distinct macrophage population mediates metastatic breast cancer cell extravasation, establishment and growth. *PLoS One* **4,** e6562 (2009).

35. Stoletov, K., Montel, V., Lester, R. D., Gonias, S. L. & Klemke, R. High-resolution imaging of the dynamic tumor cell vascular interface in transparent zebrafish. *Proc. Natl. Acad. Sci. U. S. A.* **104,** 17406–11 (2007).

36. Leong, H. S. *et al.* Invadopodia are required for cancer cell extravasation and are a therapeutic target for metastasis. *Cell Rep.* **8,** 1558–70 (2014).

37. Koop, S. *et al.* Fate of melanoma cells entering the microcirculation: Over 80% survive and extravasate. *Cancer Res.* **55,** 2520–2523 (1995).

38. Koop, S. *et al.* Independence of metastatic ability and extravasation: metastatic ras-transformed and control fibroblasts extravasate equally well. *Proc. Natl. Acad. Sci. U. S. A.* **93,** 11080–11084 (1996).

39. Lii, J. *et al.* Real-time microfluidic system for studying mammalian cells in 3D microenvironments. *Anal. Chem.* **80,** 3640–7 (2008).

40. Boussommier-Calleja, A., Li, R., Chen, M. B., Wong, S. C. & Kamm, R. D. Microfluidics: A New Tool for Modeling Cancer–Immune Interactions. *Trends in Cancer* **2,** 6–19 (2016).

41. Ganguly, K. K., Pal, S., Moulik, S. & Chatterjee, A. Integrins and metastasis. 251–261 (2013).

42. Labelle, M. & Hynes, R. O. The initial hours of metastasis: the importance of cooperative host-tumor cell interactions during hematogenous dissemination. *Cancer Discov.* **2,** 1091–9 (2012).

43. Luzzi, K. J. *et al.* Multistep nature of metastatic inefficiency: dormancy of solitary cells after successful extravasation and limited survival of early micrometastases. *Am. J. Pathol.* **153,** 865–73 (1998).

44. Albini, A. & Benelli, R. The chemoinvasion assay: a method to assess tumor and endothelial cell invasion and its modulation. *Nat. Protoc.* **2,** 504–511 (2007).

45. Roussos, E. T., Condeelis, J. S. & Patsialou, A. Chemotaxis in cancer. *Nat. Rev. Cancer* **11,** 573–87 (2011).

46. Zervantonakis, I. K. *et al.* Three-dimensional microfluidic model for tumor cell intravasation and endothelial barrier function. *Proc. Natl. Acad. Sci. U. S. A.* **109,** 13515–20 (2012).

47. Hsu, Y.-H. *et al.* Full range physiological mass transport control in 3D tissue cultures. *Lab Chip* (2012). doi:10.1039/c2lc40787f

48. Kim, J. *et al.* Engineering of a Biomimetic Pericyte-Covered 3D Microvascular Network. *PLoS One* **10,** e0133880 (2015).

49. Kim, S., Lee, H., Chung, M. & Jeon, N. L. Engineering of functional, perfusable 3D microvascular networks on a chip. *Lab Chip* **13,** 1489–500 (2013).

50. Shin, Y. *et al.* Microfluidic assay for simultaneous culture of multiple cell types on surfaces or within hydrogels. *Nat. Protoc.* **7,** 1247–59 (2012).

51. Whisler, J. a, Chen, M. B. & Kamm, R. D. Control of perfusable microvascular network morphology using a multiculture microfluidic system. *Tissue Eng. Part C. Methods* **20,** 543–52 (2014).

52. Ehsan, S. M. *et al.* A three-dimensional in vitro model of tumor cell intravasation. *Integr. Biol.* **6,** 603–610 (2015).

53. Ghajar, C. M. *et al.* The perivascular niche regulates breast tumour dormancy. *Nat. Cell Biol.* **15,** 807–817 (2013).

54. Kim, J. *et al.* Implantable microfluidic device for the formation of three-dimensional vasculature by human endothelial progenitor cells. *Biotechnol. Bioprocess Eng.* **19,** 379–385 (2014).

55. Sheikh, S., Rainger, G. E., Gale, Z., Rahman, M. & Nash, G. B. Exposure to fluid shear stress modulates the ability of endothelial cells to recruit neutrophils in response to tumor necrosis factor- _ : a basis for local variations in vascular sensitivity to inflammation. **102,** 2828–2834 (2003).

56. Nagrath, S. *et al.* Isolation of rare circulating tumour cells in cancer patients by microchip technology. *Nature* **450,** 1235–9 (2007).

57. Chrobak, K. M., Potter, D. R. & Tien, J. Formation of perfused, functional microvascular tubes in vitro. *Microvasc. Res.* **71,** 185–96 (2006).

58. Miao, H. *et al.* Effects of flow patterns on the localization and expression of VE-cadherin at vascular endothelial cell junctions: in vivo and in vitro investigations. *J. Vasc. Res.* **42,** 77–89 (2005).

59. Mierke, C. T. *et al.* Breakdown of the endothelial barrier function in tumor cell transmigration. *Biophys. J.* **94,** 2832–46 (2008).

60. Weis, S., Cui, J., Barnes, L. & Cheresh, D. Endothelial barrier disruption by VEGF-mediated Src

activity potentiates tumor cell extravasation and metastasis. *J. Cell Biol.* **167,** 223–9 (2004).

61. Mantovani, A., Cassatella, M. a, Costantini, C. & Jaillon, S. Neutrophils in the activation and regulation of innate and adaptive immunity. *Nat. Rev. Immunol.* **11,** 519–531 (2011).

62. van Zijl, F., Krupitza, G. & Mikulits, W. Initial steps of metastasis: cell invasion and endothelial transmigration. *Mutat. Res.* **728,** 23–34 (2011).

63. Quail, D. F. & Joyce, J. a. Microenvironmental regulation of tumor progression and metastasis. *Nat. Med.* **19,** 1423–37 (2013).

64. Kitamura, T., Qian, B.-Z. & Pollard, J. W. Immune cell promotion of metastasis. *Nat. Rev. Immunol.* **15,** 73–86 (2015).

65. Hynes, R. O. Integrins : Bidirectional , Allosteric Signaling Machines In their roles as major adhesion receptors , integrins. **110,** 673–687 (2002).

66. Orini, M. M. *et al.* THE _ 3 NL 1 INTEGRIN IS ASSOCIATED WITH MAMMARY CARCINOMA CELL METASTASIS , INVASION , AND GELATINASE B (MMP-9) ACTIVITY. **342,** 336–342 (2000).

67. Trikha, M., Clerck, Y. A. De & Markland, F. S. Metastatic a Snake Venom Disintegrin , Inhibits 1J @ Cell Adhesion and Blocks Experimental Human Melanoma. 4993–4998 (1994).

68. Lahlou, H. & Muller, W. J. B1-Integrins Signaling and Mammary Tumor Progression in Transgenic Mouse Models: Implications for Human Breast Cancer. *Breast Cancer Res.* **13,** 229 (2011).

69. Huck, L., Pontier, S. M., Zuo, D. M. & Muller, W. J. beta1-integrin is dispensable for the induction of ErbB2 mammary tumors but plays a critical role in the metastatic phase of tumor progression. *Proc. Natl. Acad. Sci. U. S. A.* **107,** 15559–64 (2010).

70. Mitra, a K. *et al.* Ligand-independent activation of c-Met by fibronectin and α(5)β(1)-integrin regulates ovarian cancer invasion and metastasis. *Oncogene* **30,** 1566–76 (2011).

71. White, D. E. *et al.* Targeted disruption of NL 1-integrin in a transgenic mouse model of human breast cancer reveals an essential role in mammary tumor induction. **6,** 159–170 (2004).

72. Weaver, V. M. *et al.* Reversion of the Malignant Phenotype of Human Breast Cells in Three-Dimensional Culture and In Vivo by Integrin Blocking Antibodies. **137,** 231–245 (1997).

73. Liu, Y. *et al.* Cleaved high-molecular-weight kininogen and its domain 5 inhibit migration and invasion of human prostate cancer cells through the epidermal growth factor receptor pathway. *Oncogene* **28,** 2756–65 (2009).

74. Yoshimura, K. *et al.* Integrin alpha2 mediates selective metastasis to the liver. *Cancer Res.* **69,** 7320–8 (2009).

75. Ramirez, N. E. *et al.* The α 2 β 1 integrin is a metastasis suppressor in mouse models and human cancer. **121,** (2011).

76. Brakebusch, C. *et al.* b 1 integrin promotes but is not essential for metastasis of ras-myc transformed ® broblasts. **1,** 3852–3861 (1999).

77. Zhou, B. *et al.* Integrin α3β1 can function to promote spontaneous metastasis and lung colonization of invasive breast carcinoma. *Mol. Cancer Res.* **12,** 143–54 (2014).

78. Qian, F., Zhang, Z.-C., Wu, X.-F., Li, Y.-P. & Xu, Q. Interaction between integrin alpha(5) and fibronectin is required for metastasis of B16F10 melanoma cells. *Biochem. Biophys. Res. Commun.* **333,** 1269–75 (2005).

79. Felding-habermann, B. Integrin adhesion receptors in tumor metastasis. 203–213 (2003).

80. Reticker-Flynn, N. E. *et al.* A combinatorial extracellular matrix platform identifies cell-extracellular matrix interactions that correlate with metastasis. *Nat. Commun.* **3,** 1122 (2012).

81. Desgrosellier, J. S. & Cheresh, D. a. Integrins in cancer: biological implications and therapeutic opportunities. *Nat. Rev. Cancer* **10,** 9–22 (2010).

82. Ahmed, N., Riley, C., Rice, G. & Quinn, M. Role of integrin receptors for fibronectin, collagen and laminin in the regulation of ovarian carcinoma functions in response to a matrix microenvironment. *Clin. Exp. Metastasis* **22,** 391–402 (2005).

83. Beaty, B. T. *et al.* β1 integrin regulates Arg to promote invadopodial maturation and matrix degradation. *Mol. Biol. Cell* **24,** 1661–75, S1-11 (2013).

84. Shibue, T. & Weinberg, R. A. Integrin NL 1 -focal adhesion kinase signaling directs the proliferation of metastatic cancer cells. **106,** (2009).

85. Wang, D. *et al.* The pivotal role of integrin β1 in metastasis of head and neck squamous cell carcinoma. *Clin. Cancer Res.* **18,** 4589–99 (2012).

86. Wang, H. *et al.* Tumor cell alpha3beta1 integrin and vascular laminin-5 mediate pulmonary arrest and metastasis. *J. Cell Biol.* **164,** 935–41 (2004).

87. Lamar, J. M. *et al.* The Hippo pathway target, YAP, promotes metastasis through its TEAD-interaction domain. *Proc. Natl. Acad. Sci.* **109,** E2441–E2450 (2012).

88. Stern, P. *et al.* A system for Cre-regulated RNA interference in vivo. *Proc. Natl. Acad. Sci. U. S. A.* **105,** 13895–900 (2008).

89. Chen, M. B., Whisler, J. A., Jeon, J. S. & Kamm, R. D. Mechanisms of tumor cell extravasation in an in vitro microvascular network platform. *Integr. Biol.* **5,** 1262–1271 (2013).

90. Chen, M. B., Whisler, J. a, Jeon, J. S. & Kamm, R. D. Mechanisms of tumor cell extravasation in an in vitro microvascular network platform. *Integr. Biol. (Camb).* **5,** 1262–71 (2013).

91. Gorelik, E., Wiltrout, R. H., Okumura, K., Habu, S. & Herberman, R. B. Role of NK cells in the control of metastatic spread and growth of tumor cells in mice. *Int. J. Cancer* **30,** 107–112 (1982).

92. Destaing, O. *et al.* NL 1A Integrin Is a Master Regulator of Invadosome Organization and Function. **21,** 4108–4119 (2010).

93. Haidari, M. *et al.* Integrin α2β1 mediates tyrosine phosphorylation of vascular endothelial cadherin induced by invasive breast cancer cells. *J. Biol. Chem.* **287,** 32981–92 (2012).

94. Maschler, S. *et al.* Tumor cell invasiveness correlates with changes in integrin expression and localization. *Oncogene* **24,** 2032–41 (2005).

95. Yurchenco, P. D. Basement membranes: Cell scaffoldings and signaling platforms. *Cold Spring Harb. Perspect. Biol.* **3,** 1–27 (2011).

96. Mueller, S. C. *et al.* A Novel Protease-docking Function of Integrin at Invadopodia. *J. Biol. Chem.* **274,** 24947–24952 (1999).

97. Sameni, M., Dosescu, J., Yamada, K. M. & Sloane, B. F. Functional live-cell imaging demonstrates that beta(1)-integrin promotes type IV collagen degradation by breast and prostate cancer cells. **7,** 199–213 (2009).

98. Noh, H., Eomm, M. & Han, A. Usefulness of pretreatment neutrophil to lymphocyte ratio in predicting disease-specific survival in breast cancer patients. *J. Breast Cancer* **16,** 55–59 (2013).

99. Wculek, S. K. & Malanchi, I. Neutrophils support lung colonization of metastasis-initiating breast cancer cells. *Nature* **advance on,** 1–21 (2015).

100. Coffelt, S. B. *et al.* IL-17-producing γδ T cells and neutrophils conspire to promote breast cancer metastasis. *Nature* **522,** 345–8 (2015).

101. Bald, T. *et al.* Ultraviolet-radiation-induced inflammation promotes angiotropism and metastasis in melanoma. *Nature* **507,** 109–13 (2014).

102. Huh, S. J., Liang, S., Sharma, A., Dong, C. & Robertson, G. P. Transiently entrapped circulating tumor cells interact with neutrophils to facilitate lung metastasis development. *Cancer Res.* **70,** 6071–82 (2010).

103. Spicer, J. D. *et al.* Neutrophils promote liver metastasis via Mac-1-mediated interactions with circulating tumor cells. *Cancer Res.* **72,** 3919–3927 (2012).

104. Granot, Z. *et al.* Tumor entrained neutrophils inhibit seeding in the premetastatic lung. *Cancer Cell* **20,** 300–314 (2011).

105. Granot, Z. & Jablonska, J. Distinct Functions of Neutrophil in Cancer and Its Regulation. *Mediators Inflamm.* **2015,** (2015).

106. Rebecca, S., Deepa, N. & Ahmedin, J. Cancer Statistics, 2013. *Cancer* **37,** 408–14 (2013).

107. Lin, J. K. *et al.* The Influence of Fecal Diversion and Anastomotic Leakage on Survival after Resection of Rectal Cancer. *J. Gastrointest. Surg.* **15,** 2251–2261 (2011).

108. Auguste, P. *et al.* The Host Inflammatory Response Promotes Liver Metastasis by Increasing Tumor Cell Arrest and Extravasation. *Am. J. Pathol.* **170,** 1781–1792 (2007).

109. Schussler, O. *et al.* Postoperative pneumonia after major lung resection. *Am. J. Respir. Crit. Care Med.* **173,** 1161–1169 (2006).

110. Cools-Lartigue, J. & Spicer, J. Neutrophil extracellular traps sequester circulating tumor cells and promote metastasis. *J. Clin. ...* **123,** 3446–3458 (2013).

111. Tohme, S. *et al.* Neutrophil Extracellular Traps Promote the Development and Progression of Liver Metastases after Surgical Stress. *Cancer Res.* 2015–2016 (2016). doi:10.1158/0008-5472.CAN-15-1591

112. Guller, U. *et al.* Disseminated single tumor cells as detected by real-time quantitative polymerase chain reaction represent a prognostic factor in patients undergoing surgery for colorectal cancer. *Ann. Surg.* **236,** 768-75–6 (2002).

113. Liu, Z., Jiang, M., Zhao, J. & Ju, H. Circulating tumor cells in perioperative esophageal cancer patients: Quantitative assay system and potential clinical utility. *Clin. Cancer Res.* **13,** 2992–2997 (2007).

114. Chen, M. B., Whisler, J. a, Jeon, J. S. & Kamm, R. D. Mechanisms of tumor cell extravasation in an in vitro microvascular network platform. *Integr. Biol. (Camb).* **5,** 1262–71 (2013).

115. Halden, Y. *et al.* Interleukin-8 binds to syndecan-2 on human endothelial cells. *Biochem. J.* **377,** 533–8 (2004).

116. Liang, S., Slattery, M. J. & Dong, C. Shear stress and shear rate differentially affect the multi-step process of leukocyte-facilitated melanoma adhesion. *Exp. Cell Res.* **310,** 282–92 (2005).

117. Dong, C., Slattery, M. J., Liang, S. & Peng, H.-H. Melanoma cell extravasation under flow conditions is modulated by leukocytes and endogenously produced interleukin 8. *Mol. Cell. Biomech.* **2,** 145–59 (2005).

118. Burke-Gaffney, a & Hellewell, P. G. Tumour necrosis factor-alpha-induced ICAM-1 expression in human vascular endothelial and lung epithelial cells: modulation by tyrosine kinase inhibitors. *Br J Pharmacol* **119,** 1149–1158 (1996).

119. Lämmermann, T. *et al.* Neutrophil swarms require LTB4 and integrins at sites of cell death in vivo. *Nature* **498,** 371–5 (2013).

120. Massena, S. *et al.* Achemotactic gradient sequestered on endothelial heparan sulfate induces directional intraluminal crawling of neutrophils. *Blood* **116,** 1924–1931 (2010).

121. Li Jeon, N. *et al.* Neutrophil chemotaxis in linear and complex gradients of interleukin-8 formed in a microfabricated device. *Nat. Biotechnol.* **20,** 826–30 (2002).

122. Bont, E. S. J. M. De, Nijhuis, C. S. M. O., Vellenga, E., Daenen, S. M. G. J. & Kamps, W. a. Endothelial Cells Are Main Producers of Interleukin 8 through Toll-Like Receptor 2 and 4 Signaling during Bacterial Infection in Leukopenic Cancer Patients Endothelial Cells Are Main Producers of Interleukin 8 through Toll-Like Receptor 2 and 4 Signaling . **10,** 2–8 (2003).

123. Middleton, J. *et al.* Transcytosis and surface presentation of IL-8 by venular endothelial cells. *Cell* **91,** 385–395 (1997).

124. Hiratsuka, S., Watanabe, A., Aburatani, H. & Maru, Y. Tumour-mediated upregulation of chemoattractants and recruitment of myeloid cells predetermines lung metastasis. *Nat. Cell Biol.* **8,** 1369–75 (2006).

125. Kaplan, R. N. *et al.* VEGFR1-positive haematopoietic bone marrow progenitors initiate the pre-metastatic niche. *Nature* **438,** 820–827 (2005).

126. Nguyen, D. X., Bos, P. D. & Massagué, J. Metastasis: from dissemination to organ-specific colonization. *Nat. Rev. Cancer* **9,** 274–84 (2009).

127. Spiegel, a. *et al.* Neutrophils suppress intraluminal NK-mediated tumor cell clearance and enhance extravasation of disseminated carcinoma cells. *Cancer Discov.* (2016). doi:10.1158/2159-8290.CD-15-1157

128. Jeon, J. S. *et al.* Correction for Jeon et al., Human 3D vascularized organotypic microfluidic assays to study breast cancer cell extravasation. *Proc. Natl. Acad. Sci. U. S. A.* **112,** E818 (2015).

129. Levario, T. J., Zhan, M., Lim, B., Shvartsman, S. Y. & Lu, H. Microfluidic trap array for massively parallel imaging of Drosophila embryos. *Nat. Protoc.* **8,** 721–36 (2013).

Appendix A

Protocol for extravasation assay (single device)

Materials

Device Fabrication

- Photoresist SU-8 100 (for photolithography; Microchem)
- Photomask with microdevice design (available for download in Supplementary Information)
- Dow corning Sylgard 184 Silicone Encapsulant Clear (Ellesworth, Cat. no. 184 SIL ELAST KIT 0.5KG)
- Biopsy punches (Ted Pella, Cat. no. 15110-40)
- Razor blades (Ted Pella, Cat. no. 121-32)
- Scalpel
- No.1 22X40 mm glass coverslips (VWR, Cat. no. 48393-048)
- Scotch tape

Cell seeding

- Human umbilical vein endothelial cells (p8 or lower, Lonza, Cat. no. CC-2517) and normal human lung fibroblasts (p15 or lower, Lonza, Cat. no. CC-2512)
- Fibrinogen (Sigma, Cat. no. F8630-1G)
- Thrombin (Sigma, Cat. no. T9549)
- Endothelial growth media (EGM-MV BulletKit™) (Lonza, Cat. no. CC-3202)
- Fibroblast growth media (FGM-2 BulletKit™) (Lonza, Cat. no. CC-3132)
- 0.05% trypsin (wt/vol) (ThermoFischer, Cat. no. 25300054)
- Hemocytometer or other cell counting tools
- Dulbecco's PBS (D-PBS, pH 7.2-7.4; Wisent, Cat. no. 311-010-CL)
- Sterile dH_2O
- DMEM GlutaMAX (ThermoFischer, Cat. no. 10566-016)
- FBS (ThermoFischer, Cat. no. 10437-010)
- Gel loading pipette tips (VWR, Cat. no. 37001-152)
- Pair of surgical scissors
- Humidity chambers (e.g. empty P1000 pipette tip boxes with rack, filled halfway from the bottom with sterile water) (e.g. VWR , Cat. No. 10034-060)

Equipment

- Vacuum desiccator (Cole Parmer, Cat. no. WU-06514-30)
- Drying oven (60 – 80°C)
- Benchtop centrifuge for use with 15 mL tubes
- Incubator at 37°C and 5% CO_2
- Autoclave
- Plasma cleaner (Harrick Plasma, Cat. no. PDC-001)
- Water bath at 37°C
- Confocal microscope with environmental chamber (maintained at 37°C and 5% CO_2) and motorized stage (optional)
- 3D imaging processing software (e.g. Imaris Bitplane (Belfast, UK))

REAGENT AND EQUIPMENT SET UP

Fibrinogen solution, 6 mg/mL: Dissolve 15 mg of bovine fibrinogen in 2.5 mL of sterile PBS (-/-) in a 15 mL tube by incubating the mixture in a 37°C water bath for 3 hours. Do not vortex. Sterile filter the solution (0.2 μm filter) and aliquot the dissolved fibrinogen mixture in 1 mL eppendorf tubes and store at 4°C until usage.

■ **PAUSE POINT** It is recommended that fibrinogen solutions be made on the day of or the day prior to expected use. Long-term storage of solutions is not recommended (thus dissolved solutions are generally one-time-use).

Thrombin solution, 100 U/mL: resuspend thrombin with sterile PBS (-/-) to a final concentration of 100 U/mL). Aliquot and store at -20°C until use.

HUVEC and FB cell culture: Thaw HUVECs and FBs until the required amount for the number of devices to be seeded (at least 1.5 x 10^6 HUVECs and 1 x 10^6 HLFs are required for a total of 12 devices). Cell numbers can be scaled accordingly if more or fewer devices are to be seeded.

■ **PAUSE POINT** Use lower passage HUVECs (<P8) for best μVN formation results, as endothelial cells become more senescent as passage number increases. Take care as to not allow HUVECs to become over-confluent prior to trypsinization.

Re-suspension media: Add 40 μL of thrombin stock solution to 1mL complete EGM-2MV to make 4U/mL thrombin solution. Keep media on ice until time of device seeding.

Preparation of humidity chambers: Prepare humidity chambers for device seeding by filling pipette tip boxes (with a removable rack) with water and autoclaving the whole box for 20 minutes. Set aside to cool, then transfer to a 37 °C incubator until time of device seeding.

PROCEDURE

PDMS device fabrication • TIMING 24 hrs

1. Fabricate the micro device wafer using the photo mask pattern given in this protocol. A channel height between 110-150 microns is optimal for the volumes and densities in this given protocol. Wafers can be made via SU-8 micro patterning methods that are established and detailed elsewhere [129] or via outsourcing. Silanize wafer overnight in a vacuum desiccator.
2. Fabricate and sterilize PDMS devices using the procedure outlined in our previous protocol (Steps 9-26 in Shin et al, Nature Protocols, 2012)[50]. We recommend punching 3 mm diameter holes for the media reservoirs and 1 mm diameter holes for gel injection ports (**Figure 1A**). Incubate bonded devices at 80°C for >24 before seeding to ensure that hydrophobicity is restored. Make sure to keep devices in sterile conditions until opening the device container under a sterile cell culture hood.

Seeding of endothelial cells and fibroblasts in microdevices for μVN formation • TIMING 2 hr for seeding and 4 days for culture

3. Make sure prepared devices are at room temperature.
4. Aliquot 8 μL of pre-made fibrinogen solution into 0.5mL eppendorf tubes. The number of aliquots made should be 2X the number of devices that will be seeded. Keep aliquots on ice.

▲ **CRITICAL STEP** Separate aliquots of fibrinogen are made for each individual gel region to be seeded because once thrombin is added to fibrinogen, gelation can occur in < 30 seconds.

5. Trypsinize HUVECs and FBs with 0.05% trypsin for 3 minutes, neutralize with EGM-2MV and centrifuge for 5 min at 200 g.
6. Aspirate media from the cell pellets and re-suspend the cells at 12 x 10^6/mL (HUVECs) and 6 x 10^6/mL (FBs) in re-suspension media. Keep cells on ice.

■ **PAUSE POINT** Make sure to aspirate as much of the supernatant as possible (e.g. by waiting a few seconds and aspirating the residual media), since the error in resuspended cell density can be easily increased and propagated when working with small volumes.

7. Mix 8 μL of HUVEC suspension with 8 μL of a fibrinogen aliquot by pipetting up and down 4-5 times. Withdraw 10 μL and immediately inject the HUVEC-gel mixture into the center gel region by slowly pipetting it (using a P10 pipette) via one injection port until the solution has reached halfway down the channel. Then, inject the rest of the mixture via the port on the other end of the channel, until the two interfaces of the gel meet in the middle. Retract the pipette tip slowly without releasing the injector. Repeat this process with the FBs by injecting the FB-fibrinogen mixture into the two flanking channels.

▲ **CRITICAL STEP** The cell-gel mixture must be injected slowly in order to prevent leakage into the media channels. It is recommended that injection into a single gel region be done by injecting halfway on both ends of the channel until the two interfaces meet. This decreases the risk of too much pressure building up at the inter-post interface causing gel bursting into the media channels.

■ **PAUSE POINT** Do not re-use the leftover fibrinogen-thrombin mixture in the aliquot for a subsequent device. Even if leftover the aliquot is still "liquid," injection of this leftover solution may result in gel fiber alignment in the device because the solution has already begun to polymerize.

?TROUBLESHOOTING

8. View the device in a sterile petri dish under a phase contrast or bright field microscope to ensure gels are intact and cells are homogeneously seeded.
9. Place the finished device into the humidity chamber and allow gelation for 15 minutes at room temperature. Repeat steps 7-8 with the rest of the devices.

▲ **CRITICAL STEP** Ensure that the cell solution is well mixed before withdrawing 10 μL each time as cells will sink to the bottom of the tube quickly resulting in inhomogeneous seeding densities.

10. After gelation of all devices, fill the media channels with EGM-2MV by forming a tight seal around the media port with the pipette tip. Depending on the size of the reservoir punched, the pipette tip may have to be cut to size in order to form a seal. Inject media until all reservoirs are filled.

OPTIONAL: Instead of filling with media, it is advised to dilute leftover HUVECs to 2M/mL in EGM-2MV and seed the cells in the media channels flanking the HUVEC gel region. Doing this will allow more consistent lumen opening to the media channel, since the monolayer formed in the media channel will sprout into the gel and "anastomose" with the vessel segments near the inter-post region, generating a wider opening for facilitation of tumor cell perfusion.

?TROUBLESHOOTING

11. Culture the devices at 37°C and 5% CO_2.

?TROUBLESHOOTING

12. Change the media in the devices every 24 hours by aspirating each media reservoir with a fine tipped gel-loading tip. Then fill all reservoirs on one side with media, wait until the media has flowed down the channel causing the media levels to rise in the opposing reservoir. Top off the reservoirs with more media until they are full. μVNs will be ready to perfuse on day 4-6.

Perfusion of tumor cells • TIMING 20 min to 1.5 h (if using cell tracker)

13. Briefly check the vessel openings at the inter-post regions to assess whether the vascular networks have formed connections with the media channel. Examples of connections (and lack of connections) can be found in **Supplementary Figure 2**, as well as the how perfusability is scored, and sample data on the typical number of perfusable devices that should be generated per experiment.

? TROUBLESHOOTING

14. Replace all media in the channels of the device with 0.1% BSA in PBS and incubate for 20 minutes to minimize unspecific adhesion of tumor cells to the glass during tumor perfusion. Replace with fresh EGM.
15. If live imaging will later be performed to track extravasation, HUVECs should be fluorescently labeled to robustly differentiate between intravascular and extravascular cells. This can be done by perfusing the device with cell-tracker or DiI solution in EGM-2MV and incubating for 1 hour at 37°C and 5% CO_2. After incubation, wash the device twice with EGM before proceeding. Skip this step if HUVECs have already been transfected to express a cytoplasmic or membrane fluorescent marker.

■ **PAUSE POINT** Apply a hydrostatic pressure drop across the HUVEC gel region to help the dye penetrate the entire μVN. A pressure drop of 4mm H_2O (equivalent to ~38 μL of solution in both reservoirs on one side of the gel region, for a 3 mm diameter reservoir) can be applied to promote convection and thus penetration of the dye throughout the vascular bed.

16. If tumor cells for perfusion are non-fluorescent, label cells by adding cell tracker™ or DiI solution directly to adhered cells after washing once with PBS, and following the manufacturer's instructions.
17. Aspirate the dye and wash adherent tumor cells twice with PBS. Trypsinize and re-suspend tumor cells to a final concentration of 5 x 10^5 cells/mL in EGM-2MV and store momentarily on ice. For suspended cells, dilute the dye further with buffer (PBS, HEPES or HBSS depending on the cell type) and wash via centrifugation. Re-suspend these cells to the desired concentration.
18. If perfusing platelets and/or neutrophils with tumor cells, mix the cells together to achieve the desired ratio.
19. With a gel-loading tip connected to an aspiration line, withdraw media from all 4 reservoirs directly flanking the HUVEC gel region. Mix the tumor cell suspension well, and fill one reservoir with 10 μL of cell suspension. Wait 5 seconds for the cells to flow down the medial channel (parallel to the gel). Aspirate all reservoirs again and apply 38 μL of cell suspension to both reservoirs on one side (this is creates a pressure drop of ~4mm H2O across the vascular bed). The volume should be adjusted if the reservoir diameter is different than 3 mm. Cells should now flow across the HUVEC gel region within the lumens due to the pressure drop. Check the device using bright field or phase contrast microscopy to ensure that cells are flowing through the μVNs (**Supplementary Movie 1**). Flowing cells can be clearly seen even at 10X magnification. Cells should gradually arrest in microvasculature due to size restriction. If vessel openings are small and few tumor cells flow through the capillary bed, use a fine pipette tip on an aspiration line to *gently* aspirate media from a downstream media port for 1-2 seconds.

? TROUBLESHOOTING

▲ **CRITICAL STEP** Aspirate gently and with a fine tip as to not form a tight seal with the media ports, which may cause the media channel to be fully aspirated, or cause vessels to rupture.

20. After ~5 minutes of tumor cell perfusion via hydrostatic pressure drop, fill the reservoirs on one end of the device and allow media to flow through the media channel (parallel to the gel region) to wash away remaining tumor cells. If constant perfusion of media is not required for the rest of the extravasation experiment, top off the media reservoirs with fresh EGM to prevent media drying. Devices can be maintained in an incubator until any desired time point, and extravasated cells can be imaged and analyzed by device fixation followed by confocal microscopy.

Alternatively, extravasation events on a single cell level can be monitored live via multi-area time-lapse imaging.

(Optional) Live imaging of transendothelial migration • TIMING 4 to 72 hours

21. Prepare the environmental chamber on the confocal microscope beforehand to assure that the chamber reaches a steady 37°C and 5% CO_2 by the time of tumor cell perfusion into the devices.
22. Immediately after step 19, transfer the device(s) in a sterile petri dish and secure the device onto the specimen holder in the environmental chamber.

▲ **CRITICAL STEP** Ensure that the chamber is well humidified and sealed for the entire duration of the time-lapse to prevent drying out and cell death.

■ **PAUSE POINT** Parafilm can be used to seal crevices and help create a well contained and humidified chamber.

23. Allow the device to rest on the specimen holder in the primed environmental chamber for at least 10 minutes before imaging to allow for thermal drift.
24. While waiting for equilibration of the device, set up the time-lapse parameters. For quantification of extravasation and/or real-time visualization of tumor cell protrusions during extravasation, use at least 20X objective (NA=0.75 resolution=800 X 800) or higher and at least 2 μm z-slice thickness. To track protrusion formation, image each region at least once every 20 minutes or faster, depending on the overall speed of protrusion onset and total translocation time for a particular cell type or condition. Set region locations if there are multiple areas of interest in the device. For quantification of extravasation efficiency of one device, select enough regions of interest to span the entire device – this typically yields approximately 40 to 150 tumor cells per sample. The extravasated fraction is calculated by dividing the number of extravasated cells in the entire device by the total number of tumor cells in these regions at t=0. This number is considered to be one data point. This data can be collected for both live imaging samples or fixed samples that have been incubated to a desired endpoint. For tracking of tumor cell proliferation, acquire images at least once every 5 hours for > 24 hours.

?TROUBLESHOOTING

25. Ensure the chamber is protected from other sources of light and begin the time lapse.

    ■ **PAUSE POINT** Avoid high laser intensities as this can cause photo toxicity and cell death during imaging.

?TROUBLESHOOTING

(Optional) Immunostaining and fluorescent visualization of cellular proteins and basement membrane • TIMING 24 hours (includes overnight incubation)

26. Devices can be fixed and stored for further imaging or immunofluorescent staining after a time-lapse, or directly after incubation to a desired time point. Aspirate all media reservoirs and fill all reservoirs on one side with 4% paraformaldehyde (~50 microliters per device). Allow the fluid to flow through the channels 2-3 times by aspirating the opposing reservoirs as they begin to fill. Incubate devices at RT in the dark for 10 minutes, then remove PFA from all reservoirs and replace with 1X PBS.

    ■ **PAUSE POINT** Fixed devices can now be stored for 2-3 weeks in a well sealed petri dish to prevent evaporation. Devices can later be used for imaging and/or immunofluorescent staining.

    ■ **PAUSE POINT** From this step, introduction of new solution will follow the same technique as step 25. Ensure the solution passes through the media channels at least 2-3 times before incubation.

27. To stain for intracellular proteins, permeabilize cells with 0.1% Triton X and incubate for 10 minutes. Wash twice with PBS, incubating 5 minutes per wash. For staining of basement membrane proteins, skip this step.
28. Block the device with 5% BSA and 3% goat serum in PBS for 3 hours at RT.
29. Dilute primary antibody of choice in the recommended dilution in blocking buffer (~30 microliters / device) and incubate it with the device overnight at 4°C in the dark.
30. Wash the devices with 0.5% BSA in PBS 5 times, at 15 minutes each.
31. Dilute secondary antibody of choice at 1:200 in washing buffer and incubate at RT in the dark for 3 h.
32. Remove secondary antibody from reservoirs and wash 3X with washing buffer, incubating 15 minutes per wash.
33. Image the device on a confocal microscope or store the device at 4°C. For visualization of basement membrane proteins such as collagen IV and/or laminin relative to extravasating tumor cells, acquire images at 60X for best results.

?TROUBLESHOOTING

Quantification and analysis of extravasation • TIMING 8 minutes per device

34. For quantification of extravasation for a single testing condition, images should either be acquired for the entire device (roughly equivalent to 5 regions of interest per device at 20X magnification) or the same number of arbitrary regions per device. Take images at a 2 μm z-slice size or thinner, to obtain adequate resolution during 3D image reconstruction for extravasation determination. Optimal microscope settings may depend on the fluorescent intensity of cultured cells and model of the microscope. See **Supplementary Table 1** for confocal settings used on an Olympus FV1000.
35. Using Imaris or other 3D rendering software such as the Image J "orthogonal views" function, score each individual cell as intravascular, mid-extravasation or extravascular (See **Figure 3** for examples of scoring).

?TROUBLESHOOTING

36. Calculate extravasation rate as the number of completely extravascular cells divided by the total number of cells in a single device.

    ■ **PAUSE POINT** Ensure that a sufficient number of total cells have been imaged per device before making extravasation calculations. Total number of imaged cells should ideally be in the range of 40 – 100 cells per device, given a perfusion concentration of ~0.5M/mL. Total cell counts that are too low results in large deviations in the extravasation rates between devices, and may not be very informative. However, perfusion of too many tumor cells per device (>200) should also be avoided since over-crowding of tumor cells will render it difficult to analyze via image analysis, or affect extravasation behaviors.
37. To quantify extravasation rates for a single treatment/condition, we advise to make the above quantification (Step 36) on at least 3 independent devices per experiment, and at least 3 independent experiments (i.e. a total of >9 devices per condition). The final extravasation rate can be calculated as the **mean** of the averages from each independent experiment.
38. To calculate rate of protrusion formation, analyze the status of the protrusion for individual tumor cells at multiple time frames (e.g. 20 minute frame intervals). The first time frame where a cell exhibits protrusion formation past the endothelium can be analyzed as the "time for protrusion onset" (**Figure 4A**). The same tumor cell can be followed until the cell has fully transmigrated past the endothelium. The time interval between full body transmigration and the initiation of protrusion can be analyzed as the "total time required for transmigration."

Appendix B

Modified protocol for seeding of multiplexed chips

1) Pour ~80-90 g of PDMS into wafer
2) Cure at 80C for at least 2 hours
3) Cut out PDMS carefully as to not damage/crack the SU-8 wafer (gray piece)
4) Cut and punch (3mm reservoir and 1mm gel injection port). Cut the device into rectangle following the surrounding borders of the device. Be careful to not touch any of the features.
5) Cover the device (both sides) with tape and then remove just before cleaning (step 6). Make sure ALL holes are punched at this point.
6) Clean (both devices and #1.5 coverglasses)
   a) Prepare a beaker of soapy water using soap and DI water from the tap
   b) Immerse PDMS/glass into soap
   c) Rinse thoroughly with autoclaved DI water (in the plastic Nalgene bottle with blue cap, next to the beige TC fridge. Make sure bottle has autoclave tape on it.)
   d) Spray wet device (both sides) with 70% ETOH
   e) Rinse thoroughly with autoclaved DI water
   f) Blow dry *immediately* using air in the fume hood
   g) Transfer to clean petri dish

7) **Bond (***Both 48 hours before seeding, to ensure complete and homogeneous hydrophobicity recovery***)**
   a) On for 1:30
   b) Pump until 2:00
   c) Turn on plasma slowly and treat until 3:20
   d) Bond by aligning the device with glass
   e) Press down gently with fingers on all the device features, including post areas and Christmas tree branching areas.
   f) Transfer to 60C oven

8) **Device seeding** (find 2 P200 pipettors)
   a) Remove devices and place in fridge to allow compaction
   b) Aliquot fibrin gel (2 per chip, at 25 uL each. Use a P200 pipette for this.)
   c) Re-suspend cells in EGM-thrombin mixture as usual (12M/mL EC; 4M/mL FB)
   d) Set **another** P200 pipette to 45 uL.
   e) Mix 25 ul of cell with the 25 uL fibrinogen aliquot. Mix 4 times and seed using the 45uL set pipette.
   f) Hold device so that the ECs will "sink" towards the direction of the FB channel (you might find that your right hand needs to cross over to the left side).
   g) Inject EC suspension by placing pipette as close to 90 degree a possible with device. Inject until you see the LAST gel region touch JUST the end of the channel (NOT including the downstream "neck" region).
   h) Repeat with FB. Devices should maintain in the same 90-degree orientation. Your right hand should now inject on the right side.
9) Place immediately in humid chamber.
10) Start time
11) Repeat on other CHIPS

12) Fill media when the first device has reached the 15 minute mark. Cut P200 tip.
13) Fill only to the **bottom of the downstream reservoir** and fill the downstream reservoir later. DO NOT make the media droplets coalesce.
14) Place CHIP into a 150mm dish.
15) Place a small petri dish filled with PBS on the side of the device, to maintain humidity during culture.

Changing media:

16) Aspirate ALL media reservoirs.
17) For fast media filling, take a 1mL of media and fill it in a continuous "line" down the 3mm reservoirs on the "E" side of the device. The media should flow very quickly down the channels. 20 sec later, top off the downstream "F" side channels with discrete drops of media. This should only take you <45 seconds per device.

Appendix C

Troubleshooting table for network formation

Problem	Possible cause	Potential solution
Gel does not eject from pipette into microdevice	Fibrin has gelled before injection	Pipette only 4-5 times when mixing aliquots to prevent premature gelation from shear stress Gels should be injected within 30 seconds of mixing fibrinogen with thrombin
Cell distribution is not homogeneous	Cell solution was not mixed well enough prior to combining with fibrinogen Injection speed is too high resulting in "alignment" of cells along the center region of the channel	Mix 12M/ml HUVEC solution well (with a P200 pipette) **each time** prior to withdrawing and mixing with a fibrinogen aliquot. Inject cells slowly to avoid gel "alignment" effect due to high shear-induced pre-mature polymerization.
Gel does not form a flat gel-media interface at the inter-post regions	Gel is underfilled Gel has started to evaporate	Inject with slightly more pressure, particularly giving a slight increase in pressure when reaching the region where the two gel interfaces meet in in the center of the gel channel. Make sure the device is kept in a sealed humid chamber immediately after seeding, until media injection.
Gel bursts into the media channel	Injection pressure is too high	Decrease the speed of injection into the gel region.
Bubbles form at the interpost regions after media filling	Gel was likely underfilled or was not properly humidified. This results in concavity at the gel-media interface, which traps bubbles when media is filled.	Ensure that gels are not "under-filled" by injecting slightly more gel before retracting the pipette tip. Make sure a seeded device is immediately placed into the humid chamber after seeding.
Microvascular networks do not form over 4 days	Cell seeding density may be too low Cells begin to die because media has evaporated from the reservoirs and/or was not refreshed every 24 hours Batch to batch variability of	Ensure HUVECs are seeded at a final concentration of 6M/mL. Ensure that the cell suspension is mixed well prior to mixing with a single fibrinogen aliquot since cells can settle quickly in the re-suspension. Media should completely fill the reservoir. The user may choose to fill extra media so it forms a "dome" over the reservoirs. This is helpful if the reservoir diameters are smaller than 4mm. Acquire a new batch of cells (i.e. different Lot. #), and choose pooled populations when possible

	HUVECs or NHLF	
Microvascular networks regress/die over 4 days	Improper media exchange Incorrect temperature and/or CO_2 levels Media has dried out	Ensure that both reservoirs are emptied and that fresh media is allowed to flow at least twice across the media channel before topping off the reservoirs. Devices must be kept at 37°C and 5% CO_2 at all times. The amount of media in the channel alone is less than 10 μL, thus make sure reservoirs contain an additional >50 μL of media at all times.
Networks do not form openings to the media channel	Cell seeding density is not high enough	Ensure HUVEC seeding density is around 6M/mL (final concentration) See "Optional" step at Step 10, to seed an endothelial monolayer in the media channels, which allows ECs in the media channel to "anastomose" with vessel segments at the inter-post region. See **Supplementary Figure 2** for examples of perfusable and non-perfusable openings, as well as typical number of perfusable devices that should be achieved per seeding session.
Tumor cells are not flowing through the network	Not enough of a pressure drop across the gel region Lumens have not yet opened up to the media channel to connect to the media ports	Use a pressure drop of around 4 mm to achieve an adequate flow rate through the network. This can be achieved by pipetting ~38 uL of cell suspension in both reservoirs on one side of the gel region (for a 3 mm diameter port). Continue to culture the devices for 1-2 more days to allow sufficient time for lumens to open up to the media channel
Cells are fluorescent but not clear	May be condensation on the objective lens or the glass surface of the device Poor sample placement	Decrease the humidification level of the environmental chamber Check to see that the sample is placed correctly on the specimen holder
Cells are dying over imaging time	Environmental chamber is not maintained Photo toxicity	Check to see if there are leaks resulting in less than optimal CO_2 and temperature conditions Decrease the laser intensity or the interval frequency of imaging
Unspecific staining	Not enough washing after incubation of primary or secondary antibody	Make sure when washing that solutions are completely displaced down the media channel and removed. Let the wash buffer incubate for >10 minutes between washes to facilitate diffusion.
Reconstructed cross sectional view of lumens on image processing software is "fuzzy" or not well-defined enough for robust quantification	Step size setting during image acquisition was too large	See SI Table 1 for sample microscope settings used to acquire typical data.

Appendix D

shRNA	Species	Sequence
ITGB1-1	Human	TGCTGTTGACAGTGAGCGCCAGATGAAAATAGATGTTTAATAGTGAAGCCACAGATGTATTAAACATCTATTTTCATCTGTTGCCTACTGCCTCGGA
ITGB1-2	Human	TGCTGTTGACAGTGAGCGCACCGAGCAATTTTCTGCTAAATAGTGAAGCCACAGATGTATTTAGCAGAAAATTGCTCGGTTTGCCTACTGCCTCGGA
ITGB1-3	Human	TGCTGTTGACAGTGAGCGCCCGAGCAATTTTCTGCTAAAATAGTGAAGCCACAGATGTATTTTAGCAGAAAATTGCTCGGTTGCCTACTGCCTCGGA
ITGB1-4	Human	TGCTGTTGACAGTGAGCGACCGGTGAAAATCCTATTTATATAGTGAAGCCACAGATGTATATAAATAGGATTTTCACCGGCTGCCTACTGCCTCGGA
ITGB1-5	Human	TGCTGTTGACAGTGAGCGCTCCCACAACACTGAATGCAAATAGTGAAGCCACAGATGTATTTGCATTCAGTGTTGTGGGATTGCCTACTGCCTCGGA
ITGB1-6	Human	TGCTGTTGACAGTGAGCGAAAGAGGGATAATACAAATGAATAGTGAAGCCACAGATGTATTCATTTGTATTATCCCTCTTCTGCCTACTGCCTCGGA
ITGB1-7	Human	TGCTGTTGACAGTGAGCGAAGCCACAGACATTTACATTAATAGTGAAGCCACAGATGTATTAATGTAAATGTCTGTGGCTCTGCCTACTGCCTCGGA
ITGB1-8	Human	TGCTGTTGACAGTGAGCGCCGGGTGAAAATCCTATTTATATAGTGAAGCCACAGATGTATATAAATAGGATTTTCACCCGTTGCCTACTGCCTCGGA
ITGB3-1	Human	TGCTGTTGACAGTGAGCGCTCCAACATTTGTTAATAGTTATAGTGAAGCCACAGATGTATAACTATTAACAAATGTTGGAATGCCTACTGCCTCGGA
ITGB3-2	Human	TGCTGTTGACAGTGAGCGACCGCTTCAATGAGGAAGTGAATAGTGAAGCCACAGATGTATTCACTTCCTCATTGAAGCGGGTGCCTACTGCCTCGGA
ITGB3-3	Human	TGCTGTTGACAGTGAGCGAAAGAGCAGATGTCATTCCATATAGTGAAGCCACAGATGTATATGGAATGACATCTGCTCTTGTGCCTACTGCCTCGGA
ITGB3-4	Human	TGCTGTTGACAGTGAGCGATACCCTGAGTTCATAAATTTATAGTGAAGCCACAGATGTATAAATTTATGAACTCAGGGTAGTGCCTACTGCCTCGGA
ITGB3-5	Human	TGCTGTTGACAGTGAGCGACCACGTCTACCTTCACCAATATAGTGAAGCCACAGATGTATATTGGTGAAGGTAGACGTGGCTGCCTACTGCCTCGGA
ITGB3-6	Human	TGCTGTTGACAGTGAGCGCCCGGCTACTACTGCAACTGTATAGTGAAGCCACAGATGTATACAGTTGCAGTAGTAGCCGGTTGCCTACTGCCTCGGA
ITGB3-7	Human	TGCTGTTGACAGTGAGCGCAAGGGAGAGAGTGCTATTGTATAGTGAAGCCACAGATGTATACAATAGCACTCTCTCCCTTTTGCCTACTGCCTCGGA
ITGB3-8	Human	TGCTGTTGACAGTGAGCGCTGGCAGTATGGTAGAGGGATATAGTGAAGCCACAGATGTATATCCCTCTACCATACTGCCATTGCCTACTGCCTCGGA
Firefly Luciferase (FF)		AAGGTATATTGCTGTTGACAGTGAGCGAGCTCCCGTGAATTGGAATCCTAGTGAAGCCACAGATGTAGGATTCCAATTCAGCGGGAGCCTGCCTACT GCCTCG
ITGA1-2	Mouse	TGCTGTTGACAGTGAGCGCCCCAACAAAGTGAATATTCAATAGTGAAGCCACAGATGTATTGAATATTCACTTTGTTGGGTTGCCTACTGCCTCGGA
ITGA1-3	Mouse	TGCTGTTGACAGTGAGCGACCCGGCTAATGTTATATTGTATAGTGAAGCCACAGATGTATACAATATAACATTAGCCGGGGTGCCTACTGCCTCGGA
ITGA1-5	Mouse	TGCTGTTGACAGTGAGCGCCTGGATGGTCATCTTCTGATATAGTGAAGCCACAGATGTATATCAGAAGATGACCATCCAGTTGCCTACTGCCTCGGA
ITGA2-2	Mouse	TGCTGTTGACAGTGAGCGACCCGTGATCTTTCCTAAACAATAGTGAAGCCACAGATGTATTGTTTAGGAAAGATCACGGGCTGCCTACTGCCTCGGA
ITGA2-6	Mouse	TGCTGTTGACAGTGAGCGACTGAAAGACCTTCACATGAAATAGTGAAGCCACAGATGTATTTCATGTGAAGGTCTTTCAGCTGCCTACTGCCTCGGA
ITGA2-7	Mouse	TGCTGTTGACAGTGAGCGCCAGGGCGATGGGATACTTCTATAGTGAAGCCACAGATGTATAGAAGTATCCCATCGCCCTGTTGCCTACTGCCTCGGA
ITGA3-1	Mouse	TGCTGTTGACAGTGAGCGAATGGACAATGTTCGCGATAAATAGTGAAGCCACAGATGTATTTATCGCGAACATTGTCCATCTGCCTACTGCCTCGGA
ITGA3-6	Mouse	TGCTGTTGACAGTGAGCGCCAGCTACATGATTCAGCGGAATAGTGAAGCCACAGATGTATTCCGCTGAATCATGTAGCTGTTGCCTACTGCCTCGGA
ITGA3-7	Mouse	TGCTGTTGACAGTGAGCGCCCGGATTATGCCCAAGTACCATAGTGAAGCCACAGATGTATGGTACTTGGGCATAATCCGGTTGCCTACTGCCTCGGA
ITGA4-1	Mouse	TGCTGTTGACAGTGAGCGCGGGCATCATGTGATCACCAAATAGTGAAGCCACAGATGTATTTGGTGATCACATGATGCCCATGCCTACTGCCTCGGA
ITGA4-2	Mouse	TGCTGTTGACAGTGAGCGCCGACATTTCACCATCATTATTTAGTGAAGCCACAGATGTAAATAATGATGGTGAAATGTCGTTGCCTACTGCCTCGGA
ITGA6-1	Mouse	TGCTGTTGACAGTGAGCGCCACCACAGATCTGGATATTAATAGTGAAGCCACAGATGTATTAATATCCAGATCTGTGGTGTTGCCTACTGCCTCGGA
ITGA6-2	Mouse	TGCTGTTGACAGTGAGCGCCCGATGCATAGTATTGATCTATAGTGAAGCCACAGATGTATAGATCAATACTATGCATCGGATGCCTACTGCCTCGGA
ITGA6-6	Mouse	TGCTGTTGACAGTGAGCGCTAGGGTGATTAACTTAGGCAATAGTGAAGCCACAGATGTATTGCCTAAGTTAATCACCCTAATGCCTACTGCCTCGGA
ITGA8-2	Mouse	TGCTGTTGACAGTGAGCGAAACCTATAGAATTTAAATCAATAGTGAAGCCACAGATGTATTGATTTAAATTCTATAGGTTCTGCCTACTGCCTCGGA
ITGA8-3	Mouse	TGCTGTTGACAGTGAGCGCTTGGATGATTCTACCTTTAAATAGTGAAGCCACAGATGTATTTAAAGGTAGAATCATCCAAATGCCTACTGCCTCGGA
ITGA8-5	Mouse	TGCTGTTGACAGTGAGCGCCAGATAATTATTGGCGATGAATAGTGAAGCCACAGATGTATTCATCGCCAATAATTATCTGATGCCTACTGCCTCGGA
ITGAV-9	Mouse	TGCTGTTGACAGTGAGCGCCTGCATTGTGTCTTATTGTATTAGTGAAGCCACAGATGTAATACAATAAGACACAATGCAGATGCCTACTGCCTCGGA
ITGAV-10	Mouse	TGCTGTTGACAGTGAGCGCGCATAGTACCTCTTCAGTTACTAGTGAAGCCACAGATGTAGTAACTGAAGAGGTACTATGCTTGCCTACTGCCTCGGA
ITGB1-4	Mouse	TGCTGTTGACAGTGAGCGACCAGACGGAGTAACAATAAATTAGTGAAGCCACAGATGTAATTTATTGTTACTCCGTCTGGCTGCCTACTGCCTCGGA
ITGB1-5	Mouse	TGCTGTTGACAGTGAGCGCGGCTCTCAAACTATAAAGAAATAGTGAAGCCACAGATGTATTTCTTTATAGTTTGAGAGCCTTGCCTACTGCCTCGGA
ITGB2-1	Mouse	TGCTGTTGACAGTGAGCGCGCCCATCTTTGCGGTGACAAATAGTGAAGCCACAGATGTATTTGTCACCGCAAAGATGGGCTTGCCTACTGCCTCGGA
ITGB2-4	Mouse	TGCTGTTGACAGTGAGCGAGGAAGGCTGTTGGATAACTTATAGTGAAGCCACAGATGTATAAGTTATCCAACAGCCTTCCGTGCCTACTGCCTCGGA
ITGB2-5	Mouse	TGCTGTTGACAGTGAGCGAGGAAACAGCTATCTCCACAAATAGTGAAGCCACAGATGTATTTGTGGAGATAGCTGTTTCCGTGCCTACTGCCTCGGA
ITGB3-2	Mouse	TGCTGTTGACAGTGAGCGCGCAAACAACCCGCTGTATAAATAGTGAAGCCACAGATGTATTTATACAGCGGGTTGTTTGCTTGCCTACTGCCTCGGA
ITGB3-3	Mouse	TGCTGTTGACAGTGAGCGACCTCTCAGATGCGCAAGCTTATAGTGAAGCCACAGATGTATAAGCTTGCGCATCTGAGAGGCTGCCTACTGCCTCGGA
ITGB3-9	Mouse	TGCTGTTGACAGTGAGCGAGCAGGCATTGTCCTGCCCAATTAGTGAAGCCACAGATGTAATTGGGCAGGACAATGCCTGCCTGCCTACTGCCTCGGA
ITGB3-10	Mouse	TGCTGTTGACAGTGAGCGAGGAAGGAATTTGCTAAATTTGTAGTGAAGCCACAGATGTACAAATTTAGCAAATTCCTTCCGTGCCTACTGCCTCGGA
ITGB4-4	Mouse	TGCTGTTGACAGTGAGCGACAGGGTGGAGAAGACTACGAATAGTGAAGCCACAGATGTATTCGTAGTCTTCTCCACCCTGGTGCCTACTGCCTCGGA
ITGB4-7	Mouse	TGCTGTTGACAGTGAGCGAAGGGTGGAGAAGACTACGAAATAGTGAAGCCACAGATGTATTTCGTAGTCTTCTCCACCCTGTGCCTACTGCCTCGGA